Spin-Vibronic Mechanism for Intersystem Crossing

Thomas Penfold, Etienne Gindensperger, Chantal Daniel, Christel Marian

The Spin-Vibronic Mechanism for Intersystem Crossing

Thomas J. Penfold,[*,†] Etienne Gindensperger,[*,‡] Chantal Daniel,[*,‡] and Christel M. Marian[*,¶]

†*Chemistry - School of Natural and Environmental Sciences, Newcastle University, Newcastle Upon-Tyne, NE1 7RU*

‡*Laboratoire de Chimie Quantique, Institut de Chimie, CNRS- Université de Strasbourg, Institut de Chimie UMR-7177,1 Rue Blaise Pascal 67008 Strasbourg, France*

¶*Institut für Theoretische Chemie, Heinrich-Heine-Universität Düsseldorf, Universitätsstr. 1, 40225 Düsseldorf, Germany.*

E-mail: tom.penfold@ncl.ac.uk; egindensperger@unistra.fr; c.daniel@unistra.fr; christel.marian@hhu.de

Abstract

Intersystem crossing (ISC), formally forbidden within non-relativistic quantum theory, is the mechanism by which a molecule changes its spin state. It plays an important role in the excited state decay dynamics of many molecular systems and not just those containing heavy elements. In the simplest case ISC is driven by direct spin-orbit coupling between two states of different multiplicity. This coupling is usually assumed to remain unchanged by vibrational motion, i.e. the Condon approximation. It is also often presumed that spin-allowed radiationless transitions, i.e. internal conversion, and the nonadiabatic coupling that drives them, can be considered separately from ISC and spin-orbit coupling owing to the vastly different timescales upon which these

processes are assumed to occur. However, these assumptions are too restrictive. Indeed, the strong mixing brought about by the simultaneous presence of nonadiabatic and spin-orbit coupling means that often the spin, electronic and vibrational dynamics cannot be described independently. Instead of considering a simple ladder of states, as depicted in a Jablonski diagram, one must consider the more complicated spin-vibronic levels. Despite the basic ideas being outlined in the 1960's, it is only with the advent of high-level theory and femtosecond spectroscopy that the importance of the spin-vibronic mechanism for ISC in both fundamental as well as applied research fields has been revealed with significant impact across chemistry, physics and biology. In this review article, we present the theory and fundamental principles of the spin-vibronic mechanism for ISC. This is followed by empirical rules to estimate the rate of ISC within this regime. The most recent developments in experimental techniques, theoretical methods and models for the spin-vibronic mechanism are discussed. These concepts are subsequently illustrated with examples, including the ISC mechanisms in transition metal complexes, small organic molecules and organic chromophores.

Contents

Introduction

The development of molecular spectroscopy in the mid-twentieth century made it possible to address many fundamental issues relating to the response of complex polyatomic molecules to light. However, this response often becomes quite complicated and involves many intertwined radiative and non-radiative decay processes, such as luminescence, internal conversion (IC), intersystem crossing (ISC), electron/energy transfer, which are often accompanied or driven by structural rearrangements including dissociation. Knowledge of these primary events, which often occur within the first picoseconds (ps) after excitation, is critical for understanding fundamental excited-state processes, but also controlling the functional prop-

erties of molecular excited states that are exploited for a wide number of applications across photochemistry, photophysics and photobiology.

The complexity of excited-state dynamics means that early empirical concepts,[1,2] developed for interpreting the spectral features, kinetics, lifetime and luminescence efficiency, are a matter of debate. Indeed, the interpretation of spectroscopic observables founded on the simple qualitative analyses of Kasha[3] and El-Sayed[4] can lead to erroneous conclusions as far as the photophysics and luminescent properties of polyatomic molecules are concerned. In the case of El-Sayed's rules directly concerned with ISC, early examples of this breakdown were observed in the 1960's for the phosphorescence properties of small organic molecules, such as benzene.[5–9] Importantly, understanding the dynamics of high-spin states and the mechanisms by which they are generated is of great importance as they can be both detrimental, such as non-emissive decay pathways[10] or fluorescence quenching[11] and exploited, e.g. triplet-triplet up conversion,[12] spin crossover,[13–15] photodynamic therapy,[16] energy transfer triggering,[17] building of luminescent assemblies,[18] photocatalysis[19] or triplet exciton harvesting.[20,21]

A step change in our understanding was achieved through the advent of femtosecond laser spectroscopy,[22–24] which made it possible to probe, in real time, the ultrafast dynamics in photoexcited molecules and to decipher complicated excited state dynamics over a large range of time scales. In this context, one of the most striking examples is the ultrafast ISC kinetics in transition metal complexes , which are often characterised by a high number of various electronic excited states of different multiplicities in a limited domain of energy.[25] This is exemplified by the ultrafast light induced spin-crossover dynamics of $[Fe(bpy)_3]^{2+}$.[26–29] Photoexcitation of the ^{1}MLCT band of $[Fe(bpy)_3]^{2+}$ leads to population of a non-emissive quintet MC ($^5T_2$) state within 100 fs.[30–32] Such dynamics involve two spin transitions and therefore are remarkable given that the timescales involved are significantly faster than the timescale usually expected for a single ISC event. This is accompanied in other molecules by intriguing effects such as ISC rates varying with the vibrational period of important normal

modes rather than heavy atom effects[33] or which are strongly solvent dependent.[34]

For a long time it was believed that spin-forbidden non-radiative transitions in purely organic compounds were slow in comparison to their spin-allowed counterparts and often their presence in excited state processes was neglected. However, there is increasing evidence that even in compounds composed of only light elements, ISC can occur on the subpicosecond time scale and is thus competitive with IC. This is strongly illustrated by aromatic carbonyl compounds of the xanthone type and nitro aromatic compounds. The unusual photophysical and photochemical properties of nitroarenes stimulated a series of femtosecond-resolved experiments.[35–46] Their photoexcitation decay kinetics are characterized by a biphasic decay of the lowest excited singlet state with time constants of ≤ 100 fs and < 10 ps and a very high quantum yield of triplet formation. The identity of the coordinate that tunes the initially excited singlet and the receiving triplet states into a potential curve crossing remains a matter of debate. Some authors favour the pyramidalisation,[35,36,47,48] others the torsional motion of the nitro group[37,41,44,45,47–49] while yet others believe the ONO bending to be the decisive coordinate.[50] Importantly, it is clear, however, that a strong coupling between nuclear motion, electronic structure and the electron spin magnetic moment determines the photopysics of these compounds.

All of these time-resolved experiments studying ISC dynamics have benefited from a strong insight from theory and computation. Indeed, in the aforementioned case of aromatic carbonyl compounds, quantum chemical studies along side rate constants calculated using perturbation theory have been pivotal for the understanding of the underlying mechanistic picture.[51–55] Pioneering simulations combining quantum chemistry with molecular or quantum dynamics have been proposed for both organic molecules[56] and transition metal complexes.[57,58] Indeed, prior to any experimental evidence it was shown that fast ISC (<50 ps) in a first-row transition metal complex could be described as a succession of elementary transitions occurring at critical geometries or crossing points between the singlet and the triplet potential energy surfaces (PESs) and that the efficiency of the radiationless transitions

was governed by the overlap of the propagated wave packet with the critical region of the coupled potential energy surfaces.[58] More recently by combining time-resolved photoelectron spectroscopy and quantum dynamics (QD) it was demonstrated that ISC in hydrocarbons could compete with IC.[59,60] A significant theoretical activity in this area has emerged within the past five years, of which a significant portion has focused upon studying ISC processes using non-adiabatic molecular dynamics (MD) including spin-orbit coupling (SOC).[61–76] Examples of ISC dynamics based upon quantum wavepacket dynamics are more scarce.[77–85] *On-the-fly* dynamics simulations including SOC are very powerful for the interpretation of the experiments highlighting the importance of ISC in a variety of non-adiabatic photochemical and photobiological processes with the possibility of including atomistic environment effects. But for such simulations, it remains much harder than full quantum approaches to decipher the early time photophysics and discover the subtle effects that drive the spin-vibronic mechanism in complex molecules.

In this article, we review the most recent developments in experimental techniques, theoretical methods and models for describing ISC beyond the direct spin-orbit interaction, namely the spin-vibronic mechanism. To understand this mechanism one must explicitly consider the coupling between the spin, vibrational and electronic subsystems and its role in a wide variety of different systems is being demonstrated to be increasingly important. The concepts outlined are illustrated with examples including the ISC mechanisms in transition metal complexes, small organic molecules and organic chromophores.

Background and Theory

It is often assumed that radiationless transitions, especially on the pico- to femtosecond timescale, are due to the breakdown of the Born-Oppenheimer (BO) approximation, and are thus governed by matrix elements acting between states of the same multiplicity, i.e. IC. However, as discussed throughout this review, this statement is too restrictive. For many

systems, including those containing only light elements such as C, N and H, radiationless transitions also include singlet-triplet transitions, i.e. ISC. In this regime one must not only consider scenarios in which the states are coupled by SOC, but also the possibility for states to be mixed by nonadiabatic and spin-orbit coupling simultaneously. Indeed, within a basis of spin-orbit-coupled BO states, there is no difference between IC and ISC. It is the main ideas and theory behind this which is now discussed.

The Coupling Elements

Consider an electronic Hamiltonian under the zeroth-order BO approximation:

$$\hat{\mathcal{H}} = \hat{\mathcal{H}}_0 + \hat{\mathcal{H}}_{SO} \tag{1}$$

where $\hat{\mathcal{H}}_0$ contains the usual kinetic and potential energies for the electrons. $\hat{\mathcal{H}}_{SO}$ represents the spin–orbit operator coupling the electronic and spin degrees of freedom together and mixing states of different multiplicity. Strictly speaking, the multiplicity classification for eigenfunctions of $\hat{\mathcal{H}}$ does not hold with the presence of $\hat{\mathcal{H}}_{SO}$, as it would for $\hat{\mathcal{H}}_0$, i.e. upon inclusion of $\hat{\mathcal{H}}_{SO}$ a singlet can not longer be classified as a pure singlet state. However throughout the remaining we assume it would in order to retain simplicity when discussing the states.

In this form, the nuclear coordinate, Q, is only included in $\hat{\mathcal{H}}_0$ and $\hat{\mathcal{H}}_{SO}$ as a parameter. This describes the Condon approximation, i.e. assuming that the electronic and vibrational degrees of freedom can be strictly separated, making Q a parameter. However, if this breaks down, we must consider the vibrational dependence of these Hamiltonian operators, written to first order as:

$$\hat{\mathcal{H}} = \hat{\mathcal{H}}_0 + \hat{\mathcal{H}}_{SO} + \sum_{\alpha} \left[\frac{\partial \hat{\mathcal{H}}_0}{\partial Q_\alpha} + \frac{\partial \hat{\mathcal{H}}_{SO}}{\partial Q_\alpha} \right] Q_\alpha \tag{2}$$

where the coupling elements now also depend on the vibrational degree of freedom α.

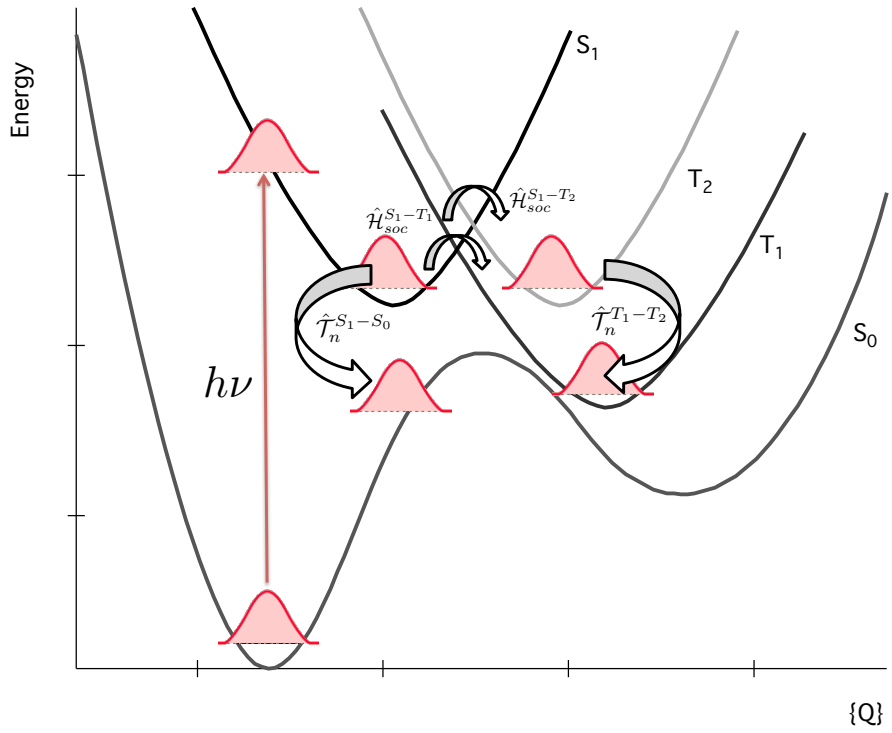

Figure 1: Schematic representation of a potential energy curve and relevant couplings as a function of an arbitrary nuclear coordinate $\{Q\}$. $\hat{\mathcal{T}}_n$ denotes nonadiabatic coupling between states of the same multiplicity and $\hat{\mathcal{H}}_{SO}$ denotes spin–orbit coupling. In the case that $\hat{\mathcal{H}}_{SO}$ between the S_1 and T_1 states was zero, decay could occur via a more complicated, second-order channel, $S_1 \rightarrow T_2 \rightarrow T_1$, involving both spin–orbit and nonadiabatic coupling. This is an example of the spin-vibronic mechanism as described in this review.

Spin–Orbit Coupling

SOC is a relativistic effect that acts on both angular momentum and spin, leading to its defining characteristic of mixing orbital and spin degrees of freedom, thus allowing electronic states of different multiplicities to couple. It is naturally incorporated within the Dirac equation, but is more commonly included as a perturbative correction to the standard, non-relativistic electronic structure theories. SOC has a wide range of important effects in chemistry and physics, such as fine-structure and band splitting in molecules, semi-conductors, and metals, molecular magnetism, spin transport in spintronics and magnetoelectronics, spin quantum dots, and qubits dynamics. In the context of this present review, SOC is also very important

for photophysics and photochemistry because it turns spin-forbidden processes, such as ISC and phosphorescence into allowed transitions.[86]

In its most common, Breit-Pauli form, the SOC operators is expressed:

$$\hat{\mathcal{H}}_{SO}^{BP} = \frac{1}{2m_e^2c^2}\sum_I\sum_i \frac{Z_I}{r_{iI}^3}\left(\hat{\mathbf{r}}_{iI}\times\hat{\mathbf{p}}_i\right)\cdot\hat{\mathbf{s}}_i - \frac{1}{2m_e^2c^2}\sum_i\sum_{j\neq i}\frac{Z_I}{r_{ij}^3}\left(\hat{\mathbf{r}}_{ij}\times\hat{\mathbf{p}}_i\right)\cdot\left(\hat{\mathbf{s}}_i + 2\hat{\mathbf{s}}_j\right) \quad (3)$$

where $\hat{\mathbf{r}}_{iI}\times\hat{\mathbf{p}}_i$ is the angular momentum of electron i with respect to nucleus I, $\hat{\mathbf{r}}_{ij}\times\hat{\mathbf{p}}_i$ is the angular momentum of electron i with respect to electron j and $\hat{\mathbf{s}}_i$ is the spin-operator of electron i. The first term is the one-electron term, involving spin-same-orbit coupling only. This describes the interaction between the magnetic spin moment of an electron with the magnetic moment induced by its orbiting in the nuclear electrostatic field. The second term is the two-electron term, describing spin-same-orbit and spin-other-orbit coupling. The former is analogous to the one-electron terms, but instead the electric field is generated by different electron. The two-electron spin-other-orbit terms arise from the interaction of the spin magnetic moment of one electron with the orbital magnetic moment of a second one, and vice versa. The two electron terms provide screening of the one-electron term and in compounds composed of light elements only, this screening is substantial and cannot be neglected. However, it can be incorporated in the one-electron terms to good approximation in a mean-field manner.[87,88] Importantly, because the one-electron contributions increase much faster with nuclear charge[89] than the two-electron terms for many cases involving heavier elements, the one-electron term is dominant. Indeed, in the total SOC matrix element (SOCME) of the valence shell, for 6d elements, such as Pt, the two-electron terms reduces the contributions of the one-electron term by approximately 10%.[90]

In a one-center approximation, the SOC operator can be expressed as:

$$\hat{\mathcal{H}}_{SO}^{eff} = \frac{1}{2m_e^2c^2}\sum_l\sum_i \frac{Z_I^{eff}}{r_{iI}^3}\hat{\mathbf{l}}_i\cdot\hat{\mathbf{s}}_i \quad (4)$$

where $\hat{\mathbf{l}}_i$ is the angular momentum and $\hat{\mathbf{s}}_i$ is the spin operator of electron i. Herein, the

screening is taken into account by replacing the nuclear charge Z_I by an effective nuclear charge Z_I^{eff} that is fitted to atomic data.[91] For each nucleus one can write a spin–orbit coupling constant, $\zeta = \frac{Z_I^{eff}}{2m_e^2c^2r^3}$, which is proportional to the effective nuclear charge and inversely proportional to the mean cubic radial distribution (r^{-3}) of the electron. This constant is therefore responsible for the so-called *heavy-atom effect*, whereby SOC is expected to increase with the atomic number. However, it is important to stress that one must also consider the integral over the two states involved:

$$[\hat{\mathcal{H}}_{SO}]_{ij} = \langle \psi_{S_i} | \hat{\mathcal{H}}_{SO} | \psi_{T_j} \rangle. \tag{5}$$

This integral, sometimes referred to as the *internal effect*, depends principally on the character of the states involved, as outlined qualitatively by El-Sayed,[4] and described in detail in section .

In quantum chemical studies of heavy-element compounds, where the inclusion of scalar and magnetic relativistic effects is mandatory, frequently effective core potentials (ECPs) are employed instead of the operators in Equations 3 and 4. The spin–orbit effective core potentials (SOECPs) are defined as the difference between the ECPs for the $j = l + 1/2$ and $j = l - 1/2$ shells derived from two- or four-component atomic calculations. In fitting this difference to a linear combination of a few Gaussian basis functions, the original $1/r_{iI}^3$-dependence has been dropped and the action of the SOC operator has been relocated to the valence region.[92–94] These atomic SOC operators can therefore be written as[95]

$$\hat{\mathcal{H}}_{SO}^{ECP} = \sum_{l=1}^{l_{\max}} \frac{2\Delta V_l(r)}{2l+1} \hat{\mathbf{l}} \cdot \hat{\mathbf{s}} \sum_{m_l=-l}^{+l} |l, m_l\rangle\langle l, m_l| \tag{6}$$

where $l_{\max}$ is the largest angular momentum quantum number for which the SOECP is defined on this atom.

To date the calculation of SOCMEs has been implemented across many different quantum chemistry methods including time-dependent Hartree-Fock theory,[96] multi-configurational

self-consistent field methods,[91,97] multi-reference configuration interaction[98–102] and multi-reference perturbation theory approaches,[103] algebraic diagrammatic construction based methods,,[104] equation-of-motion coupled-cluster theory[105–107] and semi-empirical approaches.[108] Within the framework of time-dependent density functional theory(TDDFT), Wang and Ziegler[109] developed an approach based upon an approximation of the relativistic formalism. For calculating SOC within the framework of linear-response time-dependent density functional theory (LR-TDDFT), based on a perturbative correction of the non-relativistic collinear TDDFT, similar to the work of Russo and Chiodo,[110,111] Tavernelli and co-workers[112] adopted an approach based upon a set of auxiliary many-electron wavefunctions, previously used to calculate nonadiabatic coupling vectors.[113,114] Most recently a simplification has been proposed which involves evaluation of SOC directly from the linear response amplitudes.[115,116]

Nonadiabatic Coupling

The BO approximation[117,118] represents the cornerstone of quantum theory and is used throughout quantum chemistry and condensed matter physics to decouple the motion of nuclei and electrons. However, as is well established,[119] the highly non-equilibrium electronic distribution generated upon excitation drives rapid nuclear motion leading to the breakdown of this approximation. This makes it impossible to neglect the nonadiabatic coupling terms present in the time-dependent Schrödinger equation.

The first-order nonadiabatic coupling operators are non-local derivative operators which are discussed in detail in ref.[119] They depend inversely on the mass of the system, and also the derivative coupling vector expressed:

$$\begin{aligned} \boldsymbol{F}_{ij} &= \langle \psi_i | \nabla \psi_j \rangle \\ &= \frac{\langle \psi_i | \nabla \hat{\mathcal{H}}_0 | \psi_j \rangle}{E_j - E_i} \end{aligned} \tag{7}$$

where ψ_i are the electronic basis functions that are solutions of the time-independent electronic Schrödinger equation and E_i the corresponding energies. Calculating this term is possible with a range of single[120] and multi-reference[121–125] electronic structure methods. Methods for calculating the coupling within the framework of TDDFT have also been demonstrated.[113,114,126–128]

However, within the adiabatic basis used by quantum chemistry methods, the nonadiabatic coupling diverges near intersections of the two coupled states.[129] This is illustrated in the second expression of Equation 7. The nonadiabatic coupling clearly exhibits an inverse dependence on the energy gap between surfaces. As this gap narrows, the coupling increases, but, if two surfaces become degenerate, the coupling becomes infinite. This creates a significant challenge for computational methods seeking to study the nonadiabatic dynamics. To alleviate these issues, it is possible to transform the adiabatic states into the so-called (quasi)-diabatic representation. The adiabatic picture provides a set of energy-ordered PESs and nonlocal couplings elements via nuclear momentum-like operators. In contrast, in the diabatic picture, the PESs is related to an electronic configuration and the couplings are provided by local multiplicative Q-dependent potential-like operators. Importantly, the surfaces in the diabatic picture are smooth because they are constructed so that the singular coupling terms vanish,[130] although it should be stressed that coupling can only be made rigorously zero for diatomics.[131] Consequently, they can often be described by a low-order Taylor expansion, as exploited below.

For a given set of adiabatic potential energy surfaces, diabatisation methods can be broadly classified into three groups: property-based, *by ansatz* and wave-function based.[132–134] Property based methods[132,135–142] approximate the diabatic states using observables such as transition dipole moment and change in molecular dipole moment. *By ansatz* methods define the diabatic states at a certain geometry, $\mathbf{Q_0}$ and then perform a Taylor expansion around this point.[143] The expansion is parametrised through fitting which is inexpensive, however the disadvantage is that in the absence of high molecular symmetry there might be some

ambiguity in the diabatisation because only adiabatic electronic energies are used and no information about the electronic wavefunctions is utilised. Finally, wavefunction methods explicitly calculate the coupling elements and then transform them into states which minimise the coupling and preserve the character of the diabats.[144–146] Recent developments have also included hybrid methods,[147] and important in the context of the present review SOC-diabatisation procedures based upon model space diabatization (MSD) have been proposed.[148,149]

Spin-Vibronic Coupling

The nonadiabatic coupling introduced in the previous section highlights the importance of specific vibrational degrees of freedom, along which this coupling is activated. The SOC discussed above in section is limited to a specific nuclear configuration, but as outlined in the introduction it is often not constant and also depends on the vibrational motion. In addition, in many cases it is insufficient to consider scenarios in which the states are coupled by vibronic or spin-orbit coupling, and one should account for the possibility for the states to be mixed by vibronic and spin-orbit coupling simultaneously. In ref.[5] Albrecht outlined the four mechanisms for mixing the singlet and triplet states:

I Direct spin–orbit coupling, $\hat{\mathcal{H}}_{SO}$, driven by the electronic character of the states and discussed in section .

II Vibrational spin–orbit, e.g. $(\partial\hat{\mathcal{H}}_{SO}/\partial Q_\alpha)Q_\alpha$, in which the size of the SOCME depends on the motion along a particular nuclear degree of freedom, Q_α. This is written to first order, but of course higher-orders can be included if necessary.

III Spin-vibronic, $\hat{\mathcal{T}}_N\hat{\mathcal{H}}_{SO}$, spin–orbit coupling with vibronic coupling in the singlet manifold

IV Spin-vibronic, $\hat{\mathcal{H}}_{SO}\hat{\mathcal{T}}_N$, spin–orbit coupling with vibronic coupling in the triplet manifold

The first, direct SOC has no dependence on the nuclear coordinates, while the latter three do and therefore it is these terms that make up the spin-vibronic coupling. Of these terms, only I and II can be present at first-order perturbation theory, while the terms involving a mixture of spin–orbit and nonadiabatic coupling appear only at second-order perturbation theory. Adopting each of these components, the full spin–orbit interaction, up to second order, can be written:

$$\begin{aligned}\hat{\mathcal{H}}_{SO} = \quad & \langle \Psi_{S_1} | \hat{\mathcal{H}}_{SO} | \Psi_{T_1} \rangle + \sum_\alpha \frac{\partial \langle \Psi_{S_1} | \hat{\mathcal{H}}_{SO} | \Psi_{T_1} \rangle}{\partial Q_\alpha} Q_\alpha + \sum_\alpha \sum_\beta \frac{1}{2} \frac{\partial^2 \langle \Psi_{S_1} | \hat{\mathcal{H}}_{SO} | \Psi_{T_1} \rangle}{\partial Q_\alpha \partial Q_\beta} Q_\alpha Q_\beta \\ & + \frac{\langle \Psi_{S_1} | \hat{\mathcal{H}}_{SO} | \Psi_{T_2} \rangle \langle \Psi_{T_2} | \hat{\mathcal{T}}_N | \Psi_{T_1} \rangle}{E_{T_2} - E_{S_1}} + \frac{\langle \Psi_{S_1} | \hat{\mathcal{T}}_N | \Psi_{S_2} \rangle \langle \Psi_{S_2} | \hat{\mathcal{H}}_{SO} | \Psi_{T_1} \rangle}{E_{S_2} - E_{T_1}} \end{aligned} \tag{8}$$

where Ψ represents the molecular wavefunction for a particular state, $\mathcal{T}_N$ is the nonadiabatic coupling operator and $\mathcal{H}_{SO}$ is the spin-orbit operator. Although the vibrational spin–orbit (terms 2 and 3 in Equation 8) are formally different from the interaction terms involving nonadiabatic coupling (terms 4 and 5 in Equation 8), in practice these terms can hardly be told apart, and which terms dominate will depend on the system under study.

In terms of calculating these couplings, the vibrational spin–orbit terms, which are described using first-order perturbation theory may be accounted for by calculating the vibrational dependence of the SOCME, as shown in refs.[150,151] in the framework of perturbation theory or ref.[152] in the framework of quantum dynamics. The latter terms are normally a little harder to incorporate, but can be routinely simulated using both excited state MD or quantum dynamics.[71,153–155]

Qualitative Rules for Intersystem Crossing

If the coupling between the two (initial and final) states of interest is small compared to their adiabatic energy difference, the rate of population transfer (k) between the two states can be described using perturbation theory, which to first order is Fermi's golden rule approximation

written:

$$k = \frac{2\pi}{\hbar} \sum_f |\langle \Psi_f | \hat{\mathcal{H}}_{if} | \Psi_i \rangle|^2 \delta(E_i - E_f), \tag{9}$$

where Ψ_i and Ψ_f are the total wavefunctions (electronic and vibrational) of the initial and final states and $\hat{\mathcal{H}}_{if}$ is the Hamiltonian describing the coupling between them, which in the case of ISC would be the $\hat{\mathcal{H}}_{SO}$. The δ function ensures the conservation of the molecular energy for the nonradiative transition. Assuming the Condon approximation, i.e direct SOC which has no dependency upon the vibrational degrees of freedom, the electronic and vibrational contributions are completely separable and it is possible for Equation 9 to be rewritten as:

$$k = \frac{2\pi}{\hbar} \sum_f |\langle \psi_f | \hat{\mathcal{H}}_{if} | \psi_i \rangle|^2 \sum_k |\langle \nu_{fk} | \nu_{ia} \rangle|^2 \delta(E_{ia} - E_{fk}). \tag{10}$$

This form highlights the two components, purely electronic SOC and vibrational density of states, which are crucial in determining the rate of ISC within a direct spin–orbit mechanism. The importance of these terms has led to them being widely studied leading to the development of qualitative rules making it possible to estimate the rate of ISC, which are now discussed.

El-Sayed Rules

As shown in Equation 3, the SOCME scale as Z_{eff}^4/n^3, where Z_{eff} is the effective nuclear charge and n is the principal quantum number of the valence electron. This is known as the *heavy atom effect* and therefore naively, one may expect that spin-orbit interactions increase as one moves down the periodic table. However, while this rule of thumb can work in many general cases for understanding the rate of ISC between two states, this breaks down if the two states are close in energy. In these cases, often a small coupling matrix element suffices to induce an efficient transition between the states. In addition, it does not capture any influence of the character of the states involved in the ISC process. The ISC rate dependence on the nature of the electronic transitions is described by *El-Sayed's rules*.[4]

In his work, El-Sayed highlighted that to achieve effective SOC, any change in spin must be accompanied by a corresponding change in angular momentum, so that total angular momentum is conserved. This original work was discussed in the context of organic chromophores considering the typical case of a transition from the lowest excited singlet state to the triplet manifold. El-Sayed rules predicted that $^1(\pi\pi^*) \rightsquigarrow {}^3(n\pi^*)$ ISC would be faster than $^1(\pi\pi^*) \rightsquigarrow {}^3(\pi\pi^*)$ ISC, as the latter involves the same orbitals. Therefore the requirement to conserve total angular momentum cannot be obeyed because there is no change in angular momentum associated with the transition.

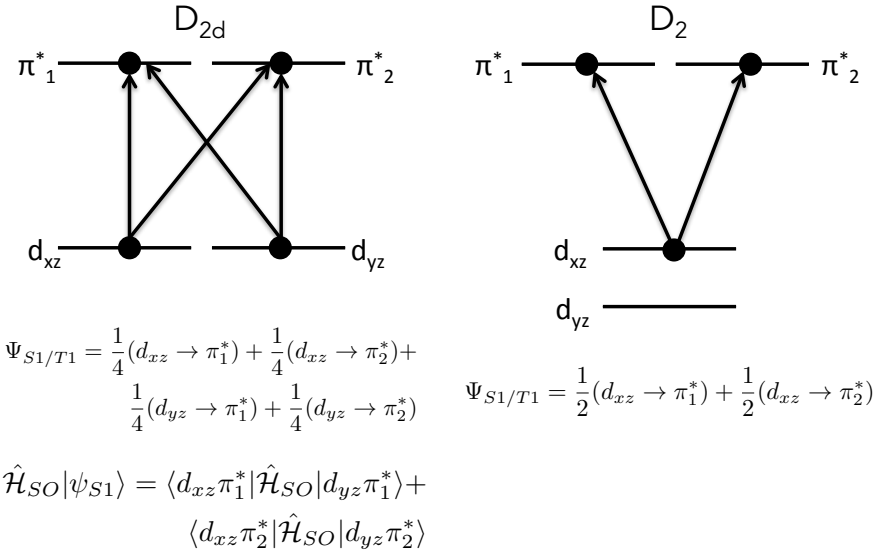

Figure 2: Schematic representation of the origin of SOCME between a singlet and triplet MLCT state, of two different molecular symmetries. Based on the SOCME of the Cu(I)-Phenanthroline complexes.[156,157] The arrows are indicative of possible one-electron transitions. At D_{2d} symmetry the singlet and triplet states are composed of four different transitions and therefore the SOCME are formed from mixing of the configurations with different d contributions, but same π^* character. In contrast, at the lower D_2 symmetry, this is no longer possible and therefore within the one-electron one-centre approximation SOC is forbidden. For the prototypical Bis-diimine Cu(I) complex, $[Cu(dmp)_2]^+$ (dmp = 2,9-dimethyl-1,10-phenanthroline), S_1-T_1 SOC at D_{2d} symmetry is $\sim$300 cm^{-1}, this falls to 30 cm^{-1} at D_2 symmetry.

Originally presented in the context of organic chromophores, *El-Sayed's rules* are generally applicable. Indeed, they can be used to explain why, despite the expected heavy atom

effect, that in some cases the SOCME between metal-to-ligand charge transfer states of Au(I) metal organic complexes are smaller than the one for analogous Cu(I) metal organic complexes. This can be understood by assuming a one-electron one-center approximation, which as described in section is expected to be dominant for heavier elements. For SOCME between two metal to ligand charge transfer (MLCT) states involving $d\pi^*$ character, the SOCME can be approximated as:

$$\langle \psi_{T1} | \hat{\mathcal{H}}_{SO} | \psi_{S1} \rangle = \langle d_i \pi_s^* | \hat{\mathcal{H}}_{SO} | d_j \pi_t^* \rangle \tag{11}$$

Since the SOC constant will be significantly larger for the metal than the lighter elements e.g. C, H, O, and N, the SOCME will be largest when the d electrons contribute, which means $i \neq j$ and $s = t$. Within the one-electron approximation, if both $i \neq j$ and $s \neq t$, then SOCME would be zero. This is shown schematically in Figure 2. In the case of Au(I) and Cu(I) complexes, because the crystal field splitting of Au(I) complexes is larger than for the corresponding Cu(I) compounds, the d electrons generally make a smaller contribution to the low-lying excited state leading to a smaller SOC.[158] Similar observations, which are essentially extensions of *El-Sayed's rules* have been made for charge-transfer states of organic chromophores.[159,160]

However, it is important to stress that the derivation of *El-Sayed's rules* is based upon pure electronic states of a single character at a fixed nuclear configuration. Mixing between states of different character will lead to the breakdown of this rule and vibronic interactions, discussed in Section , can significantly accelerate El-Sayed forbidden ISC.[150,151]

The Energy Gap Law

El-Sayed's rules address the purely electronic aspects of ISC, however Equation 10 illustrates the importance of the vibrational terms, more commonly referred to as the vibrational density of states. In the Condon approximation, the vibrational component of the rate expression is

the overlap between the initially populated and final vibrational density of states. This latter term is referred to as the Franck-Condon weighted density of states (FCWD). Assuming the high temperature limit, i.e. all modes relevant in transfer are below kT, the FCWD can be expressed:[161]

$$FCWD = \frac{1}{\sqrt{4\pi\lambda k_B T}} exp\left[-\frac{(\Delta E + \lambda)^2}{4\lambda k_B T}\right] \tag{12}$$

In Equation 12, λ denotes the reorganisation energy. In electron-transfer theory, the reorganization energy describes intramolecular and solvent reorientation energy. For ISC, λ also should include solvent (or environment) reorganization energy, but the intramolecular reorganization energy corresponds to the energy variation in the initial singlet excited state when switching from the singlet equilibrium geometry to the triplet equilibrium geometry as depicted in Figure 3. ΔE is the driving force, i.e. the adiabatic energy difference between the initial and final states at their respective minima.

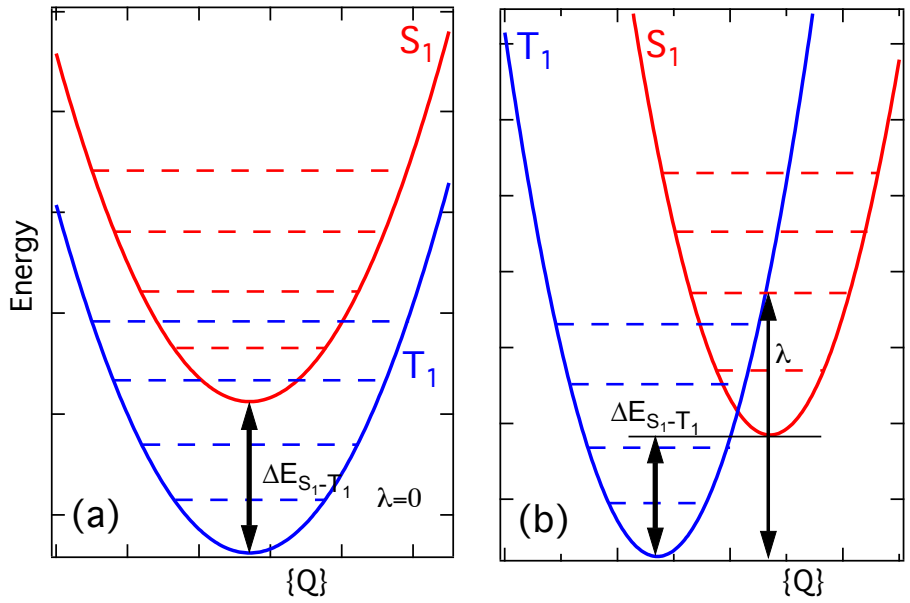

Figure 3: Schematic representation of the (a) weak and (b) strong coupling limits.

Equation 12 and Figure 3 illustrate the two regimes for radiationless transitions outlined

by Jortner and Englman,[162] namely the weak coupling limit and the strong coupling case. In the former, the displacement of final state minima (i.e. structural change) with respect to the initial state is small (Figure 3 *left*) leading to a small reorganisation energy. This is to say that the potentials are nested. In this weak coupling limit the transition probability depends exponentially on the adiabatic energy difference (ΔE). This relationship is commonly known as the *energy gap law*. Importantly, it is often forgotten that this rule applies only for a pair of nested states. In contrast, the strong coupling case is characterised by a large displacement of one potential minimum along a collective nuclear coordinate, {Q}, and so an intersection of the PESs can be expected. In this case, the rate of ISC will exhibit a Gaussian dependency on the parameter ΔE+λ. In this regime, occasionally an inverse relationship between the transition probability and ΔE is observed, i.e., the transition probability increases with increasing energy gap.[163]

Qualitative Estimation of Spin-Vibronic Coupling

Neither El-Sayed's nor the energy gap law discussed in the previous sections consider the coupled electronic, spin and nuclear dynamics which underpin the spin-vibronic mechanism. In section , three terms which compose spin-vibronic coupling mechanisms were outlined. The first (spin-vibrational) term is present at first order. Assuming a smoothly varying potential, the likely contribution of spin-vibronic coupling via these mechanisms can be estimated by determining the gradient of the SOC matrix elements and of the energy gap between the two coupled states as a function of the important reaction coordinates. While requiring additional calculations, this is not especially time-consuming.

A typical example for spin-vibrational coupling in the absence of a close-by intermediate electronic state is the ISC in free-base porphyrin following photoexcitation.[164] All low-lying electronic states of porphyrin are $\pi\pi^*$ states and ISC is thus El-Sayed forbidden. Porphyrin derivatives are nevertheless used as singlet oxygen sensitisers in photodynamic therapy (PDT). At the planar S_1 equilibrium geometry, the S_1-T_1 energy separation is $\approx$ 2400

cm^{-1} while their direct SOCME $\langle T_1|\hat{\mathcal{H}}_{SO}|S_1\rangle$ is smaller than 0.05 cm^{-1}. Out-of-plane vibrations leave the energy gap between the S_1 and T_1 states nearly unchanged, but as shown in Figure 4 increase their mutual SOC substantially by mixing some $\sigma\pi^*$ character into the electronic wavefunctions. In this way, the ISC rate constant is enhanced by two orders of magnitude to $k_{ISC} \approx 10^7$ s^{-1}, which makes ISC competitive with fluorescence in this molecule.

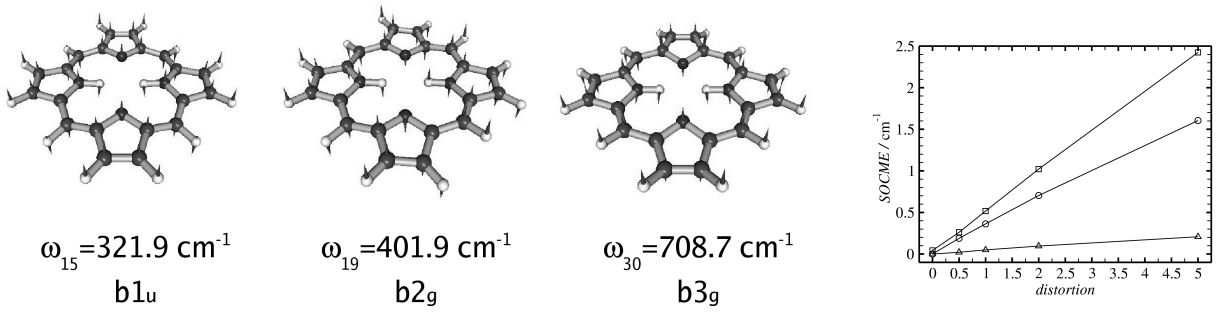

(a) (b)

Figure 4: Example for the enhancement of ISC by vibrational spin–orbit coupling:[164] (a) Out-of-plane vibrational modes of free-base porphyrin promoting SOC between $^3(\pi\pi^*)$ and $^1(\pi\pi^*)$ states. (b) Circles: Variation of $\langle T_1|\hat{\mathcal{H}}_{SO}|S_1\rangle$ along Q_{15}; Squares: Variation of $\langle T_2|\hat{\mathcal{H}}_{SO}|S_1\rangle$ along Q_{19}; Triangles: Variation of $\langle T_2|\hat{\mathcal{H}}_{SO}|S_0\rangle$ along Q_{30}.

The remaining terms in Equation 8 do not appear in first-order perturbation theory, and therefore a second-order expansion must be applied. This is written:

$$k = \frac{2\pi}{\hbar}\left|\frac{\langle\Psi_f|\hat{\mathcal{H}}_{soc}|\Psi_n\rangle\langle\Psi_n|\hat{\mathcal{H}}_{vib}|\Psi_i\rangle}{E_i - E_n}\right|^2 \delta(E_f - E_i) \tag{13}$$

whereby the initial (Ψ_i) and final (Ψ_f) states are coupled via an intermediate (Ψ_n) state. In order to develop generalised considerations, which like the energy gap rule, can be as a rule of thumb to estimate spin-vibronic contributions, we recast Equation 13 in the form of a semiclassical (Marcus-like) approach.[165,166]

$$k \sim \frac{2\pi}{\sqrt{4\pi\hbar^2\lambda_{if}k_bT}}\frac{|\mathcal{V}_{inf}|^2}{[E_n - E_i]^2 + \lambda_{in}/2} \times \exp\left(-\frac{[\Delta E_{if} + \lambda_{if}]^2}{4\lambda_{if}k_BT}\right) \tag{14}$$

Here, $\mathcal{V}_{inf}$ represents the second-order coupling matrix elements. This is equivalent to the purely electronic components of the coupling terms (Condon approximation). In the weak coupling limit, $\lambda \sim 0$, if applicable for all three states involved, this equation will exhibit an exponential dependence upon the gap between the initial and final state and quadratically on the energy gap between the initial and intermediate states. This is shown in Figure 5a.

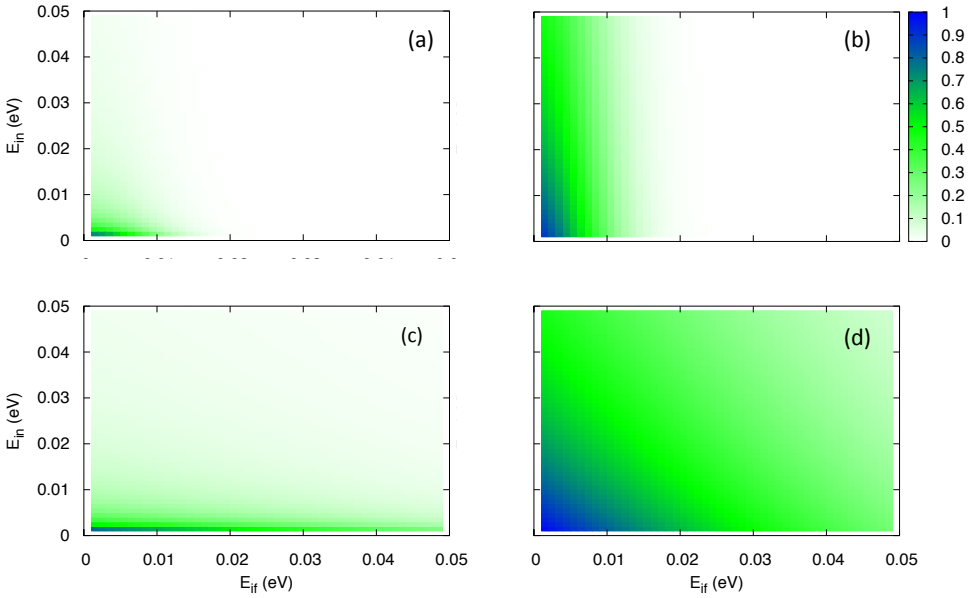

Figure 5: Normalised second-order rates calculated using Equation 14 for a single value of $\mathcal{V}_{inf}$ and λ_{if}=λ_{in}=0.001 eV (Weak coupling) (a), λ_{if}=0.001, λ_{in}=0.1 eV (a), λ_{if}=0.1 eV, λ_{in}=0.001 eV (a) and λ_{if}=0.2 eV, λ_{in}=0.1 eV (Strong coupling) (d).

In the strong coupling limit, just as in first-order perturbation theory, the second-order rate will exhibit a Gaussian dependency upon $\Delta E_{if} + \lambda_{if}$ with width $4\lambda_{if}k_BT$. This is scaled by the parameter of the energy gap and reorganisation energy between the initial and intermediate states, $[E_n - E_i]^2 + \lambda_{in}/2$. Two intermediate coupling limits can be envisioned and as shown in Figure 5b and c, exhibit the Gaussian dependency in only one of the coordinates for which $\lambda > 0$.

Theoretical Methods

Describing the rates of population transfer largely fall into two categories, i) time (in)-dependent perturbation theory (e.g. *Fermi's golden rule*) which calculate the rates at a particular nuclear geometry or ii) nuclear dynamical methods, which explicitly consider the nuclear motion over a PES. The latter, which provides a solution to the time-dependent Schrödinger equation, should yield a more precise picture of rates and corresponding dynamics. However, such approaches can be challenging for complex molecular systems with a large number of degrees of freedom.

Independent of the particular method used for addressing the nuclear degrees of freedom, the probabilities for nonradiative transitions will be very sensitive to the relative energies and to the geometric displacements of the involved PES. It is therefore mandatory to use either highly accurate electronic structure methods for their construction or to perform extensive benchmarking to accurately assess the limitations of the model developed. Experience has shown that the electronic SOCME are often less sensitive to the level of electron correlation treatment than the energetic splittings.[103,115]

In the following subsections the main approaches for describing the rate of spin-vibronic processes are described.

Perturbation Theory Approaches

The common starting point for approaches based upon perturbation theory is to approximate the initial and final states potentials typically with a harmonic oscillator model with vibrational frequencies $\mathbf{\Omega}_i$ and $\mathbf{\Omega}_f$, respectively. The mass-weighted normal coordinates of the final state, $\mathbf{Q}_f$, can be related to the ones of the initial state, $\mathbf{Q}_i$, by a Duschinsky transformation[167]

$$\mathbf{Q}_f = \mathbf{J}\mathbf{Q}_i + \mathbf{D} \tag{15}$$

where **J** is the Duschinsky matrix that accounts for the normal coordinate rotations while the displacement vector **D** expresses the geometry change between the two potentials. In molecules with common symmetry elements in the initial and final states, the Duschinsky matrix is block diagonal and the displacement vector has nonzero elements only for totally symmetric modes. Although the eigenfunctions of a harmonic oscillator form a complete set, the linear transformation proposed by Dushinsky is only an approximation. This is a consequence of the center-of-mass and Eckart conditions for the transformation from $3N$ space-fixed to $3N-6$ internal coordinates of non-linear molecules ($3N-5$ for linear ones). Due to these conditions, two electronic states with different equilibrium geometries and different normal modes give rise to two different internal coordinate systems. An axis-switching matrix, originally introduced by Watson and Hougen,[168] can be used for the transformation of the Eckart systems and for an approximate factorisation of the rotational coordinates from the vibrational subspaces $\mathbf{Q}_i$ and $\mathbf{Q}_f$.[169,170] The zeroth-order axis-switching matrix $\mathbf{T}_0$ which connects the equilibrium geometries of the two states has to be totally symmetric with respect to the largest common point group of these geometries. An alternative method for the determination of Duschinsky matrices and normal-mode-projected displacements for large floppy molecules using (redundant) internal coordinates has been presented by Reimers.[171]

In the harmonic oscillator model, the vibrational wavefunctions are factorised further into a product of lower-dimensionality (in most cases one-dimensional) oscillators carrying n quanta each.

$$v_{ia} = \prod_{\alpha} v_{i\alpha}^{n_{a\alpha}}(Q_{i\alpha}) \tag{16}$$

$$v_{fk} = \prod_{\beta} v_{f\beta}^{n_{k\beta}}(Q_{f\beta}) \tag{17}$$

To evaluate the integrals over vibrational wavefunctions of the initial and final states, Eq. (15) is used to transform one set of vibrational functions into the basis of the other. In the following, we choose the normal coordinates and harmonic oscillator functions of the inital

electronic state as the common basis and drop the index i in the denomination of the normal coordinates again.

To include vibrational SOC terms in the calculation of ISC rate constants, the Hamiltonian is typically expanded about the equilibrium geometry $\mathbf{Q_0}$ of the initial electronic state. In addition to the direct SOC term

$$k_{\mathrm{ISC}}^{\mathrm{FC}} = \frac{2\pi}{\hbar} \left| \langle \psi_f \,|\, \hat{\mathcal{H}}_{\mathrm{SO}} \,|\, \psi_i \rangle \right|^2_{\mathbf{Q_0}} \sum_k |\langle v_{fk} \,|\, v_{ia} \rangle|^2 \, \delta(E_{ia} - E_{fk}) \tag{18}$$

two contributions to the ISC rate are obtained from the derivative couplings, a cross term that contains Franck-Condon- and Herzberg-Teller-like expressions

$$\begin{aligned} k_{\mathrm{ISC}}^{\mathrm{FC/HT}} = \frac{4\pi}{\hbar} \Re \Bigg(& \langle \psi_f \,|\, \hat{\mathcal{H}}_{\mathrm{SO}} \,|\, \psi_i \rangle \Big|_{\mathbf{Q_0}} \sum_k \langle v_{fk} \,|\, v_{ia} \rangle \, \delta(E_{ia} - E_{fk}) \\ & \sum_\alpha \frac{\partial \langle \psi_f \,|\, \hat{\mathcal{H}}_{\mathrm{SO}} \,|\, \psi_i \rangle}{\partial Q_\alpha} \Big|_{\mathbf{Q_0}} \sum_k \langle v_k \,|\, Q_\alpha \,|\, v_a \rangle \, \delta(E_{ia} - E_{fk}) \Bigg) \end{aligned} \tag{19}$$

and a term that stems exclusively from the derivative couplings

$$\begin{aligned} k_{\mathrm{ISC}}^{\mathrm{HT}} = \frac{2\pi}{\hbar} \Re \Bigg(& \sum_\alpha \frac{\partial \langle \psi_f \,|\, \hat{\mathcal{H}}_{\mathrm{SO}} \,|\, \psi_i \rangle}{\partial Q_\alpha} \Big|_{\mathbf{Q_0}} \sum_k \langle v_{fk} \,|\, Q_\alpha \,|\, v_{ia} \rangle \, \delta(E_{ia} - E_{fk}) \\ & \sum_\beta \frac{\partial \langle \psi_f \,|\, \hat{\mathcal{H}}_{\mathrm{SO}} \,|\, \psi_i \rangle}{\partial Q_\beta} \Big|_{\mathbf{Q_0}} \sum_k \langle v_{fk} \,|\, Q_\beta \,|\, v_{ia} \rangle \, \delta(E_{ia} - E_{fk}) \Bigg) \ . \end{aligned} \tag{20}$$

Herein $\Re$ denotes the real part of the expression. Note that SOCMEs may have imaginary phase and that, depending on the relative phase of the coupling terms, the off-diagonal contributions to the rate may be positive or negative.

In principle, individual rates for the non-radiative transition from an initial singlet state to the three fine-structure levels of a triplet state could be determined. This would require to go beyond first-order perturbation theory and to determine the detailed composition of the triplet substates, followed by a diabatisation procedure to determine the individual singlet-

triplet coupling. In practice, the individual ISC rates are added up because the energetic splittings of the fine-structure levels are very small in spatially nondegenerate states. This is equivalent to adding the transition rates determined for the three Cartesian components of $\hat{\mathcal{H}}_{\mathrm{SO}}$. If the initial state is a triplet state, the procedure how to handle the *de facto* degeneracy in the initial state is not so clear cut. If spin relaxation among the triplet sublevels is faster than reverse-ISC (rISC), then each triplet sublevel is statistically populated by one third of the triplet density only and the rate constant for the total rISC will have to be divided by 3 after summation over all possible channels.

To evaluate the rate constants defined in Equations 18-20, different approaches have been pursued to approximate the Dirac δ distributions in these expressions. They can roughly be divided into integration schemes in the energy domain and in the time domain and will be briefly reviewed in the following.

Evaluation of ISC Rates in the Energy Domain

Toniolo and Persico proposed to replace the Dirac δ function in Eq. 9 by a step function of finite width 2η.[172]

$$k_{\mathrm{ISC}} \approx \frac{\pi}{\hbar\eta} \sum_{f \text{ for which } |E_i - E_f| \leq \eta} |V_{fi}|^2 \tag{21}$$

In Condon approximation, the vibrational part of the rate is obtained by explicitly summing over the Franck-Condon factors (FCFs) of the initial state (typically the vibrationally cold state $v_{i\mathbf{0}}$ with zero quanta in all normal modes) with all final states v_{kf} in the interval 2η. Integrals of the type $\langle v_{kf} \,|\, Q_\alpha \,|\, v_{i\mathbf{0}} \rangle$, appearing in Equations 19 and 20, are products of FCFs in all but one normal coordinates and an integral over Q_α which is readily reduced to a sum of FC integrals in harmonic approximation. The authors applied this approach successfully to study the temperature-independent predissociation dynamics in nitrosoalkanes.[173] Later, this scheme has been extensively used by the Marian group to determine rate constants for

El-Sayed forbidden ISC.[51,150,164,174–177]

In practical applications, the interval width 2η has to be chosen with great care. The vibrational density of states (VDOS) grows exponentially with the number of vibrational modes and the adiabatic energetic separation between the initial and final states.[178] For psoralen, an organic compound with 54 normal modes and an S_1-T_1 energy separation of about 7100 cm^{-1}, a VDOS of $\rho \approx 10^{10}$ cm in the triplet state at the energy of the initial state has been estimated,[150] *i.e.* approximately 10^{10} vibrational states are located in an interval of width 1 cm^{-1}. To reduce the computational effort, the interval is typically chosen to be very narrow and the number of coupling modes and the maximum number of quanta allowed in each accepting mode is limited. It has become standard practice to vary these parameters to determine a confidence interval for the computed rate constants.

While integration schemes in the energy domain give detailed insight into which vibrational modes promote the nonradiative transition, they scale very unfavourably with the size of the problem. Pre-screening of the FCFs,[179,180] sum rules[181] and mode selection[150] can be used to alleviate the computational demands and to extend the applicability of this approach. The fundamental difficulties nevertheless persist: With increasing number of normal modes and increasing adiabatic electronic energy difference, the VDOS grows to an extent that the computation of rate constants for nonradiative transitions, even for vibrationally cold molecules and in Condon approximation, becomes prohibitive in the energy domain.

Time-Dependent Methods

A way to avoid the explicit calculation of FC integrals, without resorting to high-temperature limits or estimated values for the VDOS, is to transform Fermi's golden rule into the Heisenberg picture.[130] To this end, the Dirac δ function is expressed as the Fourier integral

$$\delta(E_i - E_f) = \frac{1}{2\pi} \int_{-\infty}^{+\infty} e^{i(E_i - E_f)t/\hbar} dt \tag{22}$$

and substituted into the rate equations. Making use of the properties of conjugation and the resolution of the identity

$$\mathbf{1} = \sum_{k}^{\infty} \mid \psi_f v_{fk} \rangle \langle \psi_f v_{fk} \mid$$

yields

$$k_{\mathrm{ISC}} = \frac{1}{\hbar} \int_{-\infty}^{+\infty} \langle \psi_i v_{ia} \mid \hat{\mathcal{H}}_{\mathrm{SO}}(0) \hat{\mathcal{H}}_{\mathrm{SO}}(t) \mid \psi_i v_{ia} \rangle dt \tag{23}$$

where $\hat{\mathcal{H}}_{\mathrm{SO}}(t) = e^{i\hat{\mathcal{H}}_0 t/\hbar} \hat{\mathcal{H}}_{\mathrm{SO}} e^{-i\hat{\mathcal{H}}_0 t/\hbar}$ is a spin–orbit operator in the Heisenberg picture. Expression 23 is not necessarily limited to the harmonic oscillator model, but the evaluation of the autocorrelation function becomes particularly easy in this case.

Making use of Mehler's formula for Hermite polynomials,[182,183] Etinski *et al.* derived an analytical expression for the generating function $G(t)$ of a vibrationally cold molecule in Condon approximation.[184] The ISC rate constant is then obtained by integrating the time correlation function

$$k_{\mathrm{ISC}} = \frac{1}{\hbar} \left| \langle \psi_f \mid \hat{\mathcal{H}}_{\mathrm{SO}} \mid \psi_i \rangle \right|^2 \int_{-\infty}^{+\infty} G(t) e^{i(E_i - E_f + 0.5\,\mathrm{tr}(\mathbf{\Omega}_i))t/\hbar} dt \ . \tag{24}$$

To speed up the numerical integration, a Gaussian damping function was introduced. Like the interval width 2η in Eq. 21, the width of the damping function is a technical parameter which has to be chosen with care and ought to be varied to make sure that the calculated rate constants are converged. Furthermore, Etinski derived a short-time expression which gives the rate constant in closed form without any need for numerical integration. The time-dependent integration schemes were later extended to include thermal effects[185] as well as vibrational spin–orbit coupling.[151] In parallel, Peng *et al.* derived similar analytical formulae for the nonradiative decay rate between triplet and singlet states using a thermal vibration correlation function approach.[186,187] The resulting formulae are lengthy and the reader is referred to the original literature for the details. In the context of time-dependent correlation function methods for computing ISC rate constants, Reimers' extension to internal coordinates has been implemented recently into a new code by Barone and co-workers.[188]

Technically, the time-dependent approach can even be (and has been) used to determine rate constants for non-radiative transitions between pairs of singlet and triplet states with very large adiabatic energy gap, for example the ISC from the first-excited triplet state to the electronic ground state ($T_1 \rightsquigarrow S_0$).[187,188] It should be kept in mind, however, that the harmonic oscillator approximation underlying the analytic expressions may not be well suited to describe the highly excited vibrational states of S_0 at the energy of the T_1 state.

Summarising, the time-dependent perturbational approaches allow the computation of ISC rate constants for molecules with many vibrational degrees of freedom and substantial singlet-triplet splittings with reasonable computational expense. They are difficult to apply if many electronic states are involved in the nonradiative process simultaneously. As shown in the following, they are easily extended to take account of thermal effects.

Including Temperature

In some cases, such as thermally activated delayed fluorescence (TADF), the singlet-triplet crossing occurs from an adiabatically lower-lying electronic state to a higher-lying one. As nonradiative transitions proceed under energy conservation, these can only be achieved if the initial state is vibrationally excited (Fig. 6), be it thermally or kinetically. Temperature can

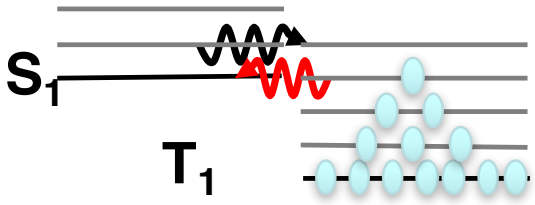

Figure 6: Thermal activation of the T_1 state vibrational levels (schematic) facilitating reverse intersystem crossing

be introduced quite easily in the perturbation theory approaches by assuming a Boltzmann distribution function for the population of the initial vibronic manifold according to

$$p(E_{ia}) = \frac{1}{Z} \exp\left(-E_{ia}/k_B T\right) \tag{25}$$

where $Z = \sum_a^\infty \exp\left(-E_{ia}/k_BT\right)$ is the canonical partition function, k_B is the Boltzmann constant and T is the absolute temperature. In Condon approximation, the rate constant for an incoherent population transfer at temperature T is then given by

$$k_{\mathrm{ISC}}^{\mathrm{FC},T} = \frac{2\pi}{Z\hbar}\left|\langle\psi_f \,|\, \hat{\mathcal{H}}_{\mathrm{SO}} \,|\, \psi_i\rangle\right|^2 \sum_a \sum_k \exp\left(-E_{ia}/k_BT\right) \left|\langle v_{fk} \,|\, v_{ia}\rangle\right|^2 \delta(E_{ia} - E_{fk}) \quad (26)$$

and the derivative coupling terms in Eqs. 19 and 20 are modified accordingly.

Because of the high computational demands caused by the explicit summation over all pairs of vibrational states, inclusion of temperature effects is not feasible in the energy-based integration schemes. In the framework of the time-dependent approaches, formulae for the temprature dependence of rate constants were presented for both, direct and vibrational SOC, by Peng *et al.* [187] and by Etinski *et al.* [151,185]

Quantum Dynamics Methods

As described in the introduction, an alternative approach is to explicitly simulate the excited state dynamics over a manifold of spin-vibronically coupled levels. Here all of the couplings between the excited states considered can be included into the Hamiltonian and therefore this approach can naturally incorporate all types of spin-vibronic interactions. The biggest challenge for these methods, as described below, is to calculate the multi-dimensional PES also the timescales accessible within these simulations are typically limited to few ps domain.

Multi-Configurational Time-Dependent Hartree Approach

Traditionally excited state dynamics have been studied with grid-based quantum dynamics. These methodologies are based upon solving the time-dependent Schrödinger equation (TDSE) for the nuclei, thus taking into account all quantum effects. The simplest way of solving the time-dependent Schödinger equation is to expand the nuclear wavefunction into

a time-independent basis set, with time-dependent coefficients:

$$\Psi(x_1, x_2, ..., x_f, t) = \sum_{j_1=1}^{n_1} ... \sum_{j_f=1}^{n_f} C_{j_1 ... j_f}(t) \prod_{k=1}^{f} \chi_{j_k}^{(k)}(x_k) \tag{27}$$

where χ_j is an orthonormal basis, such as the eigenfunctions of the harmonic oscillator and x_k is the nuclear coordinate. The analogous approach to Equation 27 in electronic structure theory is full configuration interaction (full CI). Consequently, while it rigorously describes the motion of a nuclear wavepacket, like full CI, it suffers from a severe computational expense, scaling exponentially with the number of degrees of freedom. This makes it difficult to describe nuclear dynamics in systems containing more than 5-6 degrees of freedom.

A particularly powerful approach which reduces this problem and which has become extensively used is the Multi-Configurational Time-Dependent Hartree (MCTDH) method.[189] In this approach the nuclear wavefunction *ansatz* takes the form:

$$\Psi(Q_1, ..., Q_f, t) = \sum_{j_1=1}^{n_1} ... \sum_{j_f=1}^{n_f} A_{j_1 ... j_f}(t) \prod_{k=1}^{f} \varphi_{j_k}^{(k)}(Q_k, t) \tag{28}$$

where $Q_1, \cdots, Q_f$ are the nuclear coordinates, $A_{j_1 ... j_f}$ are the MCTDH expansion coefficients and $\varphi_{j_k}^{(k)}$ are the n_k expansion functions for each degree of freedom k known as single particle functions (SPFs).

The *ansatz* for the MCTDH nuclear wavefunction appears rather similar to standard nuclear wavepacket approach (Equation 27), however crucially the basis functions are now time dependent. This means that fewer basis functions are required to converge these variational calculations as they adapt to provide the best possible basis for the description of the evolving wavepacket. In addition, the coordinate for each set of SPFs, Q_k, can be a composite coordinate of one or more system coordinates. Thus the basis functions are d-dimensional, where d is the number of system coordinates within the specific SPF, usually between 1-4. This reduces the effective number of degrees of freedom for the purpose of the simulations.

The memory required by the standard method is proportional to N^f, where N is the number of grid points for each f degree of freedom. In contrast, the memory needed by the MCTDH method scales as:

$$memory = fnN + n^f \tag{29}$$

where the first term is due to the (single-mode) single-particle function (SPF) representation, and the second term the wavefunction coefficient vector A. As $n < N$, often by a factor of five or more, the MCTDH method needs much less memory than the standard method, so allowing larger systems to be treated. Indeed the standard implementation of MCTDH can treat, depending on the exact details of the calculations, $\sim$50 nuclear degrees of freedom.

Importantly, the full strength of the MCTDH class of methods for solving the time-dependent Schrödinger equation is revealed in its so-called Multi-Layer variant (ML-MCTDH),[190,191] which has treated systems containing over 1000 degrees of freedom. The mode combinations contained within each SPF discussed above is a very powerful way of reducing the effective number of degrees of freedom. However past 3-4 combinations, the SPFs become very complicated and unfeasible to propagate. But, it has already been discussed that the MCTDH approach is an efficient approach for propagating complicated wavefunctions. Therefore, in the ML-MCTDH, the complicated SPFs arising from many mode combinations are themselves propagated by the MCTDH equations of motion. It can be seen as using the MCTDH method to propagate the complicated SPFs of an underlying MCTDH simulation. This can in principle be repeated for multiple layers where the biggest challenge is the complexity of the underlying methods. A detailed discussion on all of these aspects, beyond the remit of the present chapter can be found in ref.[192]

Including Temperature

The standard MCTDH wavefunction approach outlined in the previous section, describes the evolution of a particular well-defined initial state, and therefore calculations are effectively performed at 0 K or given some initial, but specific vibrational excitation. However, given the

importance of the thermal energy in some cases, it can be important to explicitly address the temperature of the system. This is most applicable for energetically uphill reaction dynamics. In the case of ultrafast deactivation, it is stressed that even if an experiment is carried out at room temperature, a significant fraction of the initial excitation energy is often rapidly transferred into the vibrational degrees of freedom (vibronic coupling), given that only 0.1 eV is ∼1160 K, the temperature of the nuclei can very quickly exceed room temperature, making the initially temperature of the system a minor perturbation to the dynamics.

In the most rigorous approach, the effect of temperature may be included by adopting a density matrix approach. In density operator form, the 0 K state is expressed:

$$\rho = |\Psi\rangle\langle\Psi| \tag{30}$$

i.e. it is a pure state. However a system at finite temperature is an incoherent mixture of very many thermally excited states, $|\Psi_n\rangle$ and therefore the correct description is in the form of a density matrix:

$$\rho = \sum_n p_n |\Psi_n\rangle\langle\Psi_n| \tag{31}$$

where p_n is a probability, not an amplitude of finding a system in state Ψ_n. So in addition to a probability of finding a particle described by a wavefunction at a specific location, there is now also a probability for being in a different state.[130]

The equation of motion for the density matrix follows naturally from the definition of ρ and the time-dependent Schrödinger equation leading to the well known Liouville-von Neumann equation:

$$i\hbar\frac{\partial\rho}{\partial t} = [H, \rho] \tag{32}$$

This applies to a so called closed quantum system, i.e. the Hamiltonian is not in contact with a dissipative environment. When used to describe an open quantum system, the equation has an additional term used to describe dissipation or population decay, however this was

not considered for the examples discussed below.

In common with the multi-configuration wavefunction expansion used in the MCTDH scheme for wavefunctions, a similar expansion can be used in the case of density operators, in this case expressed:

$$\rho(Q_1,...,Q_f,Q'_1,...,Q'_f,t) = \sum_{j_1=1}^{n_1} ... \sum_{j_f=1}^{n_f} B_{j_1...j_f}(t) \prod_{k=1}^{f} \sigma_{j_k}^{(k)}(Q_k,Q'_k,t) \tag{33}$$

where $B_{j_1...j_f}$ denotes the MCTDH coefficients and σ presents the single-particle density operators (SPDO's) analogous to the single-particle functions of the conventional scheme. The implementation of this approach is described in detailed in refs.[193,194]

It is important to bear in mind that compared to the wavefunction approaches described in the previous section, the numerical treatment of density operators is more difficult since the dimensionality of the system formally doubles.[130] To overcome this, a number of approximate approaches have been proposed which retain the computationally less intensive wavefunction formalism.[195] An example is simply to sample various initial conditions of the vibrational levels for each normal mode according to the Boltzmann distribution.

Spin-Vibronic Model Hamiltonian

MCTDH and its multi-layer variant are able to simulate the dynamics of sizeable molecular systems and therefore, the largest challenge is the description of multidimensional PES. For excited states this is especially challenging owing to the breakdown of the BO approximation and the subsequent presence of nonadiabatic coupling. For quantum dynamics, as described in section , the diabatic picture is the method of choice as it provides smooth PES, that can often be described by a low-order Taylor expansion. However, the output of most quantum chemistry is in the adiabatic basis and so obtaining a diabatic representation is a crucial step.

One approach for obtaining an appropriate PES and the method of choice for all spin-

vibronic studies presented below is the vibronic coupling model.[143] Its extension, the spin-vibronic Hamiltonian matrix ($\mathbf{H}^{SO-vib}$) is expressed as the sum of the non-relativistic vibronic model Hamiltonian matrix ($\mathbf{H}^{vib}$), and the spin–orbit, ($\mathbf{H}^{SO}$) Hamiltonian matrix:

$$\mathbf{H}^{SO-vib} = \mathbf{H}^{vib} + \mathbf{H}^{SO} \tag{34}$$

The $\mathbf{H}^{SO}$ is comprised of the SOC off-diagonal terms, which can either be Q-dependent[154] or independent.[81] These are incorporated in a spin-diabatic manner,[153] which is very convenient as one can use the usual SOC- free quantum chemistry methods and introduce the SOCs only to run the dynamics. It is important to note that rigorously, each triplet state should be described by the three m_s levels (m_s=–1,0,1) and consequently, each triplet state adds an additional three states to the simulation. An approximation to contract the three sub-levels can be made and the SOC be treated as the square root of the sum of the squares of each component. This clearly reduces the computational cost. However, the use of the absolute (real spherical) SOC representation is not straightforward when many singlet and triplet states are coupled and should be rigorously tested, especially if SOC is large.

The multistate vibronic interactions within the spin-free electronic excited states are contained within $\mathbf{H}^{vib}$. The starting point for $\mathbf{H}^{vib}$ is a Taylor series expansion of the PES around a reference nuclear geometry $\mathbf{Q}_0$, usually the FC point using dimensionless (mass-frequency scaled) normal-mode coordinates:

$$\mathbf{H}^{vib} = (T_N + V_0)\mathbf{1} + \mathbf{W}^{(0)} + \mathbf{W}^{(1)} + \ldots \tag{35}$$

Here T_N is the kinetic energy operator and V_0 is the ground state potential. V_0 is not restricted to a particular form but is often defined as harmonic with vibrational frequencies ω_i along dimensionless normal coordinates Q_i. $\mathbf{W}$ describes the multistate vibronic coupling matrix within the spin-free representation.[143] Truncation at first order, as shown here, is referred to the linear vibronic coupling (LVC) model, while truncation at second order is

referred to the quadratic vibronic coupling (QVC) model. Both have been largely used and have provided good agreement with experimental observations. The advantage of the LVC is that it can be relatively straightforward to obtain, but the disadvantage is that it can become inaccurate for larger displacements away from $\mathbf{Q}_0$ when anharmonic effects become more important. The disadvantage of the QVC model, is that the number of expansion coefficients needed to describe the model can become quite numerous and require additional quantum chemistry data.

The zeroth-order coupling matrix contains the adiabatic state energies at $\mathbf{Q}_0$. The adiabatic potential surfaces are equal to the diabatic surfaces at this point, so $\mathbf{W}^{(0)}$ is diagonal and is expressed as,

$$W_{ij}^{(0)} = \sum_{\alpha} \langle \Phi_i(\mathbf{Q}_0) | \hat{\mathcal{H}}_{el} | \Phi_j(\mathbf{Q}_0) \rangle \tag{36}$$

where $\hat{\mathcal{H}}_{el}$ is the standard clamped nucleus electronic Hamiltonian and Φ are the diabatic electronic functions. The first-order linear coupling matrix elements are written:

$$W_{ij}^{(1)} = \sum_{\alpha} \langle \Phi_i(\mathbf{Q}_0) | \frac{\partial \hat{\mathcal{H}}_{el}}{\partial Q_\alpha} | \Phi_j(\mathbf{Q}_0) \rangle Q_\alpha \tag{37}$$

where the on-diagonal and off-diagonal terms are written:

$$W_{ii}^{(1)} = \sum_{\alpha} \kappa_{\alpha}^{(i)} Q_\alpha \tag{38a}$$

$$W_{ij}^{(1)} = \sum_{\alpha} \lambda_{\alpha}^{(i,j)} Q_\alpha \tag{38b}$$

κ and λ are the expansion coefficients corresponding to the on- and off- diagonal matrix elements. The on-diagonal elements are the forces acting within an electronic surface and are responsible for structural changes of excited-state potentials compared to the ground state. They are therefore responsible for the reorganisation energy; they are called tuning modes. The off-diagonal elements are the nonadiabatic couplings responsible for transferring wavepacket population between different excited states; they are called coupling modes.[143]

For the case of the LVC, in the limit of two interacting states, the coupling constants can be obtained from the following expressions[143] evaluated at $\mathbf{Q}_0$.

$$\kappa_\alpha^{(i)} = \left.\frac{\partial V_i}{\partial Q_\alpha}\right|_{\mathbf{Q}_0} \tag{39a}$$

$$\lambda_\alpha^{(i,j)} = \left.\left(\frac{1}{8}\frac{\partial^2}{\partial Q_\alpha^2}(|V_j - V_i|^2)\right)\right|_{\mathbf{Q}_0}^{1/2} \tag{39b}$$

where V_i is the adiabatic PES of the spin-free state i. These show that in this model, only the gradients and the Hessians at Franck-Condon geometry are needed to obtain the model Hamiltonian, meaning that the number of quantum chemistry calculations required is quite small. Second-order terms, $\mathbf{W}^{(2)}$ are expressed in a similar way. The off-diagonal terms at second order are rarely used, however the on-diagonal terms can be very important. The quadratic terms (i.e. $Q_\alpha = Q_\beta$) are responsible for changes in frequency of the excited state potential compared to the ground state, while the bilinear terms (i.e. $Q_\alpha \neq Q_\beta$) are responsible for mixing the normal modes in the excited state, i.e. the so called Duschinsky rotation effect (DRE).[152,196]

For the spin-vibronic model which goes beyond the LVC model, the expansion coefficient of the potential are usually obtained using step wise fitting procedures.[152,196,197] This takes advantage of the fact that while transformations from the adiabatic to the diabatic representation are normally difficult to perform, the opposite way (i.e. diabatic to adiabatic) is relatively simple.[197] Consequently, starting from an initial guess, the diabatic potential can be refined using least squares fit to the computed adiabatic potential by means of standard quantum chemical methods. At each iteration of the fit, the diabatic Hamiltonian is transformed into the adiabatic basis to assess the quality of the fit. This approach is often referred to as *diabatisation by ansatz*. While in the preceding section the diabatisation is basically performed on the spin-free states and the SOC then added, it is possible to go beyond this assumption by including the SOC directly in the construction of diabatic states.[149] A more rigorous and quite involved treatment to include the nuclear coordinate dependence of the

SOC has been proposed by Poluyanov and Domcke,[198] and succesfully applied to several problems[199–203] implying intricate Jahn-Teller and SO effects. Very recently, a related approach was developed by Weike and Eisfeld[204] and applied to the general $a_1 + e$ Jahn-Teller case. Finally, Zeng[148] proposes an extension of the model space diabatisation technique[205] to include SOC. Robust and accurate diabatisation techniques are a cornerstone for quantum dynamical treatment of spin-vibronic problems, and developments will allow for a better theoretical description of ISC.

An important consideration when setting up a model Hamiltonian for large polyatomic molecules is which nuclear degrees of freedom are required in the model to ensure an accurate description of the dynamics of interest. In addition, it is clear that for large systems the number of relevant terms, especially at second order, can rapidly become very large making it challenging to refine all of them. The former can be addressed by identifying important excited state structures, such as energy minima and conical intersections, and expressing them as a function of the normal mode displacements from $\mathbf{Q}_0$[82,83] or using trajectory approaches combined with post-analysis.[206] This helps to clearly identify the modes responsible for significant structural changes in the excited state, but will not necessarily identify nonadiabatic coupling modes as they do not always induce structural changes in the excited states. Here additional help is provided using, if present, molecular symmetry. Indeed, a linear vibronic coupling matrix element will only be non-zero if the direct product of the vibrational mode symmetry Γ_α and the irreducible representations of the states Γ_i and Γ_j contains the totally symmetric representation A:

$$\Gamma_i \otimes \Gamma_j \otimes \Gamma_\alpha \supset A \ . \tag{40}$$

Therefore off diagonal elements (nonadiabatic coupling elements) will only be non-zero if the product of the two state symmetries gives the symmetry of the specific mode. Without symmetry, accurate quantum dynamics are still possible, but the development of the Hamiltonian is more involved.

Finally, it is emphasised that these model Hamiltonians confine nuclear motion within a

reduced number of vibrational modes. It is therefore crucial that the most important modes to the dynamics are identified. Indeed, it is often possible to identify a subset of important vibrational degrees of freedom in any excited state dynamics process. This can usually be achieved using the methods described above. However such models will not capture accurately effects such as vibrational relaxation and intramolecular vibrational redistribution. Therefore simulations longer that a few picoseconds must carefully consider the influence of this effect on the interpretation of the dynamics.

On-the-fly Dynamics Methods

Grid-based quantum dynamics suffer from two limitations: i) Exponential scaling associated with the use of a direct product grid[207] and ii) the requirement to pre-compute the PES meaning that such simulations are limited to only a few degrees of freedoms or models. Motivated primarily by the desire to overcome these limitations, a number of approaches based upon trajectories have been developed. These range from fully quantum approaches, which explicitly address the nuclear motion according to the TDSE[208] to mixed quantum-classical approaches, such as Tully's Trajectory Surface Hopping (TSH).[209,210] The appeal of methods based upon trajectories is that it becomes easier to apply them within a framework of direct dynamics, where the electronic properties of the system are calculated *on-the-fly* at each time step as and when it is required. This removes the need to calculating model PES before the simulations and may allow the system to evolve into the fully unconstrained configurational space. Moreover, these methods can easily be combined with a Quantum Mechanics / Molecular Mechanics (QM/MM) scheme which treats explicitly the solute/solvent interactions.[211]

Trajectory Surface Hopping

One of the most commonly used approaches is Tully's TSH.[210] This approach discretises the nuclear wavepacket into a swarm of independent classical trajectories, which are subsequently

propagated classically according to Newton's equations of motion. The effects of nonadiabatic coupling, forbidden within the framework of classical nuclear mechanics, are included by means of trajectory *hops* between different PES and are controlled by the nonadiabatic couplings within a stochastic algorithm. Convergence of these simulations is achieved by sampling a number of initial conditions and requires many trajectories to be run, usually on the order of 10^3 because of the slow convergence associated with the underlying classical equations of motion. In addition, it is stressed that the classical foundation of TSH means that such simulations will not necessarily converge onto the correct quantum solution.[212] In particular, quantum effects such a tunneling or interferences are not taken into account.

Excited-state dynamics including both nonadiabatic and spin–orbit couplings have a long history within surface hopping.[213] However, as mentioned above the main advantage of these approaches is the ability to calculate the potential and all relevant couplings *on-the-fly* allowing simulations to be performed in full nuclear configuration space. Here the group of González *et al.*[214] has developed an approach of TSH which incorporates spin–orbit and nonadiabatic couplings, using it extensively to study ISC in DNA bases and analogous structures.[64,72,215–218] (see section). Other groups have also used surface hopping in a similar manner either explicitly[65,66] or by post processing the dynamics.[61,206]

Atkins *et al.* recently used TSH including all relevant spin-vibronic couplings, to study the ultrafast dynamics of $[Ru(bpy)_3]^{2+}$ in the gas phase.[219] The authors found ISC within 30 fs (Figure 7), in good agreement with experimental observations[220] and reported that ISC competes with an internal conversion relaxation process within the singlet manifold to the lowest singlet state. They also reported, consistent with the spin-vibronic mechanism, that ISC is not only driven by the high density of states and the large SOC of the system but also by the vibrational motion. However, this was achieved by freezing the vibrational motion. By doing this, the authors are also preventing the structural changes in the triplet state, taking the wavepacket away from the crossing point between the two states. Consequently, this creates an equilibrium between the singlet and triplet states at a fixed geometry, as shown in

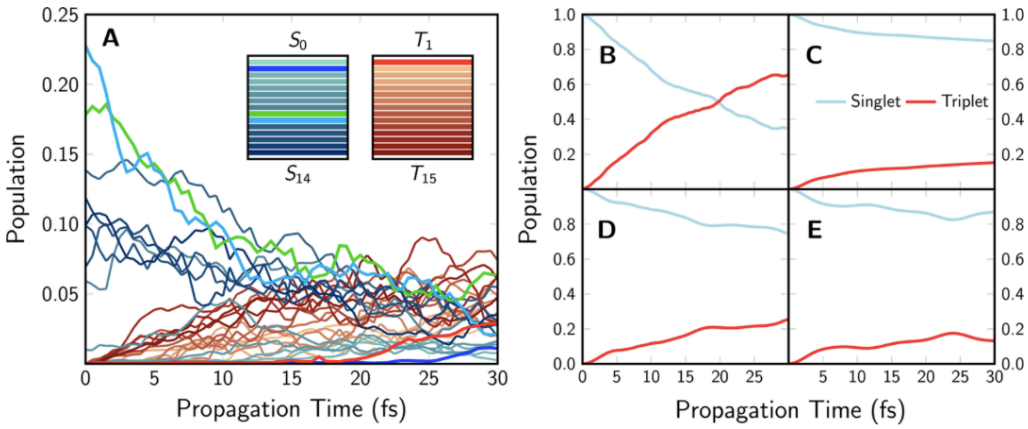

Figure 7: (a) Time-resolved normalized singlet (bluish) and triplet (brownish) populations over 30 fs. For the triplet states, the different ms states are summed as one. Highlighted states are the S1 in blue, the S8 in green, the S9 in light blue, and the T1 in red. (b) Normalised total population of all of the singlets (pale blue) and all of the triplets (red) summed over all of the trajectories. (c) Normalized total population of the singlets and triplets summed over all trajectories when the initial geometries are frozen (case I). (d) Normalized total population of the singlets and triplets summed over all trajectories run from the FC geometry allowing geometrical changes (case II). (e) Normalized total population of the singlets and triplets summed over all trajectories run from the frozen FC geometry (case III). Figure reproduced from ref.[219]

Figure 7. This equilibrium will reflect the mixing, driven by the magnitude of the coupling and size of the energy gap at that geometry. While this does not exclude a spin-vibronic mechanism in $[Ru(bpy)_3]^{2+}$, it does show that identifying refined spin-vibronic effects in transition metal complexes by means of trajectories-based methods remains a challenge because of the high density of excited states. This emphasises the importance of post-processing of *on-the-fly* simulations. Indeed, for complex systems, direct analysis of the results can become quite cumbersome due to high dimensionality, especially in terms of determining the important nuclear motions. Consequently, there is great merit in adopting excited state dynamics based upon model Hamiltonians, which only include the most important nuclear degrees of freedom. Indeed, excited state dynamics, especially at early times, are usually dominated by a subset of full nuclear configuration space.[206]

Methods based upon Gaussian Wavepacket

To overcome the approximations introduced in TSH, a number of groups have developed sophisticated trajectory approaches based upon Gaussian wavepackets (GWP) instead of independent point trajectories. These include multiple spawning,[221,222] coupled-coherent states (CCS),[223] multi-configurational Ehrenfest (MCE),[224] variational multi-configurational Gaussian wavepacket (vMCG)[208,225] and most recently the multiple cloning method.[226] All of these approaches derive from the work of Heller[227,228] and include the delocalised nature of quantum mechanics, while conveniently maintaining the localised trajectory representation of classical mechanics for the mean position of the GWPs. Importantly, the spatially localized nature of the GWP means that it remains possible to perform direct dynamics, during which the potential can be evaluated *on the fly*.

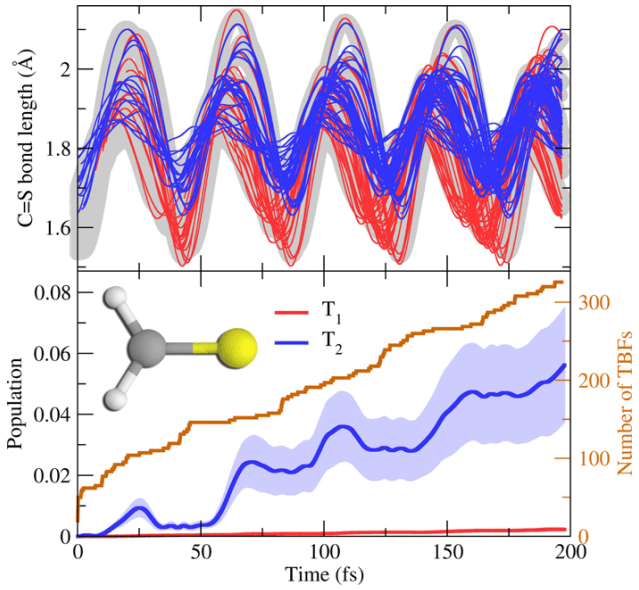

Figure 8: Dynamics of thioformaldehyde after photoexcitation to S_1. Upper panel: C=S bond length for all basis functions. Basis functions are associated with the S_1 (light gray), T_1 (red), or T_2 (blue) electronic state. Lower panel: Population of the two triplet states during the dynamics (light area indicates the standard error). The total number of basis functions is given in orange. Figure reproduced from ref.[155]

Most present implementations of GWP approaches consider only dynamics within states of a single multiplicity, however there is no formal limitation to include SOC. Given the recent

progress made in these areas, many examples can be expected in the near future. Indeed, Curchod *et al.*[155] have recently extended the formalism of the most established approach, *ab initio* multiple spawning to include SOC as well as nonadiabatic couplings and used it to study the excited state dynamics of thioformaldehyde, seen in Figure 8. This showed that after excitation into the first excited electronic state (S_1), ISC occurs principally to the T_2 state. This is consistent with El-Sayed rules, as these states have different character, $n\pi^*$ and $\pi\pi^*$, respectively, while the T_1 state which is barely populated has $n\pi^*$ character. While not discussed within ref.,[155] Figure 8 shows a clear involvement of the C=S bond during ISC, however whether this points to a spin-vibronic contribution to the ISC process or is simply related to dynamics in the T_2 state is unclear.

While the present example has a fairly modest size, this work sets the foundation for these approaches to be applied to larger systems. This is enhanced by the recent developments in quantum chemistry accelerated by graphical processing units (GPUs)[229] which when coupled to *on-the-fly* dynamics can make larger problems more tractable.[230–232]

Excited State Dynamics of Sulfur Dioxide: A Case Study

A number of recent studies have reported upon the ISC dynamics of SO_2, including both spin–orbit and nonadiabatic couplings.[62,71,80] This provides an interesting point of comparison between quantum and trajectory-based dynamics.

Experimental and theoretical interest in the excited state dynamics of SO_2 is due mainly to its fundamental role in atmospheric photochemistry. Two low-lying singlet states, the absorbing one $^1B_1$ and the $^1A_2$ and three triplet states ($^3B_1$, $^3B_2$, $^3A_2$) may contribute to the ultrafast dynamics (< 1 ps) and to the lowest part of the absorption spectrum characterised by three bands in the UV domain, corresponding to one forbidden and two allowed transitions. The vibrational structure of the band observed between 3.8 - 5.1 eV exhibits a complicated vibrational structure hardly deciphered experimentally. Moreover only the $^3B_1$ state has been put in evidence by means of phosphorescence experiments.[233] A pioneering

study based on full-dimensional quantum dynamics and MRCI electronic structure data by Xie et al.[84] including the two lowest singlet ($^1B_1$ and $^1A_2$) and the lowest triplet ($^3B_1$) states has been revisited by Leveque et al.[80] pointing to the importance of the $^3B_2$ state in a complicated mechanism combining conical intersections and SOC (Figure 9). The overall ISC process has been carefully analysed on the basis of the time evolution (0-200 fs) of the populations of the excited states including the individual spin–orbit components of the triplet states showing clearly that a spin-vibronic mechanism is operated as illustrated in (Figure 10).

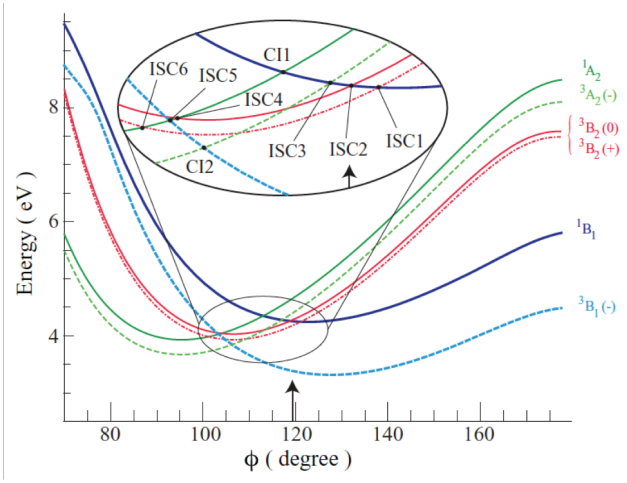

Figure 9: One-D cuts of the A" PES associated to the low-lying singlet and triplet excited states of SO_2 as function of the bending angle ϕ. Figure reproduced with permission from ref.[80]

The mechanism shows short time-scale elementary steps driven either by singlet/triplet crossing (ISC) or singlet/singlet and triplet/triplet conical intersections (CI) and controlled by spin-vibronic coupling. The three triplet states are marginally populated at the early time-scale (< 10 fs) via $^1B_1$ to $^3B_2$ and $^3A_2$ ISC and $^3A_2$ to $^3B_1$ CI. At longer time-scale (> 50 fs) the population of the $^1A_2$ and $^3B_1$ states is assisted by the angular bending mode whereas population of $^3B_2$ increases via $^1A_2$ to $^3B_2$ ISC. Despite modest $^1A_2$ / $^3B_2$ SOC values (a few tens of cm^{-1}) the transfer of population to $^3B_2$ driven by the landscape of the PES and the position of the critical geometries (ISC or CI) is rather efficient. After one ps

the population of the $^3B_1$ and $^3A_2$ states remain marginal whereas the one of the $^3B_2$ state amounts to 25% with an overall population of the two singlet states of 65%.

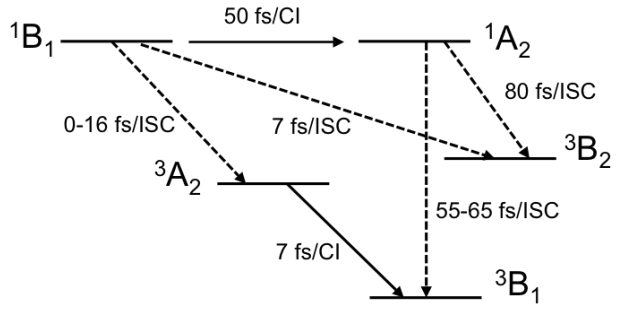

Figure 10: Short time-scale mechanism of singlet to triplet states ISC processes in SO_2 adapted from ref.[80]

Interestingly two recent nonadiabatic molecular surface hopping dynamics based on MR-CIS PESs including arbitrary couplings[62] and on TD-DFT[71] have also been performed. The latter study focuses on the comparison between gas- and liquid-phase dynamics. These two studies based on different electronic structure methods converge to comparable time-scales of the global ISC process, namely about 540 fs[62] and about 250 fs.[71] Both simulations overestimate the population of the triplet states with 50% in the $^3B_2$ state[62] and 60% in the $^3B_1$ state[71] when reaching 1 ps as compared to the simulation based on full-dimensional quantum dynamics, namely 25% when the three triplets are included[80] and 30% when $^3B_2$ is excluded.[84] Other discrepancies between time scales and excited-state populations deduced from quantum dynamics and trajectory approaches cannot be rigorously analysed, mainly because *on-the-fly* dynamics are interpreted in terms of adiabatic states. However, as pointed out by Köppel *et al.* [80] and put in evidence in SO_2, strong interference effects between different singlet to triplet coupling channels, not taken into account in surface hopping trajectories, play a central role in the population transfers.

To the best of our knowledge SO_2 is the only system for which full-dimensional quantum dynamics and non-adiabatic molecular dynamics, both including SOC applied to two singlets and three triplets have been performed. Further sophisticated experiments are certainly

needed to validate the theoretical findings and to understand the photochemistry of this simple triatomic but complex molecule.

Experimental Observation of Spin-Vibronic Dynamics

From an experimental perspective, directly observing spin-vibronic dynamics calls for techniques that provide sensitivity to the spin and electronic states and vibrational motion of the system under study. Achieving such simultaneous detail within one technique is challenging and consequently a combination of approaches, usually supplemented with theory, is often used. In the following subsections, information about spin-vibronic dynamics obtained using different spectroscopic techniques is discussed.

Transient Optical Absorption and Time-resolved Fluorescence Spectroscopy

Two of the most commonly used techniques to resolve excited state dynamics are transient optical absorption spectroscopy and time-resolved emission (fluorescence or phosphorescence) spectroscopy. For the former, the pump pulse excites the sample into an excited state, while the probe pulse measures the change in absorption as a function of time. Transient absorption spectra track the excited-state dynamics through a number of dominant spectral features including i) the ground-state bleach, i.e. a loss of signal at the ground-state absorption due to a fraction of the sample becoming promoted into the excited state, ii) stimulated emission originating from the probe pulse driving the excited-state population back to the ground state and iii) excited-state absorption (ESA), arising from the absorption of excited-state species promoting them to higher-lying excited states. It is important to stress that for ESA the final states are not often known and even for relatively simple molecules can result in broad and unresolved bands. An alternative approach, which avoids these overlapping bands, is time-resolved emission spectroscopy, which detects the light emitted as a function

of time after the pump pulse. This has the advantage of not involving higher lying unknown excited states. It is therefore in principle simpler than transient absorption but is limited to bright states, i.e. those that give out light.

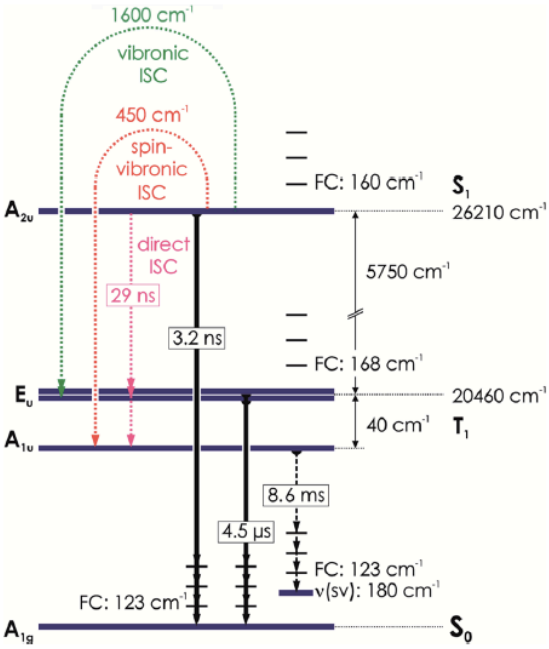

Figure 11: Energy level diagram and relaxation mechanisms of the lowest states of Pt(POP-BF_2). Figure reproduced from ref.[234]

One of the clearest examples of spin-vibronic dynamics is the binuclear d^8-d^8 molecular complexes of platinum bridged by various ligands, which have been extensively studied due to their interesting photochemical and photophysical properties arising from the lowest singlet and triplet $^{1,3}A_{2u}$ excited states (Figure 12).[234–242] In particular the room temperature ISC of $[Pt_2(P_2O_5H_2)_4]^{4-}$ (PtPOP)[235,238] and $[Pt_2(P_2O_5(BF_2))_4]^{4-}$ (PtPOP-BF_2)[242] occur on the timescale of 10s to 100s of picoseconds, remarkably slow for transition metal complexes. They also exhibit a strong solvent dependence.[238,242]

To investigate this for PtPOP-BF_2, Hofbeck *et al.*[234] used emission (fluorescence and phosphorescence) spectroscopy over a range of temperatures. Direct ISC, via SOC alone is forbidden due to the symmetry of the state involved ($^{1,3}A_{2u}$)[243] and the poor Franck-Condon overlap associated with two nested potentials which are separated by >0.5 eV. The authors

reported that when adopting a classical Arrhenius analysis, the temperature dependent data could only be fit with two channels, in agreement with the proposal of ref.[244] At room temperature the authors concluded that ISC was driven by two different thermally activated pathways which are promoted by spin-vibronic and vibronic mechanisms, respectively, hence thermal activation energies of 450 cm^{-1} and 1600 cm^{-1} (Figure 11) are required to initiate the spin-vibronic ISC mechanism.

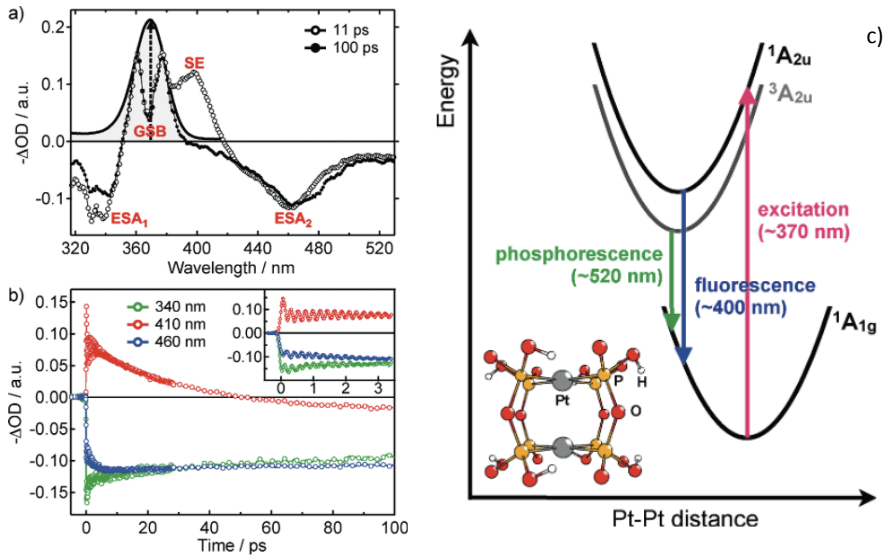

Figure 12: (a) Representative transient absorption spectra of PtPOP at 11 (open circles) and 100 ps (closed circles) after excitation at 370 nm into the $^1A_{2u}$ absorption band (dashed vertical arrow), together with a static absorption spectrum (black curve). (b) Time traces at fixed wavelengths. The upper-right inset zooms into the initial 3.5 ps time window, showing the wavepacket dynamics of the Pt-Pt stretch. (c) Simplified potential energy scheme of the ground state and $^{1,3}A_{2u}$ lowest-excited states of PtPOP. Figure reproduced from ref.[238]

Ultrafast transient absorption and fluorescence spectroscopies of PtPOP[238] and PtPOP-BF_2[242] identified clear signatures of excited state wavepacket dynamics assigned to the Pt-Pt stretching vibration. This is associated with the contraction of the Pt-Pt bond[237,245] in the excited state (Figure 12), caused by excitation of an electron from the antibonding $d\sigma^*$ orbital (d_z^2-derived, z-axis along Pt-Pt) into the bonding $p\sigma$ orbital (p_z-derived). However, with a frequency of $\sim$150 cm^{-1} and symmetry-based consideration, this mode cannot promote the spin-vibronic mechanism. Indeed, this mode, which dominates the spectral signature and the

vibrational dynamics in the excited state, can be classed as a *tuning mode*. Such modes are responsible for the change of frequency between the ground and excited states and therefore are responsible for the largest structural distortions. However, they do not necessarily contain the coupling responsible for the spin-vibronic mechanism. Importantly, the *coupling modes* need not show any significant displacement between the ground and excited state minima and will therefore not drive strong nuclear motion making them hard to observe using transient optical absorption and time-resolved fluorescence spectroscopies. Although these modes do not drive strong nuclear relaxation, they can induce sizeable nonadiabatic interstate coupling. Finally, in the context of the d^8-d^8 molecular complexes of platinum, the strong solvent effect on the rate of ISC means that one should also consider the role of a solvent coordinate alongside any potential coupling modes.[238,242]

Time-resolved Vibrational Spectroscopy

Despite the detailed information that can be extracted from optical pump-probe techniques, the broad, unresolved and overlapping bands often observed can make extracting the vibrational dynamics besides a couple of dominant tuning modes challenging. In contrast, time-resolved vibrational spectroscopy including time-resolved infrared[246,247] and transient 2-dimensional infra-red (2D-IR),[248,249] offer appealing alternatives because they can directly track the activated normal modes during the excited-state dynamics. Indeed, because of the narrow vibrational bands and their sensitivity to electronic and geometric structure, very fine changes, on the orders of hundredths of an Ångström, can be determined.

Recently, nonlinear Raman spectroscopies such as femtosecond stimulated Raman scattering (FSRS),[250–252] have provided new opportunities for ultrafast vibrational spectroscopy, circumnavigating Heisenberg's uncertainty principle by including a second probe pulse. After the initial pump pulse, the probing is performed by the simultaneous interaction of a narrow-bandwidth picosecond Raman pulse and a broadband, femtosecond continuum probe pulse, which disentangles the time and energy resolution.[253] Similar information can be achieved

by converting this frequency-domain approach into a time-domain ones, such as Broadband Impulsive Vibrational Spectroscopy (BB-IVS).[254] The principle motivation for time-domain implementations of vibrational spectroscopy is the ability to record the entire spectrum of molecular vibrations, but also simultaneously achieving higher spectral and temporal resolution than would be possible spontaneous by Raman scattering alone.

FSRS has been used to study the ultrafast ISC dynamics of an Fe(II) spin crossover system[255] and the nature of ISC in $[Ru(bpy)_3]^{2+}$.[256] Indeed, before the development of FSRS, it was not possible to probe ISC processes on this time-scale with vibrational spectroscopy because of its ultrafast nature and the problems associated with Heisenberg's uncertainty principle. From ref.,[256] the authors concluded, consistent with other experiments,[257] that ISC occurs within $\sim$ 100 fs and were able to identify key modes during the dynamics, such as C=C stretching modes, and assigned solvent-mediated ISC process consistent with TSH simulations.[61] However it is not clear whether ISC is dominated by the rate of solvation, spin conversion or vibrational relaxation in the triplet metal-to-ligand-charge-transfer (^{3}MLCT) state or a convolution of all three since they are expected to occur on similar time scales. Consequently, at present direct evidence of spin-vibronic coupling using these approaches has not been reported, although they have been used to elucidate the important modes in nonadiabatic dynamics, such as the singlet fission mechanism[258] or the photoisomerisaiton of retinal in channel rhodopsin[259] and therefore there is no technical barrier to understanding the spin-vibronic mechanisms.

Besides probing spin-vibronic dynamics, the ability of IR radiation to directly excite vibrational modes means that once vibrational roles are understood they can in principle be manipulated. Weinstein and co-workers have recently used an infrared pulse between the pump and probe pulses to control electron transfer.[260–262] Based on this knowledge and understanding of the vibronic pathways, the possibility of achieving similar control by chemical design opens new research directions for the future.

Multidimensional Electronic Spectroscopy

Linear spectroscopy is inherently one-dimensional, and provides an absorption spectrum as a function of excitation energy. As mentioned above, one of the limitations of optical transient absorption spectroscopy is the number of overlapping bands as systems become more complicated. Taking a cue from the correlation between spins routinely used in NMR, multidimensional infrared and optical spectroscopies are becoming increasingly common.[263–265] The former provides information about the coupling between vibrational degrees of freedom whereas 2D electronic spectroscopy is able to reveal couplings between electronic degrees of freedom.[266]

Recently, Carberry *et al.*[267] used 2-dimensional electronic spectroscopy (2D-ES) to probe the excited state decay of $[IrBr_6]^{2-}$ and measured the couplings between all of the ligand to metal charge transfer (LMCT) states. Indeed, Figure 13, shows the magnitude 2D spectrum, 6 ps after excitation. It exhibits a number of off-diagonal peaks, as predicted by mapping the linear absorption transitions onto the excitation and emission axes (dashed horizontal and vertical lines) and is consistent with 6 spin-orbit coupled LMCT states. Exploiting the dynamics of the off-diagonal elements, the authors were able to show that vibronic contributions, measurable for dynamics on surfaces of a single multiplicity,[268] play very little role in this case, and that the dominant source of coupling is SOC. Although this is not unexpected, given the elements involved, it does outline the potential for resolving spin-vibronic dynamics and potentially disentangling the two components within the approach.

2D-ES has also been used to probe singlet fission[269] and reveals the crucial role of vibrational degrees of freedom in this conversion from singlet to triplet states. However, it is stressed that in singlet fission, the two generated spin-triplet excitons are initially correlated to form an overall spin-singlet state. This spin-allowed process differs from the spin-vibronic mechanism discussed here within the context of ISC.

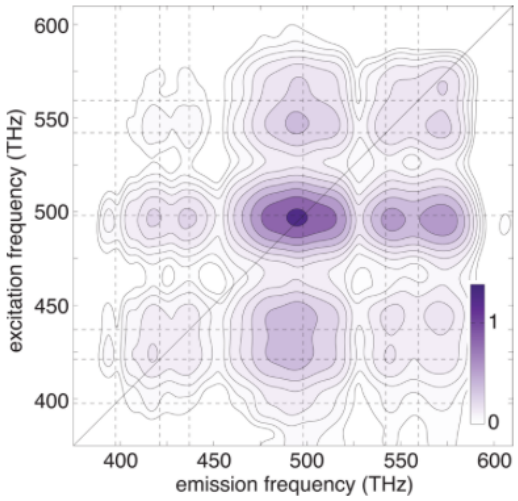

Figure 13: The magnitude of the 2D spectrum 6 ps after excitation. The off-diagonal peaks among all six LMCT transitions are induced by SOC. Figure reproduced from ref.[267]

Time-resolved X-ray Spectroscopy

The desire to resolve structural dynamics in excited-state deactivation mechanisms, which is important in the context of spin-vibronic dynamics, has led to a significant research effort that aimed at exploiting short wavelength probe pulses. This has led to the development of time-resolved diffraction methods using X-rays[270–272] or electrons[273,274] and core level spectroscopies using either X-rays[275–278] or electrons.[279,280] Among these, X-ray spectroscopy is particularly appealing owing to its ability to deliver geometric, electronic and spin state information about the system under study.

For the implementation of time-resolved X-ray spectroscopy, third generation light sources (i.e. storage rings that generate synchrotron radiation) are most suited because of their wide tunability, stability and high photon flux. However, the physics of storage rings limits the X-ray pulse duration to 50-100 ps, making direct observation of vibrational motion in real time challenging. This limitation has been overcome by the laser-electron slicing scheme[281–284] and the so-called *low-alpha* modes,[285,286] albeit at the sacrifice of beam intensity, making experiments very challenging. Recent advances in technological developments, such as X-ray Free Electron Lasers (X-FELs) and High Harmonic Generation (HHG),[287,288] has led

to a paradigm shift in the capability of X-ray Spectroscopy to deliver simultaneously high temporal and spectral resolution on an extremely broad range of samples in a wide array of different environments.[275,278] Recently X-FELs have been exploited by Zhang *et al.*[27] and Lemke *et al.*[29] who used X-ray emission and absorption, respectively, to probe the evolution of the spin-state of $[Fe(bpy)_3]^{2+}$ during light-induced spin crossover dynamics, identifying an intermediate triplet state, discussed in more detail below.

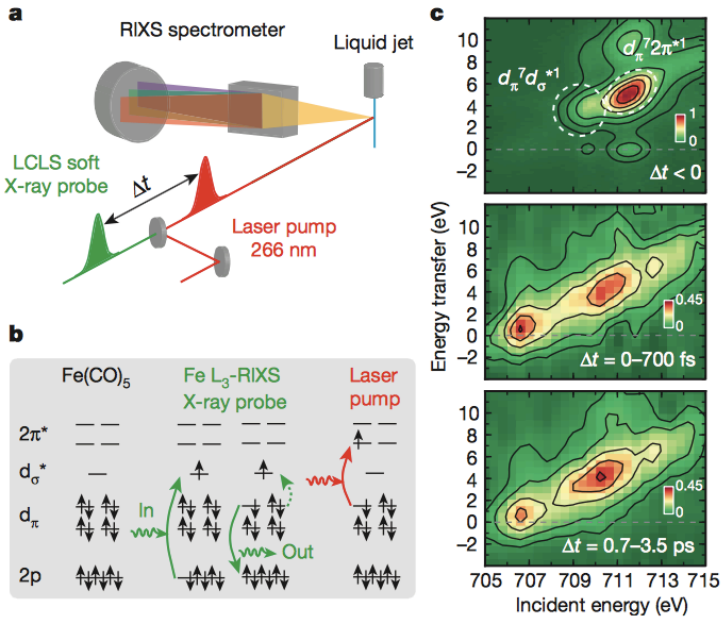

Figure 14: Scheme with optical-laser pump and soft X-ray probe after the pump-probe time delay Δt. The intensity of RIXS is measured at the Fe L_3-absorption edge with a dispersive grating spectrometer. b) Electron configuration of ground-state $Fe(CO)_5$ with single- electron transitions of X-ray probe and laser-pump processes (orbital assignments according to Fe 2p and 3d or ligand 2p character and according to symmetry along the Fe-CO bonds; the asterisk marks antibonding orbitals). RIXS at the Fe L_3-absorption edge with $2p \rightarrow d^*_\sigma$ excitation involves scattering to final $d^7_\pi d^*_\sigma$ ligand-field excited states. Optical $d_\pi \rightarrow 2\pi^*$ excitation triggers dissociation. c) Measured Fe L_3-RIXS intensities (encoded in colour) versus energy transfer and incident photon energy. Top: ground-state $Fe(CO)_5$ (negative delays, probe before pump). Middle and bottom: difference intensities for delay intervals of 0-700 fs and 0.7-3.5 ps, respectively, isolating transients by subtracting scaled intensities of unpumped $Fe(CO)_5$ from the measured intensities. Figure reproduced from ref.[289]

In terms of future perspectives for time-resolved X-ray Spectroscopy in the context of

spin-vibronic dynamics, it is noted that the X-ray flux of X-FELs is typically 10-11 orders of magnitude higher than the slicing source at 3^{rd} generation light sources. This is offering new opportunities in photon-greedy second-order X-ray spectroscopies, such as resonant X-ray emission spectroscopy (RXES), also referred to as resonant inelastic X-ray scattering (RIXS)[290–292] to be performed with femtosecond resolution. RXES, displays its spectral information in 2 dimensions (Figure 14), absorption and emission energy, which separate overlapping bands and can provide more dynamical insight. By measuring pump-probe RXES signal, sensitivity of the spin and electronic states and vibrational motion of the system under study could be achieved in a synergistic way. This represents an exciting route towards unravelling new insights into spin-vibronic dynamics.[293,294]

Recently, Wernet *et al.*[289] used time-resolved RIXS to probe the ligand exchange dynamics of $Fe(CO)_5$ in solution and in particular the role of states of different spin-multiplicity. Figure 14 shows a scheme of the experimental set and the measured spectra. The authors were able to observe that after photo-excitation, $Fe(CO)_4$ is formed in an excited singlet state that undergoes ISC to the triplet ground state or combines with a CO or solvent molecule to regenerate a penta-coordinated Fe species on a sub-picosecond timescale. While this present study does not offer direct relevance in the context of the spin-vibronic mechanism, it illustrates the power of time-resolved RIXS and motivates future studies in the area.

Spin-Vibronic Intersystem Crossing in Transition Metal Complexes

Owing to their strong absorption in the UV-visible region of the spectrum and long-lived excited states, transition metal complexes have become a central component for a variety of applications, such as photocatalysts,[295] dye-sensitised solar cells (DSSCs)[296,297] and organic light emitting diodes (OLEDs).[298] The rich electronic flexibility associated with their ability to bind various ligands and to link polymers, wires, proteins and DNA open the route to

a number of functions, such as luminescent or conformational probes,[299,300] diagnostic or therapeutic tools,[301–303] photoswitches[304,305] and long-range electron transfer trigger.[306,307] Their extensive use for photophysical, photochemical and photobiological applications has provided a strong driving force for a large research effort directed to their fundamental photophysics[308–311] in order to control these functions or elucidate rational material design.

This work has strongly highlighted the complexity of the dynamics that occurs on the ultrafast timescales,[25] but also the breakdown of long held expectations. Indeed, the concepts of IC, driven by vibronic coupling and ISC, controlled by SOC, become rather artificial in the case of polyatomic molecules characterised by a high density of electronic excited states. Within the basis of spin–orbit and vibronically-coupled BO states, a realistic picture is provided by a spin-vibronic mechanism as illustrated by recent work reported in the proceeding subsections.

Jahn-Teller and Spin-Orbit Coupling Effects in Transition-Metal Trifluorides

One of the most well studied results of vibronic coupling is the Jahn-Teller effect. The interplay between Jahn-Teller (JT) and SOC effects has been explored in high-spin doubly-degenerate electronic states of first-row transition metal trifluorides, the vibronic spectra of which have been computed from first principles.[85,312] Whereas JT vibronic coupling is quenched by strong SOC effects in vibronic spectra of electronic states of even number multiplicities, the vibronic structure is conserved in the spectra of states characterised by odd number multiplicities. This has been demonstrated for MnF_3 in its $^5E'$ ground state and $^5E''$ excited state, for CoF_3 in its $^5E'$ and $^5E''$ excited states, for NiF_3 in its $^4E'$ excited state and for CoF_3 in its $^5E'$ and $^5E''$ excited states. These systems are particularly instructive because they show limiting cases of strong JT/ weak SOC, weak JT/weak SOC and strong JT/ strong SOC (Table 1) that affect differently either the vibronic fluorescence spectra (MnF_3 and CoF_3) or the internal vibronic infrared spectra (MnF_3 and NiF_3). These systems

have been studied considering SOC together with vibrational strongly JT active normal modes including linear and up-to sixth order JT couplings, JT stretching normal modes including up-to fourth order JT couplings within a two-state four-mode model in the case of fluorescence spectroscopy.

Table 1: JT and Spin-Orbit coupling terms of MnF_3, CoF_3 and NiF_3 in low-lying high-spin states together with the normal mode frequencies (in cm^{-1}) from Ref.[85,312]

	MnF_3	MnF_3	NiF_3	CoF_3	CoF_3
	$^5E'$	$^5E''$	$^4E'$	$^5E'$	$^5E''$
Linear JT	764	311	548	548	264
Quadratic JT	40	-17	26	28	-12
Spin-Orbit	145	82	234	293	155
Bending	176	176	198	184	193
Stretching	769	824	-	780	799

The experimental assignment of the refined spin-vibronic spectra in these high-spin states systems is still a challenge and quantum dynamics based on accurate electronic structure data (here from CASSCF calculations)[85,312] help at pointing to the combined JT/SOC effects on the adiabatic PES and consequently on the spectral characteristics. A strong JT effect as in MnF_3 or CoF_3 in their ($^5E'$) state will give rise to different characteristics depending on the SOC as illustrated in Figure 15. In the case of MnF_3 (Figure 15 left) the SO splitting is completely quenched by the strong JT effect and the weak SOC leads to an increase in density together with an enhancement of the double-hump shape of the spectrum as compared to the spectrum without SOC. Because of the stronger SOC effect in CoF_3 (Figure 15 right) a significant difference is observed in terms of shape and structure between the spectra simulated without and with SOC.

NiF_3 in its $^4E'$ excited state is characterized by strong JT and spin–orbit couplings (Table 1). Interestingly and as illustrated by the internal infrared spectra computed without and with SOC, the strong original non-adiabatic effects (Figure 16) are dramatically reduced by SOC and the structure of the spectrum becomes much more simple.

Strictly speaking these pioneering studies are not related to ISC processes because they

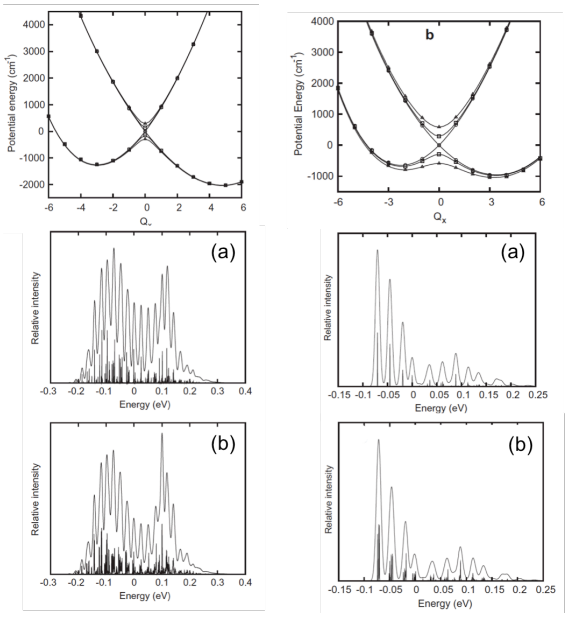

Figure 15: Potential energy curves of the ${}^5E'$ states of MnF_3 (top left) and CoF_3 (top right) along the bending normal mode with SOC and associated vibronic fluorescence spectra, without (a) and with (b) SOC with the permission of ref.[312]

focussed on isolated doubly degenerate electronic states ignoring the pseudo-JT (PJT) couplings between states of different multiplicities. However the tools developed in this context are ready for investigating more complex situations including other states of different multiplicities, degenerate or not, not only for recording high-resolved electronic spectra but also for mechanistic investigations. The mutual quenching of the two effects, namely JT and SOC, via a spin-vibronic mechanism has been observed in a number of cases (M=Cr, Ni) as well as the predominance of the role of the degenerate bending mode. Of course, an analysis of this complexity needs theoretical simulations based on QD.

Fe(II) Complexes

Fe(II) is a system with six d-electrons and, consequently, Fe(II) complexes exhibit either a high spin ${}^5T_2$ ground state in a weak ligand field or a low spin ${}^1A_1$ ground state in a strong ligand field. A transition between the two configurations, thereby controlling the magnetic properties of the complex, can be achieved by changes in temperature or by light. The latter

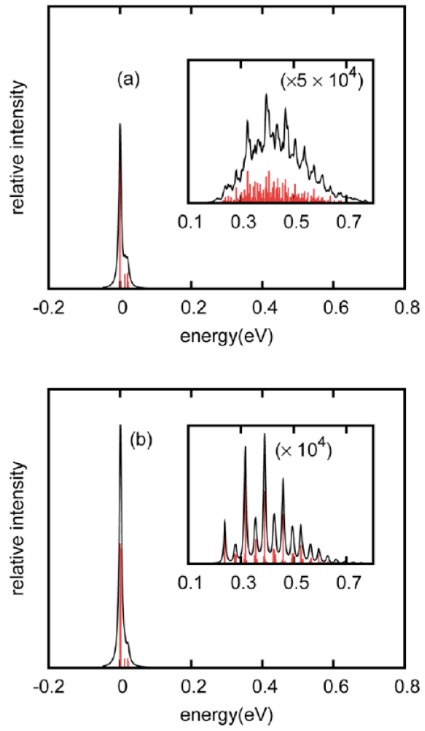

Figure 16: Internal infrared vibronic spectrum of NiF_3 in its $^4E'$ excited state without (a) and with (b) SOC at T = 0K. Reproduced from Ref.[85]

is usually referred to as light-induced excited spin-state trapping (LIESST).[313–316]

The high density of electronically excited states in many Fe(II) complexes, which derives from the simultaneous presence of metal-to-ligand charge transfer (MLCT) and metal-centered (MC) states means that the excited-state dynamics of LIESST are usually extremely rich and ultrafast. Consequently, this process has received significant attention,[14,317–321] a lot of which has been focused upon the prototypical LIESST complex, Iron(II)-tris-bipyridine ($[Fe(bpy)_3]^{2+}$),[284,322? –324] shown in Figure 17. These studies have shown that after optical excitation into the ^{1}MLCT band, $[Fe(bpy)_3]^{2+}$relaxes into the non-emissive quintet MC ($^5T_2$) state, therefore undergoing two spin forbidden transitions, within 200 fs,[30–32] Figure 17. This decay is significantly faster than the usual time scales expected for a single ISC event, let alone two (singlet→quintet), and consequently direct observation of the intermediate states and description of the full mechanism was a significant challenge.

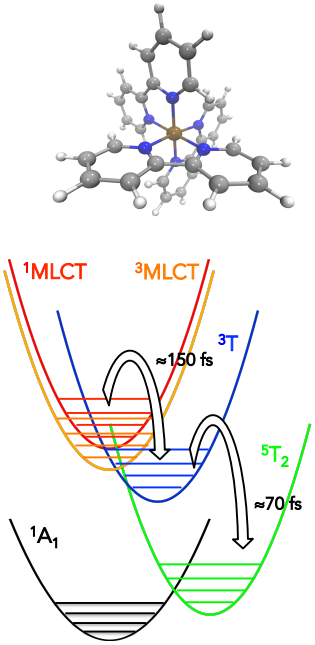

Figure 17: Schematic of the potential energy surfaces, proposed decay pathways, and time scales involved in the excited-state deactivation of $[Fe(bpy)_3]^{2+}$. Figure reproduced from ref.[78]

Using the time-dependent perturbation approach outlined in section , Sousa *et al.*[325] characterise the excited-state decay mechanism including all possible intermediate electronic states along the decay pathway. Given the high density of excited states and strong coupling, it can be argued because the coupling between excited states is likely to be much greater than the energy gap between them, that perturbation theory is not strictly valid. However, the calculations gave a total deactivation time in good agreement with the experimentally determined rate and indicate that the complex can reach the final high-spin state by different deactivation channels, both of which include intermediate MC triplet states (^{3}MC) and require spin-vibronic interactions.

These mechanisms were later used to explain the femtosecond X-ray emission study of Zhang *et al.*[27] The authors reported that at 50 fs after photoexctiation, the transient XES spectrum, which is particularly sensitive to the spin state of the absorbing iron atom,[275,278] could only be described invoking the intermediate ^{3}MC. This conclusion was subsequently

challenged by Aubock *et al.*[28] who used pump-probe optical transient absorption spectroscopy to argue that the quintet state is impulsively populated in < 50 fs, the same time measured for the depopulation of the MLCT manifold. The authors did not exclude the contribution of an intermediate triplet state, but claimed its lifetime must be <20 fs. Most recently, Lemke *et al.*[29] used ultrafast X-ray absorption spectroscopy reporting that the transient spectra were consistent with the short-lived ^{3}MC state which is populated within 50 fs and decays within 120 fs (Figure 18), similar to the conclusion of Zhang *et al.*[27] They were also able to probe not only the position, but the width of the wavepacket as predicted in ref.[293]

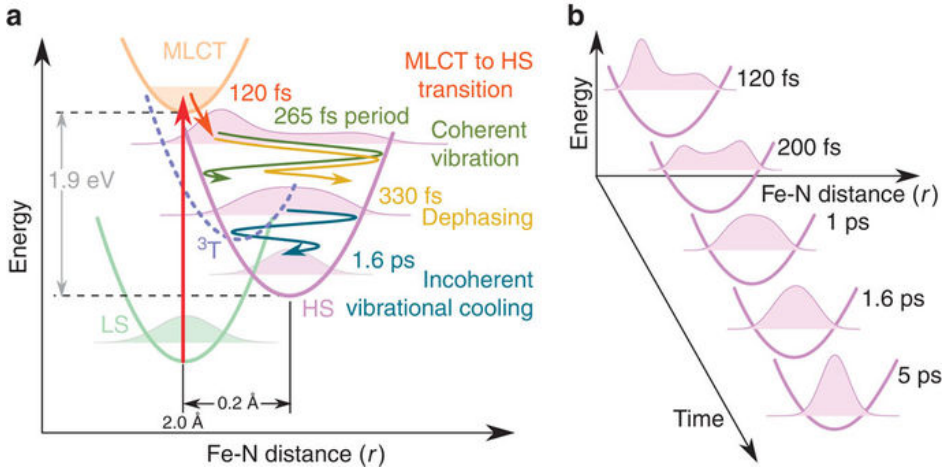

Figure 18: Schematic representation of the structural trapping during the light-induced spin-state conversion in $[Fe(bpy)_3]^{2+}$ from LS to HS state along the Fe-N distance reaction coordinate. The photoexcited MLCT (manifold) decays, through the ^{3}T state ($t_{2g}^5 e_g^1 L^0$), towards the HS state within (120(10) fs) and a large fraction of energy is dissipated. It expands and coherently oscillates (breathing mode, 265?fs period) around the HS equilibrium structure while losing energy. The wave packet disperses at 330?fs time constant and vibrationally cools inside the HS state potential within 1.6?ps. (b) Schematic time evolution of the wave packet in the HS potential based on the simulated distribution model. Figure reproduced from ref.[29]

While the conclusions from these recent experimental works are slightly different, the most important point in the context of the present review is that all of these results illustrate that the deactivation process is significantly non-BO involving presence of spin–orbit and nonadiabatic coupling, which in the presence of a high density of electronically excited states

leads to a heavily mixed spin-vibronic manifold of excited states.[255] Indeed, this relaxation process is one of the most stark examples of strongly inter-winded spin, electronic and structural dynamics occurring in a molecular system.

The spin-crossover phenomenon makes Fe(II) complexes very appealing for single-molecule magnets, but the photoexcited decay route makes $[Fe(bpy)_3]^{2+}$and related complexes unsuitable for applications seeking to exploit the MLCT properties, as the MC states transfer the photoexcited electrons away from outer ligand-based regions of the complex, preventing charge transfer and/or injection.[326] Recently, motivated by the desire to achieve photosensitisers using earth abundant elements,[297] there have been many attempts to destabilise the MC states to achieve longer-lived MLCT states. Liu *et al.*[327] demonstrated this by exploiting strongly σ-donating N-heterocyclic carbene ligands to create $[Fe(bmip)_2]^{2+}$(bmip=2,6-bis(3-methyl-imidazole-1-ylidine)pyridine). Using ultrafast transient absorption, the authors reported a ^{1}MLCT-^{3}MLCT conversion of $\sim$100 fs, no population of a high spin $^5T_2$ state and a ^{3}MLCT lifetime of $\sim$9 ps, which is $\sim$100 times longer than the MLCT lifetimes of other Fe(II) complexes. Harlang *et al.*[328] then exploited this long ^{3}MLCT lifetime to implement $[Fe(bmip)_2]^{2+}$as a photosensitiser attached to titanium dioxide, reporting photoelectrons in the conduction band of titanium dioxide generated by injection from the ^{3}MLCT state of $[Fe(bmip)_2]^{2+}$with quantum yield of 92%. However, unfortunately, >85% of the injected electrons at the $[Fe(bmip)_2]^{2+}$-TiO_2 interface undergo fast (<10 ns) electron-cation recombination. Papai *et al.* used quantum wavepacket dynamics simulations to understand the photoexcited decay mechanism of $[Fe(bmip)_2]^{2+}$[78] and a tert-butyl substituent analogue.[79] These simulations, which provide good agreement with the experimental decay timescales, rationalise the strong differences between the dynamics of these two complexes and highlight the interplay between the spin and nonadiabatic (spin-vibronic) coupling which influences the rate of decay from the MLCT to the MC states. However, the most important factor in the development of these complexes is the relative energetic position of the ^{1,3}MC and MLCT states, especially close to the FC geometry, which largely determines the lifetime of

the MLCT states.

Cu(I) Complexes

For potential applications in OLEDs,[329–331] and light emitting electrochemical cells (LEECs),[332,333] or as chemo- and biosensors,[334,335] it is widely acknowledged that complexes containing 2^{nd} and 3^{rd} row transition metal ions presently form the most stable and versatile emitters. However, these metals are unappealing for commercial applications due to their high cost and low abundance. Consequently, one of the most attractive methods is to simply remove the metal centred states by adopting a complex based upon d^{10} metal ions, such as Cu(I), Ag(I), Au(I), Zn(II) and Cd(II).[336] Among the most popular are those containing Cu(I) ions.[337]

Amongst the most extensively studied is Cu(I) complexed with phenanthroline ligands (see ref.[338] and references therein) because they have many photophyscial properties which are similar to the ruthenium polypyridines.[157,339–342] One of the first time-resolved spectroscopic studies of $[Cu(dmp)_2]^+$ was performed by Chen *et al*,[343] who used time-resolved absorption spectroscopy to probe the dynamics following photoexcitation of the optically bright S_3 state.[344] They reported two principal dynamical processes occurring in 500-700 fs and 10-20 ps. Based upon the ultrafast ISC occurring in $[Ru(bpy)_3]^{2+}$,[257] they assigned the first to ultrafast ISC and the second to the structural relaxation. At the same time Nozaki and co-workers[156] reported that the 10-20 ps relaxation was due to ISC, which is relatively slow in $[Cu(dmp)_2]^+$ due to a strong effect of the structural rearrangements on the magnitude of the SOC matrix elements. Indeed, at the FC geometry the coupling between S_1 and T_1 was estimated to be $\sim$300 cm^{-1}, but at the distorted excited-state geometry, expected to be most important on the timescale of tens of picosecond, it is only $\sim$30 cm^{-1} (See Figure 2).

Later, Tahara and co-workers[346] probed the excited state dynamics using femtosecond fluorescence up-conversion. Following photoexcitation at 420 nm they found three principal time-components. An initial strong fluorescence, which decayed with a time constant of $\sim$45 fs, was attributed to the decay of the initially populated excited state via IC. This was

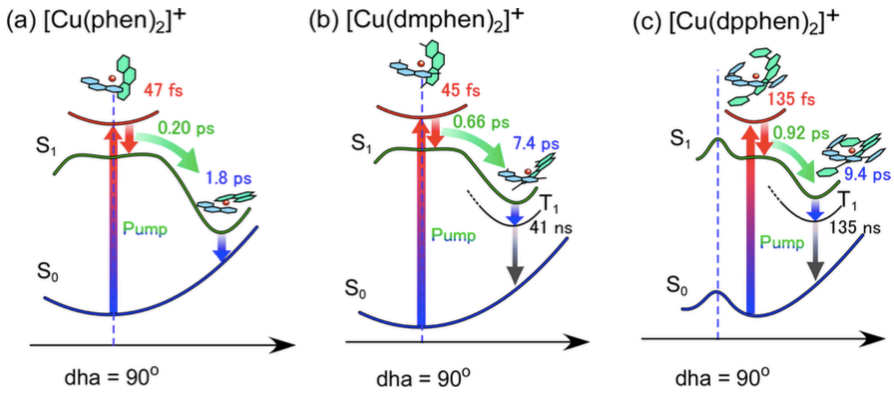

Figure 19: Schematic potential curves and ultrafast relaxation processes of (a) $[Cu(phen)_2]^+$, (b) $[Cu(dmp)_2]^+$, and (c) $[Cu(dpp)^2]^+$. phen = 1,10-phenanthroline, dmp = 2,9-dimethyl-1,10-phenanthroline and dpp = 2,9-diphenyl-1,10-phenanthroline. Figure reproduced from ref.[345]

followed by two time components of 660 fs and 7.4 ps, assigned to the PJT distortion and ISC, respectively. Later Chen and co-workers[347] reported similar time-components, 80 fs, 510 fs and 10-15 ps. They concluded, in agreement with Tahara that the longer timescale was ISC, and assigned the shortest time constant (80 fs) to IC and the PJT distortion. Finally Tahara and co-workers[348] used transient absorption spectroscopy to investigate the dynamics following excitation at 550 nm. This transition corresponds to the lowest singlet MLCT state (S_1), which is dipole forbidden but gains intensity through vibronic coupling with the main absorption band. They observed distinct wavepacket dynamics corresponding to the PJT distortion, and were able to obtain a low-frequency vibrational spectrum of the important modes.

All of these latter studies[346–349] have ruled out ultrafast ISC. However, the analysis of these experiments only considered SOC between the S_1 and T_1 states, and the SOC at a minimum of the S_1 geometry. As pointed out by Zgierski,[350] there are four closely spaced and vibronically coupled triplet states in close proximity to S_1, and therefore the S_1-T_1 coupling is not the only relaxation channel into the triplet states. Indeed it was shown in ref.[344] that along a flattening distortion mode, identified to be important in the wavepacket dynamics of ref.[348] the T_2, T_3 and T_4 states all intersect the S_1 state.

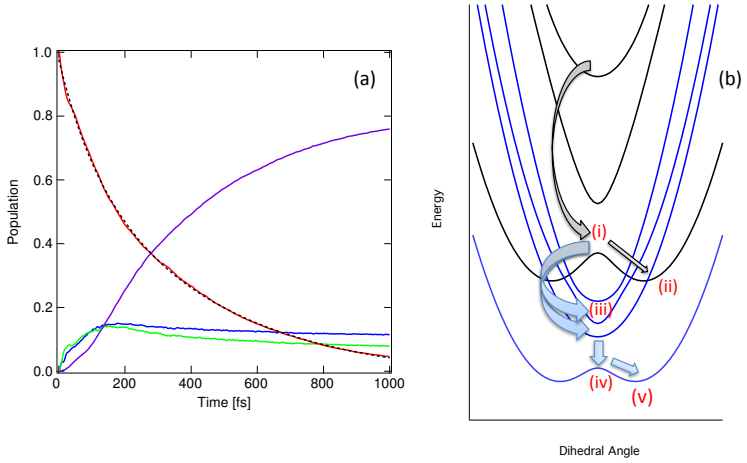

Figure 20: (a) Relative diabatic state populations of S_1 (blue), S_2 (green), S_3 (red), the triplet (T_{1-4}) states (purple), for 1 ps following photoexcitation. The black dashed line is the biexponential fit of the S_3 diabatic state populations. (b) Schematic representation of the key dynamical steps occurring within the ultrafast nonadiabatic dynamics of $[Cu(dmp)_2]^+$. (i) Internal conversion from S_3 to S_2. (ii) Vibrational relaxation from S_1^{FC} to S_1^{JT}. (iii) Ultrafast ISC from S_1^{FC} to T_2^{FC} and T_2^{FC}. (iv) IC within the triplets. (v) Vibrational relaxation from T_1^{FC} to T_1^{JT}. FC is the Franck-Condon geometry and JT is the JT flattened geometry. Figures reproduced from ref.[154]

A recent quantum dynamics study using a model spin-vibronic Hamiltonian[154,344] found that after photoexcitation a component of ultrafast intersystem crossing, shown in the population kinetics of Figure 20a, occurs at the same time as the structural JT distortion. The mechanism for ISC is shown to be a dynamic effect, in the sense that it arises from the system traversing the PJT coordinate where the singlet and triplet states become degenerate, leading to efficient crossing. It is enhanced by the strong vibronic coupling within the triplet manifold and the small energy gap between the states. This contribution of ultrafast ISC does depend on the rate of vibrational cooling leading to a wavepacket relaxed in the minimum of the S_1 state at which geometry the SOC is significantly weaker and the crossing is only between the S_1 and T_1 state. However, as demonstrated this occurs in about 1 ps,[351] after most of the ISC shown in Figure 20a has occurred. In addition, these conclusions were recently supported using excited-state molecular dynamics simulations, explicitly including the effect of the solvent in a QM/MM fashion.[206]

This illustrates again the entwined nature of electronic, spin and structural relaxation associated with the spin-vibronic mechanism which suggests that both processes are intimately coupled in all molecules in this series, making decoupling them into different mechanism steps an approximation.[352] In the context of these Cu(I) complexes, this spin-vibronic dynamics leading to an ultrafast component of ISC is actually detrimental. Indeed, Huang *et al.*[353] recently demonstrated that when attached to a TiO_2, charge injection for a related Cu(I)-phenanthroline complex, from the ^{1}MLCT is two orders of magnitude faster than from the ^{3}MLCT. Consequently for efficient charge injection one needs to restrict ISC.

The research of Cu(I) complexes has largely focused upon the four-coordinate systems. However, unlike four-coordinate tetrahedral Cu(I) compounds, the three-coordinate geometry eliminates the possibility of flattening distortion in the excited state.[354] However, reports on luminescent linear Cu(I) complexes are rare.[355–360] Particularly interesting with regard to spin-vibronic coupling are linear Cu(I) complexes involving the standard N-heterocylic carbene IPR (1,3-bis(2,6-diisopropylphenyl)imidazol-2-ylidene) as σ-donor and various pyridine derivatives as π-chromophore ligands that were reported to be highly efficient blue to blue-green phosphorescence emitters.[360] For each of these complexes, the luminescence quantum yield was found to depend on the excitation wavelength. The highest quantum yield was measured for excitation wavelengths close to the origin of the S_1 band. Difference densities obtained from DFT/MRCI calculations (Fig. 21) show the S_1 state of the pyridyl and methylpyridyl complexes to be an MLCT state resulting mainly from a $d_\sigma \rightarrow \pi_{\text{pyridyl}}$ excitation. The corresponding triplet state exhibits a very similar electronic structure and therefore the direct SOC between these states is small. In second order, their interaction is mediated by another close-lying triplet state of mixed MLCT and ligand-centered (LC) type, wherein the MLCT configuration corresponds to a $d_\pi \rightarrow \pi_{\text{pyridyl}}$ excitation. As the dominant ^{1}MLCT and ^{3}MLCT configurations differ from the leading term of the ^{3}MLCT/LC wavefunction by a $d_\sigma \rightarrow d_\pi$ single excitation, their mutual spin–orbit interaction is expected to be substantial. And indeed, due to the large SOCME (267 cm^{-1}) and the close ener-

getic proximity of the states, the vibrationally relaxed S_1 state is predicted to convert very rapidly within 16 ps to the ^{3}MLCT/LC state, leading to complete suppression of prompt fluorescence. The ^{3}MLCT/LC state can further interact via SOC of comparable magnitude (266 cm^{-1}) and/or derivative coupling with the ^{3}MLCT state, establishing a temperature-dependent equilibrium so that TADF becomes conceivable in addition to phosphorescence. Photoexcitation with shorter wavelengths may reach locally excited triplet states of the diisopropylphenyl substituents which do not phosphoresce and hence diminish the luminescence quantum yield.

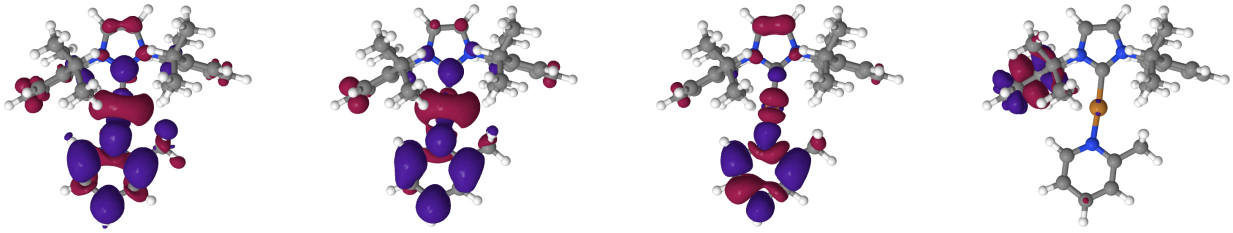

(a) (b) (c) (d)

Figure 21: Difference densities of the low-lying singlet and triplet excitations in the linear IPR-Cu(I)-methylpyridyl complex. Figures reproduced from ref.[360]

In contrast, the fast and efficient ISC and rISC in some linear coinage metal carbene-metalamide (CMA) complexes proceed for a co-planar orientation of the cyclic amino(alkyl) carbene (CAAC) and carbazolate (Cz) ligands even in Condon approximation without invoking spin-vibronic interactions.[361] The rotationally assisted spin-state inversion (RASI) mechanism postulated by Di *et al.* [359] to explain the luminescence properties of linear carbene-metalamide (CMA) complexes, is considered an artefact of the unbalanced quantum chemical treatment of the first excited singlet and triplet states by these authors. They had computed the T_1 state at the level of unrestricted density functional theory (UDFT) whereas the energy of the S_1 state energy had been determined by TDDFT finding that the S_1 TDDFT potential energy curve intersects the T_1 UDFT potential upon intramolecular rotation of the Cz ligand. A consistent quantum chemical treatment at the TDDFT or DFT/MRCI levels of theory finds the T_1 state to lie energetically below the S_1 state at all

nuclear arrangements.[361] Multiconfiguration effects decrease the singlet-triplet energy gap to values below 0.1 eV in the gold complex and lead to non-negligible SOCMEs enabling ISC and rISC to proceed with rate constants of the order of 10^9 s^{-1} at room temperature.

Re(I) α-diimine Complexes

Rhenium(I) tricarbonyl α -diimine complexes $[Re(X)(CO)_3(L)]^{n+}$ with X being a halogen, an alkyl group or a pyridyl ligand and L a bidentate-diimine ligand or two monodentate pyridyl ligands, play a central role in the photochemistry and photophysics of 3^{rd} row transition metal complexes since their discovery in the 1970s.[362] Indeed, thanks to their synthetic flexibility, tunable photo activity and rich photophysics and photochemistry, these molecules are easily linked to bio systems or incorporated in polymers, wires and supramolecular assemblies finding various applications in the fields of photocatalysis, light-emitting devices, electron/energy transfer processes, non-linear optics and cancer treatments.[363–369] The control of their excited-state activity is essentially driven by the character of the lowest long-lived triplet state, MLCT, IL, MC or LLCT, easily tunable by the nature of X and L and accessible via ultrafast vibrational decay.[370] In order to investigate in detail the role of SOC in this class of complexes, pioneering time-resolved spectroscopic experiments and theoretical studies have been performed on a number of complexes.[33,364,371,372,372–382] Surprisingly, fs-ps ultra-fast luminescent decay, measured in this family of Re(I) complexes, does not follow the heavy atom SOC effects, all the complexes investigated so far exhibiting the same particularities, namely an ISC process characterized by three time domains $\tau_1 \sim$ 85-150 fs, $\tau_2 \sim$ 0.3-1.7 ps and $\tau_3 \sim$ 40 ns - 7.5 μ s and three domains of energy, namely 500-550 nm, 550-600 nm and >610 nm whatever the ligands X and L are as illustrated by fs fluorescence up-conversion, transient absorption and time-resolved infra-red experiments.[33,373,383]

After careful theoretical investigations of the static absorption and emission properties of a series of $[Re(X)(CO)_3(L)]^{n+}$ (X = Cl, Br, I; L= 2,2'-bipyridine, n=0; X= imidazole or

pyridine; L = 1,10-phenanthroline, n= +1) of C_s symmetry, depicted in Figure 22,[372,384–388] a model Hamiltonian for solving a multi-state multimode problem including vibronic and SOC within the LVC approximation and the assumption of harmonic potentials has been developed (see section 3.2.3). The simulation of the ultrafast dynamics by wavepacket propagations using MCTDH[192] is based on DFT and its TDDFT electronic structure data.[81–83,385]

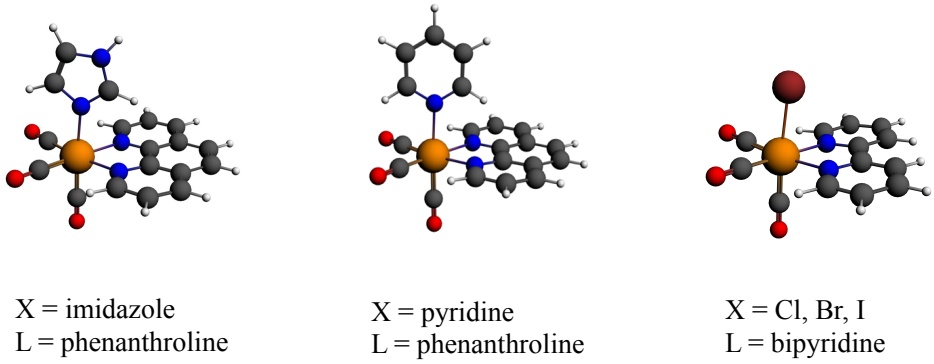

Figure 22: Schematic representation of $[Re(X)(CO)_3(L)]^{n+}$ (X = Cl, Br, I; L= 2,2'-bipyridine, n=0; X= imidazole or pyridine; L = 1,10-phenanthroline, n= +1)

The diabatic populations extracted from the quantum dynamic simulations based on five electronic excited states coupled vibronically and by spin–orbit, namely the three low-lying triplet $^3IL_{bpy}$, ^{3}MLCT/XLCT and two singlet ^{1}MLCT/XLCT states, the electronic densities of which are depicted in Figure 23, are represented in Figure 24 for $[Re(X)(CO)_3(L)]$ (X= Cl, Br; L= 2,2'-bipyridine).

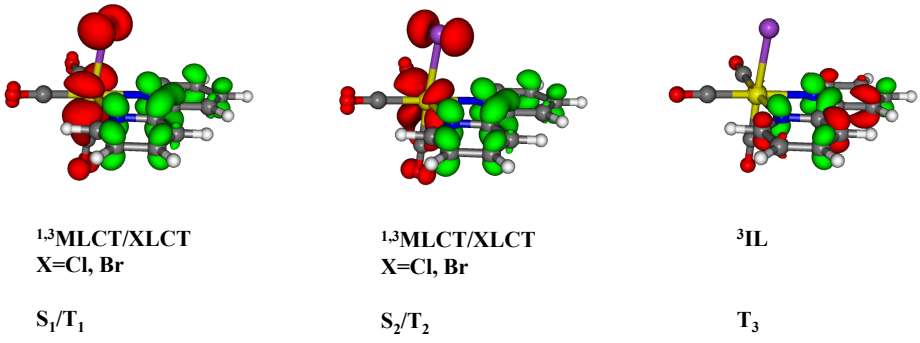

Figure 23: Electronic densities of the five lowest singlet and triplet states of $[Re(X)(CO)_3(L)]$ (X = Br and L= 2,2'-bipyridine).

One important question is the choice of the active normal modes that have to be incorporated in the reduced dimensionality quantum model within the spin-vibronic model Hamiltonian as defined in section 3.2.3. In the case of the Re(I)- halide complexes fourteen modes have been taken into account and eleven spin–orbit states have been included in the simulation. The choice of the tuning modes (a') is based on a systematic analysis of the shifts in energy and position of the diabatic potentials generated at the FC point by the intrastate coupling κ (see section 3.2.3). For instance, Harabuchi *et al.*[83] have shown that the normal modes corresponding to the carbonyl vibrations are crucial for inducing the population of the two intermediate S_1 and T_2 states that play a key role in the spin-vibronic mechanism. Indeed when switching off these modes we observe a minor population of the lowest triplet T_1 state. When activating these modes the diabatic potentials of S_2/T_2 and S_1/T_1 are shifted differently as indicated by the change of sign of the corresponding κ generating potential crossings close to FC.[81] The diabatic populations as function of time, exhibited in Figure 24 for X=Cl and X=Br, show an ultrafast decay of the S_2/T_3 excited states within about 100 fs that correlates perfectly with the experimental kinetics of τ_1 estimated at 85 ± 8 fs for X=Cl and 128 fs for X=Br ± 12 fs.[33] This decay is concomitant with a nearly instantaneous population of T_1 and S_1 / T_2 within a few tens of fs. For both complexes the population of the two intermediate states S_1 and T_2 reaches about 45 % within 200 fs. At about 300 fs and 400 fs an exchange of population between the intermediate states S_1/T_2 and T_1 is observed in $[Re(Cl)(CO)_3(bpy)]$ and $[Re(Br)(CO)_3(bpy)]$, respectively, agreeing well with the experimental τ_2 values estimated at 340 ± 50 fs for X=Cl and 470 fs ± 50 fs for X=Br.[33]

The following spin-vibronic mechanism has been proposed for the interpretation of the ultrafast luminescent decay in $[Re(Cl)(CO)_3(bpy)]$ and $[Re(Br)(CO)_3(bpy)]$ Figure 25 (left): At early times, below 200 fs, both vibronic S_2/S_1 and SOC S_2/T_1 and S_1/T_2 effects are operating; The intermediate states S_1 and T_2 play a central role in the population of T_1 at longer time scales via both vibronic and SOC.

The trends in the decay kinetics measured experimentally for X=Cl, Br, I confirmed

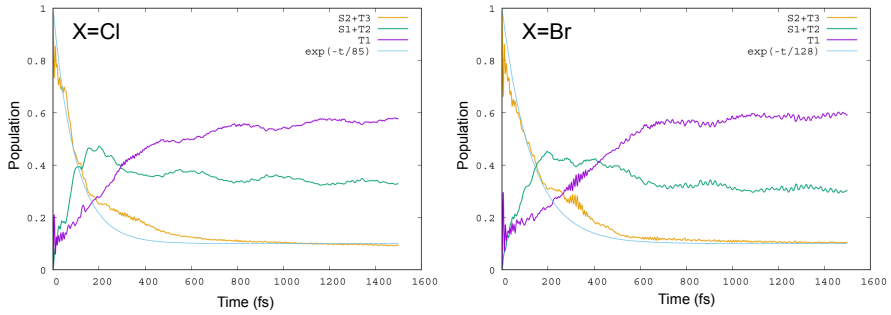

Figure 24: Time-evolution of the diabatic populations of the low-lying singlet and triplet excited states of [Re(X)(CO)$_3$(L)] (X = Cl, right; X = Br, left and L= 2,2'-bipyridine).

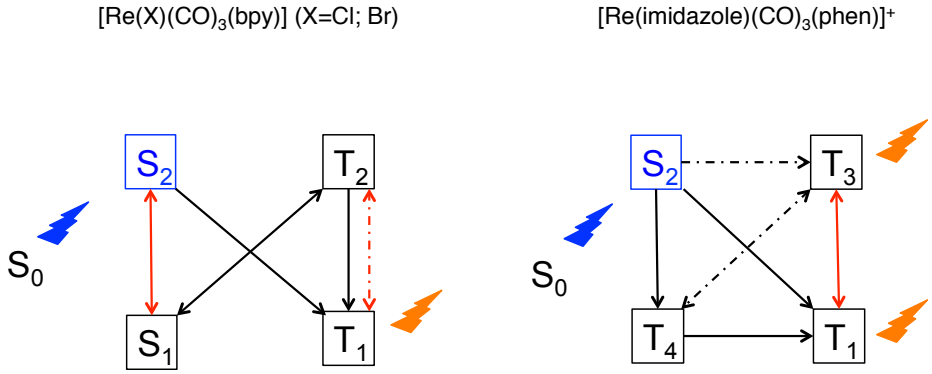

Figure 25: Spin-vibronic mechanism of the ultra-fast luminescent decay observed in [Re(X)(CO)$_3$(L)]$^{n+}$ (X = Cl, Br and L = 2,2'-bipyridine, n=0) left and [Re(X)(CO)$_3$(L)]$^{n+}$ (X = imidazole and L = 1,10-phenanthroline, n= +1), red arrows: vibronic; black arrows: SOC.

theoretically along the halides series and counter intuitively to the heavy atom effect, namely a faster decay for the light elements substituted complexes has been explained by the change of electronic character of the involved excited states, nearly mostly MLCT in X=Cl to mostly XLCT in X=I that correlates with a decreasing contribution of intrastate coupling via the key tuning modes (carbonyl vibrations) that populate the intermediate states S_1 and T_2.

As illustrated for the imidazole-substituted complex Figure 22 similar experimental luminescent decay characteristics together with comparable chemical properties can lead to a very different spin-vibronic mechanism paving the way to laser pulse control in transition

metal complexes. The two lowest ^{1}MLCT, the three lowest ^{3}MLCT and the $^3IL_{phen}$ states of [Re(imidazole)$(CO)_3$(phen)]$^+$, the electronic densities of which are depicted in Figure 26, have been included in the simulation because potentially populated by ultrafast decay from the absorbing state S_2. This leads to six electronic states coupled vibronically and by SOC within a fifteen modes model generating fourteen adiabatic spin–orbit states.[82] The $^3IL_{phen}$ (T_3) state is stabilized as compared to the ^{3}IL state localized on the bpy ligand in the halide complexes.

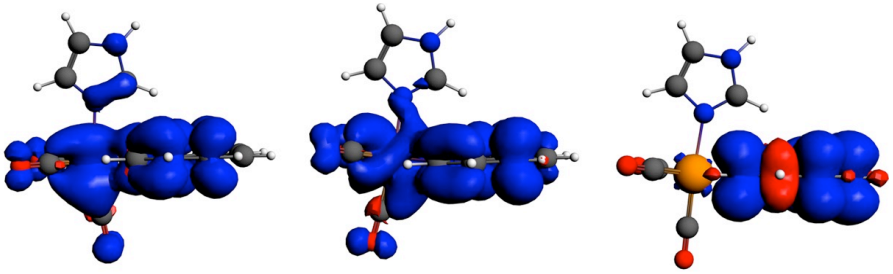

^{1,3}MLCT **^{3}IL**

$S_1/T_1/S_2/T_2$ **T_3**

Figure 26: Electronic densities of the six lowest singlet and triplet states of [Re(X)$(CO)_3$(L)]$^+$ (X = imidazole and L = 1,10-phenanthroline, n= +1)

In contrast to the Re(I) halide-substituted complexes (Figure 25 left) the T_3 state will drive the mechanism of population of the lowest long-lived T_1 state in [Re(imidazole)$(CO)_3$(phen)]$^+$ whereas the S_1 and T_2 states will play a minor role (Figure 25 right). It is worth noting that both the T_3 state in the imidazole complex and the S_1 and T_2 states in the halide complexes have been put in evidence experimentally as intermediate states. Interestingly, the populations of T_3 and T_1 can be quenched by switching off selected tuning modes corresponding to the carbonyl or phenanthroline vibrations as exemplified in Figure 27. This is mainly due to the important shifts in position and energy experienced by T_3 under the influence of these modes.

As illustrated by the time evolution of the diabatic populations represented in Figure

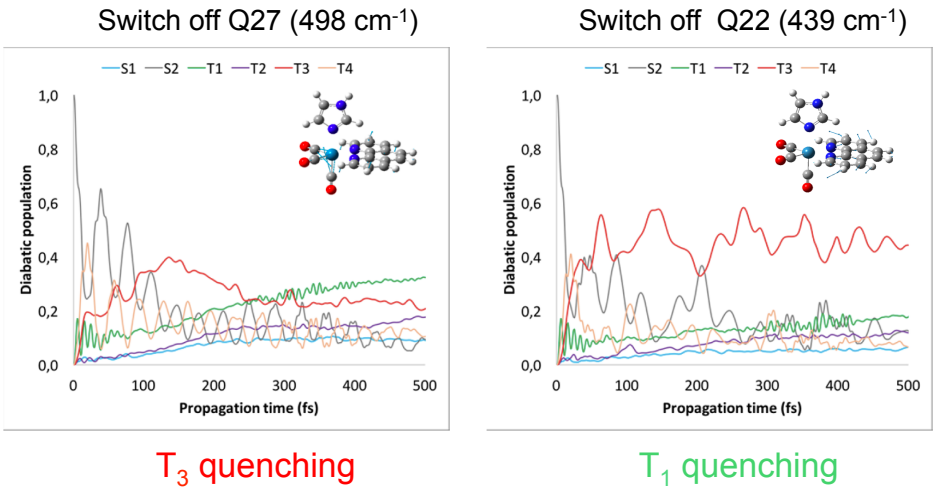

Figure 27: Time evolution of the diabatic populations of the six lowest excited states of $[Re(imidazole)(CO)_3(Phen)]^{n+}$ when switching off Q27 (left) and Q22 (right)

28[82] this key ^{3}IL (T_3) state will play a major role in the spin-vibronic mechanism of the luminescent decay of this complex (Figure 25); the early time (<100 fs) population of T_3 and T_1 correlated to the depopulation of S_2 and T_4 is driven essentially by SOC. The estimated time scale τ_1 of 75 fs can be compared to the experimental decay of 144 $\pm$ 7 fs measured in DMF.[373]

Within $\tau_2 = 1.5 \pm 0.2$ ps the population of two triplet states, one of them with a significant IL contribution, is put in evidence experimentally by means of fs fluorescence up-conversion complemented by transient absorption and time-resolved infra-red spectroscopy.[373] From the simulation reported in Figure 28 we can conclude that these states correspond to T_3 and T_1 that exchange population within this time-scale.

The two examples reported above illustrate the power of the spin-vibronic model in deciphering the relaxation mechanisms in transition metal complexes. Of course improvement of the electronic structure data extracted here from DFT/TD-DFT/SOC calculations and expansion of the model Hamiltonian to higher order is mandatory to develop more quantitative studies. Combining and comparing the different methods described in section 3 should open the way to the investigation and control of spin-vibronic mechanism not only by laser

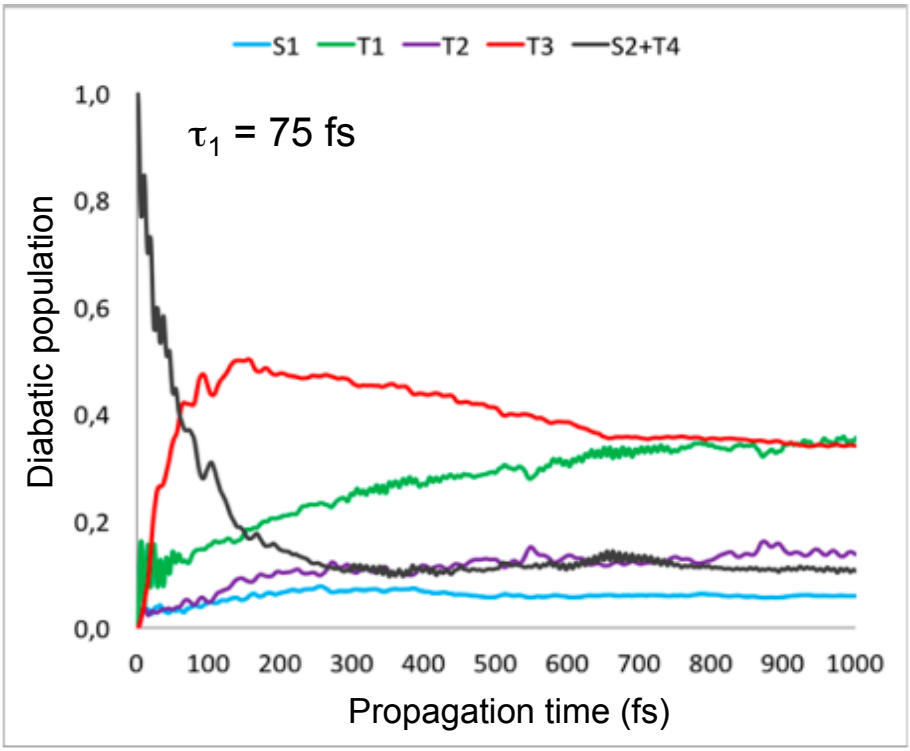

Figure 28: Time-evolution of the diabatic populations of the low-lying singlet and triplet excited states of $[Re(X)(CO)_3(L)]^+$ (X = imidazole and L= 1,10-phenanthroline adapted from[82]

pulses but also chemically or by environment effects.

Spin-Vibronic ISC in Small Molecules and Organic Chromophores

Small Aromatic Molecules

The earliest examples of studies characterising the spin-vibronic nature of spin-flip transitions were observed in the phosphorescence properties of small aromatic hydrocarbons, such as benzene.[5–9] Indeed in aromatic hydrocarbons, the triplet-ground state transition is often forbidden under the Condon approximation and therefore vibrations must be involved for phosphorescence to be activated.

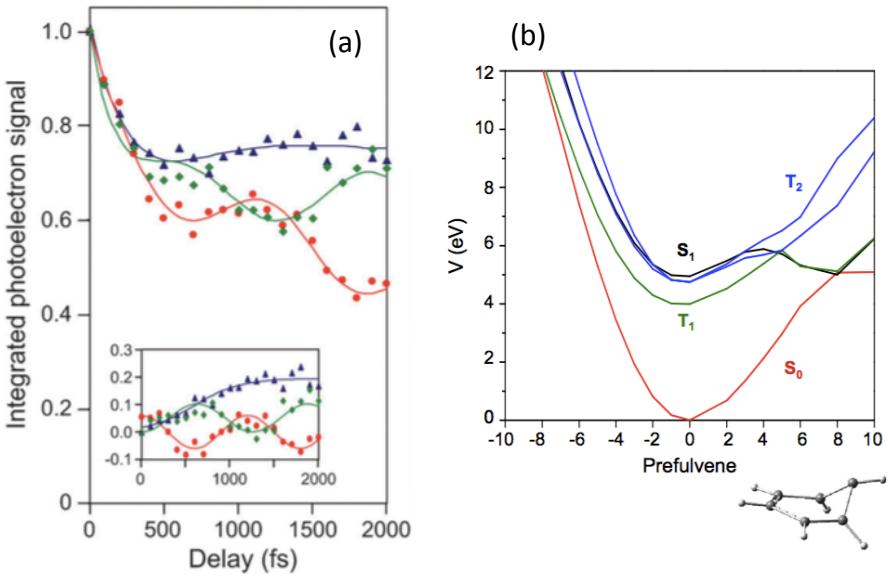

Figure 29: (a) Experimental integrated photoelectron yields as a function of delay for a probe wavelength 243 nm. Inset: Partial integrated photoelectron yields. (b) Cut through the potential energy surfaces of benzene along the prefulvene mode: The vector from the Franck-Condon point to the S_1/S_0 conical intersection. Figure reproduced from ref.[59,60]

Benzene is a classic example of a photochemically rich molecule, with a number of competing pathways that can result after photoexcitation.[389,390] Extending these studies into the femtosecond time domain, Fielding and co-workers used time-resolved photoelectron spectroscopy (TRPES) to show the involvement of ISC competing with the IC in the photoexcited decay of benzene on a sub-picosecond timescale (Figure 29a).[59,60,152,196] Although this still remains a minor channel, any ultrafast ISC in a simple hydrocarbon is surprising due to the very weak SOCME. Despite the small magnitude of the SOCME,[391] supporting quantum dynamics simulations[59,60,152,196] demonstrated that ultrafast ISC occurs via spin-vibronic effect activated by the prefulvene mode (Figure 29b) where weakly-coupled (S_1, T_1 and T_2) states are near degenerate, leading to efficient crossing.

Another small aromatic molecule, which has been widely studied due to its potential application in optoelectronic is thiophene.[392] Just like many other small hetroaromatic molecules, thiophene exhibits ultrafast deactivation of the S_1 state and is non-fluorescent.[393–396] These previous studied have indicated that a ring opening mechanism is responsible for the

internal conversion from the excited to the ground state. Recently, Schnappinger *et al.*[397] studied the relaxation of thiophene including both singlet and triplet states. They reported that after internal conversion, at the ring opening conical interactions, there are two possible pathways. One returns the system to the closed ring ground state, while the other leads to a flat potential, along which the SOCME increases and the singlet–triplet energy gaps nearly vanish. This leads to efficient intersystem crossing promoted by this vibrational motion in a mechanism which is very similar to as described above for benzene.

Deactivation of DNA bases by ISC

In living organisms exposed to UV light, DNA is being continuously damaged and repaired. Interaction with UV light generates an excited electronic state in DNA which will decay via either photophysical or photochemical pathways.[398,399] Photophysical relaxation is characterised by nonradiative decay from an excited state to the ground state, resulting in repopulation of the ground electronic state. Consequently, these pathways have been widely studied for understanding intrinsic photoprotection mechanisms. Research into these photoprotection mechanisms dynamics is dominated by femtosecond time-resolved spectroscopic studies of single nucleobases in either the gas[400–406] or solution phase,[407–411] often supported by theoretical work.[215,406,412–421]

Despite extensive studies, the precise role of ISC in photostability is not well established. To address this, the González group have extensively used excited state molecular dynamics to probe the competition between IC and ISC in DNA bases.[64,72,75,215–217,422] Recently, using nonadiabatic dynamics simulations at the multi-state complete active space second-order perturbation theory (MS-CASPT2) level of theory, Mai *et al*[72] studied the deactivation mechanism of 2-thiouracil. As show in Figure 30, the authors report two sub-picosecond ISC channels promoted by out of the ring plane motions of the S atom which leads to near degeneracy of singlet and triplet states and sizeable of SOCME $\sim$150 cm^{-1}

For the related natural DNA base cytosine, excited state molecular dynamics simula-

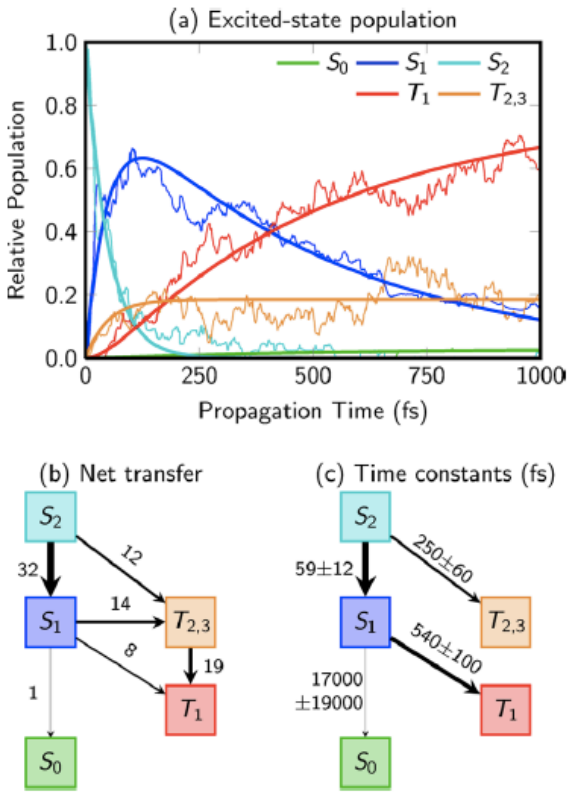

Figure 30: (a) Excited-state populations from 44 trajectories (thin lines) and global fits (thick lines) to the populations. (b) Net population transfer (numbers of trajectories) among the electronic states. (c) Fitted time constants (in femtoseconds) from the global fit. The T_3 population was absorbed into the T_2 population in all panels. The thickness of the lines in panels b and c relates to the amount of transferred population. Figure reproduced from ref.[72]

tions[215,216] employed potentials, non adiabatic and spin–orbit couplings determined at the state-averaged complete-active-space self-consistent-field (CASSCF) level. On the basis of these simulations, the authors reported a decay of the S_1 population via ISC to the T_2 state to be ultrafast. At least for vibrationally cold S_1 populations, these results are at variance with the experimental findings on supersonic jet-cooled cytosine by Lobsiger *et al.* [423,424] A recent combination of experimental and theoretical studies implies that the main deactivation channel for S_1 populations with an excess energy below 550 cm^{-1} is IC to the electronic ground state and that the $S_1 \rightsquigarrow T_1$ ISC is moderately fast (nanosecond time scale), and not ultrafast.[406] The slight out-of-plane distortion of the S_1 minimum geometry

of cytosine and the concomitant small admixture of $^1n_O\pi^*$ character in the S_1 wavefunction makes the $S_1 \rightsquigarrow T_1(^1\pi\pi^* \rightsquigarrow^3 \pi\pi^*)$ ISC nearly as fast as an El-Sayed allowed transition. The presumable reason for these contradictory findings is the electronic structure of the S_1 state. The CASSCF wavefunction is reported to have predominantly $n_O\pi^*$ character at the S_1 minimum whereas the spectral signature clearly identifies S_1 to be a slightly out-of-plane distorted $^1\pi\pi^*$ state. Higher-level correlated methods, such as CASPT2 and spin-component scaled coupled cluster with approximate treatment of doubles (SCS-CC2), place the $^1\pi\pi^*$ state adiabatically below the $^1n_O\pi^*$ state in cytosine.[406,415] This underpins the importance of basing photodynamical studies of heteroaromatic compounds on reliable correlated electronic structure methods.

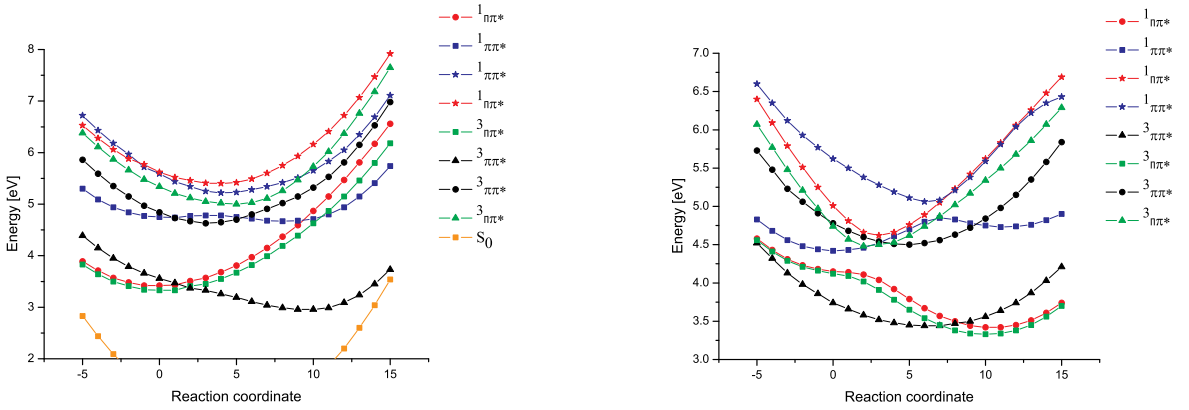

(a) 0: $S_2(^1\pi\pi^*)_{min}$; 10: $S_1(^1n\pi^*)_{min}$

(b) 0: $S_1(^1n\pi^*)_{min}$; 10: $T_1(^1\pi\pi^*)_{min}$

Figure 31: CC2 linearly interpolated paths between the S_2, S_1 and T_2 minima illustrating IC (a) and ISC (b) decay pathways in 6-azauracil. Photoexcitation primarily populates the S_2 state (blue squares). Figures reproduced from ref.[163]

Using the perturbation theory methods described in section based on CC2 potentials to determine ISC rate constants of the photoexcited pyrimidine bases uracil and thymine, Etinski *et al.* [425] predicted ISC to play an important role in the electronic relaxation of the initially exicted $^1\pi\pi^*$ state in the gas phase. This was confirmed later experimentally.[426] The triplet quantum yield of uracil may be even enhanced if a nitrogen atom is substituted for the CH group in 6-position.[427] Energy profiles and SOCMEs computed along linearly

interpolated reaction paths (Figure 31) point towards strong nonadiabatic and spin-vibronic coupling in 6-azauracil. Absorption of UV light excites the $S_2(^1\pi\pi^*)$ state. Essentially, two different decay pathways were proposed.[163,428] The first one involves the $T_2(^3n\pi^*)$ state as a transient. Due to the non-BO nature of these states, a strong variation of the $\langle ^1S_2|\hat{\mathcal{H}}_{SO}|^3T_2\rangle$ with the nuclear coordinates is observed. The second one involes a conical intersection of S_2 with $S_1(^1n\pi^*)$ which acts as a doorway state from which ISC to the $T_1(^3\pi\pi^*)$ state proceeds. Remarkably, an inverse energy gap behaviour for the $S_1 \rightsquigarrow T_1$ ISC was predicted by theory:[163] A blue shift of the S_1 potential energy surface by about 0.2 eV places the intersection between the S_1 and T_1 potentials close to the S_1 minimum, thus increasing the overlap of the vibrational wavefunctions and consequently speeding up the ISC from $\tau_{ISC} = 125$ ps in the gas phase to $\tau_{ISC} = 30$ ps in acetonitrile solution. Recent femtosecond transient absorption spectroscopy measurements confirm the predominance of the second pathway: The $S_2 \rightsquigarrow S_1$ IC is found to proceed at the subpicosend time scale whereas a time constant of 5.2 ± 0.1 ps is measured for the $S_1 \rightsquigarrow T_1$ ISC in acetonitrile. The experiments also reveal a clear dependence of the $S_1 \rightsquigarrow T_1$ rate constant on the polarity of the solvent, showing a faster formation of the T_1 state in more polar solvents. In contrast, aqueous solution markedly diminishes ISC in uracil and the other pyrimidine nucleic acid bases.[429,430] The reduced triplet quantum yield is traced back to the substantial blue shift of the $n_O\pi^*$ states relative to the $\pi\pi^*$ excited states in polar protic environments, making their direct or indirect participation in spin-vibronic decay mechanisms of the photoexcited $^1\pi\pi^*$ states less probable.[425,431] Similar blue shifts are encountered in many aromatic carbonyl compounds (see also section). In the xanthone family of dyes, the polarity and proticity of the solvent environment can be applied to actively control the triplet quantum yield.[53,432]

Heteroaromatic Photosensitisers for Photodynamic Therapy

PDT uses photosensitisers, *i.e.* photo-addressable molecules with little or no toxicity, to initiate programmed cell death (apoptosis). PDT is applied to cure tissue related diseases

such as skin cancer, vitiligo, or psoriasis, but may also be used to kill microbial cells, *e.g.* in blood samples. Type I photosensitizers trigger radical reactions and are not of interest in the context of the present review. Type II photosensitizers either undergo photochemical reactions in the triplet state or transfer spin and excitation energy to molecular oxygen to form singlet dioxygen which in turn initiates apoptose.[433–435]

$$(\mathrm{PhSens}) \overset{h\nu}{\rightarrow} {}^1(\mathrm{PhSens})^* \overset{\mathrm{ISC}}{\rightsquigarrow} {}^3(\mathrm{PhSens})^*$$

$$^3(\mathrm{PhSens})^* + \mathrm{O_2}(^3\Sigma_g^-) \rightarrow (\mathrm{PhSens}) + \mathrm{O_2^*}(^1\Delta_g)$$

Prerequisites for a potent photosensitiser are the existence of a long-lived triplet excited state and its efficient population via ISC. Three prototypical type II photosensitisers are displayed in Fig. 32. All of them are heteroaromatic compounds with a $^3\pi\pi^*$ state as the lowest triplet state. Photoexcitation initially populates a $^1\pi\pi^*$ state. So, unless intermediate $n\pi^*$ states are present, ISC is El-Sayed forbidden and it is necessessary to envoke spin-vibronic coupling to form triplet states in appreciable amounts. PUVA therapy combines

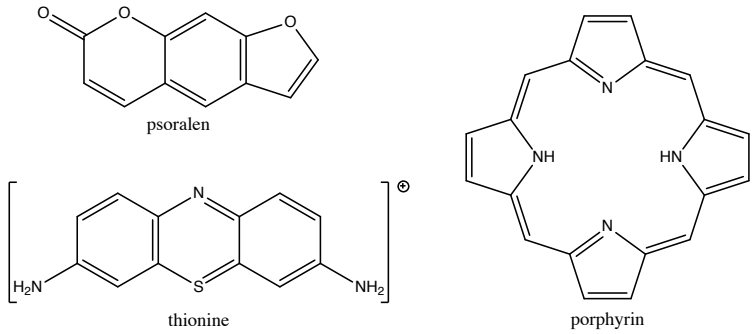

Figure 32: Prototypical type II photosensitisers

the topical application of psoralen derivatives with UV-A irradiation of $\sim 365 - 320$ nm wavelengths.[436] In the longer wavelength regime, porphyrin or phenothiazine derivatives are used.[433,437] Some of the porphyrin derivatives, e.g. protoporphyrin IX, can be synthesised by the patient's body after administration of 5-aminolevulinic acid.[438]

Psoralens are light-sensitive compounds naturally occurring, e.g., in cow parsnip. Pho-

toexcited psoralens have been found to perform [2 + 2]-cycloadditions with thymine bases at the pyrone and the furan sides, linking two DNA strands covalently together and thus preventing replication of diseased cells.[436] In addition, singlet oxygen formation is observed. Theoretical studies by Tatchen *et al.* [150,439,440] have shown that the ISC pathways involving $n\pi^*$ states are energetically not accessible in aqueous solution and that the rate constants for the $^1\pi\pi^* \rightsquigarrow {}^3\ \pi\pi^*$ transitions are small ($< 10^5\ \mathrm{s}^{-1}$) in Condon approximation. Out-of-plane vibrational distortions enhance the spin–orbit coupling (Figure 33) to an extent that the $S_1 \rightsquigarrow T_1$ ISC outcompetes the fluorescence by two orders of magnitude and triplet formation becomes the dominant process in aqueous solution.[150]

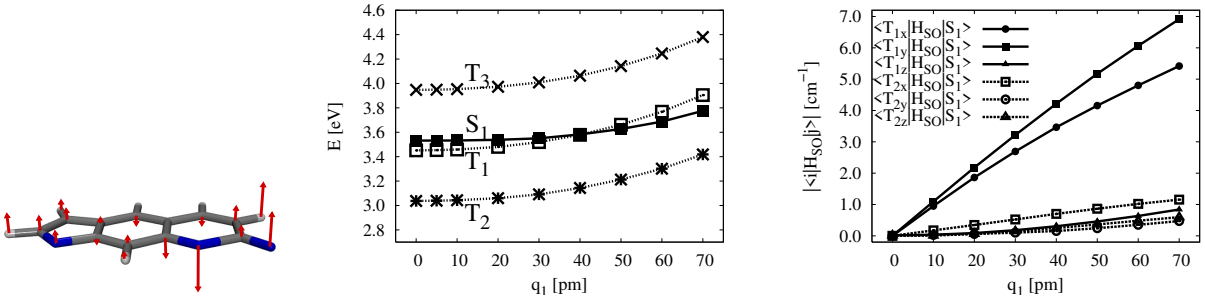

(a) q_1 normal mode (b) (c)

Figure 33: (Out-of-plane normal mode q_1 (a), potential energy curves (b) and SOCMEs (c) of psoralen plotted against q_1. Figures reproduced from ref.[150]

As already mentioned in section , there are no low-lying states of $n\pi^*$ character in porphyrin derivatives. Upon excitation to the Soret band, free-base porphyrin (FBP) relaxes to the lowest excited singlet state. Afterward, about 5 % of the population decays back to the ground state while the majority goes to the first excited triplet state by ISC transfer.[441] Although FBP belongs to the D_{2h} molecular point group, its π system is almost D_{4h} symmetric. Accordingly, the two highest occupied π molecular orbitals, π_H and π_{H-1}, are quasi degenerate. The same is true for the lowest π^* molecular orbitals, π^*_L and π^*_{L+1}. In line with the Gouterman four-orbital model,[442] the wavefunction of the $S_1(^1B_{2u})$ state is dominated by two nearly equally large terms corresponding to $\pi_{H-1} \rightarrow \pi^*_{L+1}$ and $\pi_H \rightarrow \pi^*_L$ excitations. Although each of these terms exhibits a large transition dipole moment with

the electronic ground state, the probability for a radiative transition is very low in Condon approximation because the individual contributions to the electric dipole transition moment nearly cancel. In-plane deformation vibrations lift this cancellation and make the Q-band transitions vibronically allowed.[151,164,181,443,444] As a consequence, the Q bands of porphyrins exhibit a very characteristic intensity pattern with a weak 0–0 peak and substantially more intense vibronic transitions.[445,446] Although the spin–orbit interaction between the $S_1(^1B_{2u})$ and $T_1(^3B_{3u})$ states is formally allowed in D_{2h} symmetry, it is very weak at the S_1 minimum because both states have $\pi\pi^*$ character. The squared matrix element which enters the perturbation expression 18 has a value of merely 0.004 cm^{-2} which may be compared to an energy separation of about 2400 cm^{-1} at the DFT/MRCI level.[164] In-plane deformations do not change the SOCME markedly, but out-of-plane vibrational distortions mix some $\sigma\pi^*$ character into the electronic wavefunctions thereby enhancing the spin–orbit interaction (Figure 4(b)). Not surprisingly, the $S_1 \rightsquigarrow T_1$ ISC rate constant is found to be temperature dependent with calculated values of $\sim 1 \times 10^7$ s^{-1} at 0 K and $\sim 9 \times 10^7$ s^{-1} at room temperature.[151]

Thionine (3,7-diamino-phenothiazin-5-ium cation) is a photosensitiser which belongs to the phenothiazine (PTZ) family of dyes. While the PTZ core is a ubiquitous donor in TADF donor–acceptor compounds (see also section), its cationic diamino-substituted derivatives are efficient singlet oxygen sensitisers absorbing in the 590-660 nm wavelength regime. Although only two $\pi\pi^*$ excited triplet states are located adiabatically below the first excited singlet state $S_1(\pi_H\pi_L^*)$,[447] thionine exhibits a sizeable triplet quantum yield of 0.55 in dilute water solutions. Based on computed potential energy curves and ISC rate constants in Herzberg-Teller approximation, it was suggested that the triplet formation in water proceeds primarily through the $S_1(\pi_H\pi_L^*) \rightsquigarrow T_2(\pi_{H-1}\pi_L^*) \rightsquigarrow T_1(\pi_H\pi_L^*)$ channel.[176] The $T_2(\pi_{H-1}\pi_L^*)$ state is seen to cross the $S_1(\pi_H\pi_L^*)$ potential close to the minimum of the latter so that even small out-of-plane distortions are sufficient to speed up the El-Sayed forbidden nonradiative transition substantially. Also in this case, the spin-vibronic transition is markedly enhanced

by thermal effects.[151]

Thermally Activated Delayed Fluorescence (TADF)

TADF, also known as E-type delayed fluorescence (DF),[448] has recently emerged as a very attractive approach for harvesting the 75% of triplet excited states generated by electrical excitation in organic light emitting diodes (OLEDs).[449,450] One of the key components of TADF is the rate of the conversion from the triplet state into the singlets, as long lifetimes in the triplet state lead to excited state quenching mechanisms such as triplet-triplet annihilation, reducing efficiency.[451] This calls for a detailed understanding of the factors affecting TADF.

Due to the importance of charge transfer states,[450] which are used to minimise the energy gap between the low-lying singlet and triplet states, it was initially assumed that the states involved in the rISC were the singlet (^{1}CT) and triplet (^{3}CT) charge transfer. However, SOC between these intramolecular CT states is formally zero (See section). This means that other electronic states are likely to be involved. Using D-A and D-A-D molecular TADF systems[452–454] Monkman, Bryce and co-workers demonstrated that two of the excited states involved could be independently tuned and therefore they must be of different character. Further insight into the mechanism was provided by Ward *et al.*[455] who showed that different D-A-D molecules with very similar energy gaps ($\Delta E_{S_1-T_1}$) exhibit large variations in k_{rISC}. They found that by sterically hindering the motion of D and A group, the emission could be switched from TADF to phosphorescence. This indicates a mechanism which goes beyond the Condon approximation and is dynamic in nature, in the sense that it depends on molecular vibrations.

These observations were recently rationalised by Gibson *et al.*[456] using QD to study the rISC of a D-A molecule composed of a phenothiazine donor and a dibenzothiophene-S,S-dioxide acceptor (PTZ-DBTO2), shown in Figure 34a. In this work, as shown schematically in Figure 34b, the authors showed that for PTZ-DBTO2, three states were crucial to de-

scribe the rISC mechanism. These were the ^{1}CT, ^{3}CT and a local $\pi\pi^*$ (^{3}LE) excited state on the donor unit. The rates obtained were in good agreement with those reported experimentally[457] (Figure 34c black trace), but most importantly the authors show that the non-adiababtic coupling between the two triplet states was critical for describing the rISC. Indeed, if this was removed the rate become close to zero (Figure 34c dark blue trace).

Importantly, the critical role of vibronic coupling between the two triplet states for rISC between the ^{3}LE$\rightsquigarrow^1$CT states cannot be described within first-order perturbation theory approach and therefore must involve spin-vibronic coupling. In addition, for PTZ-DBTO2 in low polarity environments as shown in Figure 34b, a direct second-order coupling for ^{3}LE$\rightsquigarrow^1$CT would require population transfer between the two CT states. However, as shown in Figure 34c the coupling between these two states has an insignificant role. Consequently, the relevant terms are:

$$k_{rIC} = \frac{2\pi}{\hbar} \left|\langle \Psi_{^3CT} | \mathcal{H}_{vib} | \Psi_{^3LE} \rangle\right|^2 \delta(E_{^3CT} - E_{^3LE}) \tag{41}$$

and

$$k_{rISC} = \frac{2\pi}{\hbar} \left| \frac{\langle \Psi_{^1CT} | \hat{\mathcal{H}}_{\mathrm{SO}} | \Psi_{^3LE} \rangle \langle \Psi_{^3LE} | \mathcal{H}_{vib} | \Psi_{^3CT} \rangle}{E_{^3CT} - E_{^3LE}} \right|^2 \delta(E_{^1CT} - E_{^3LE}) \tag{42}$$

Firstly, the vibronic coupling between ^{3}LE and ^{3}CT promotes, on a timescale much faster than the rISC, an equilibrium between the two states. Obviously, the position of this equilibrium depends both on the size of the nonadiabatic coupling and the energy gap. Subsequently, the second-order term, Equation 42, couples the ^{3}CT and the ^{1}CT, using the ^{3}LE as an intermediate state. This latter second-order term is very efficient because of the good vibrational overlap between the almost degenerate initial and final states, ^{3}CT and ^{1}CT, respectively. Importantly, this explains recent experimental results which demonstrated that steric hindrance of D-A dihedral angle switches the main pathway from TADF to phosphorescence[455] .This steric hindrance is equivalent to removing the vibronic coupling term, which is shown herein to be strongest along modes exhibiting a distortion of the D-A dihedral angle.

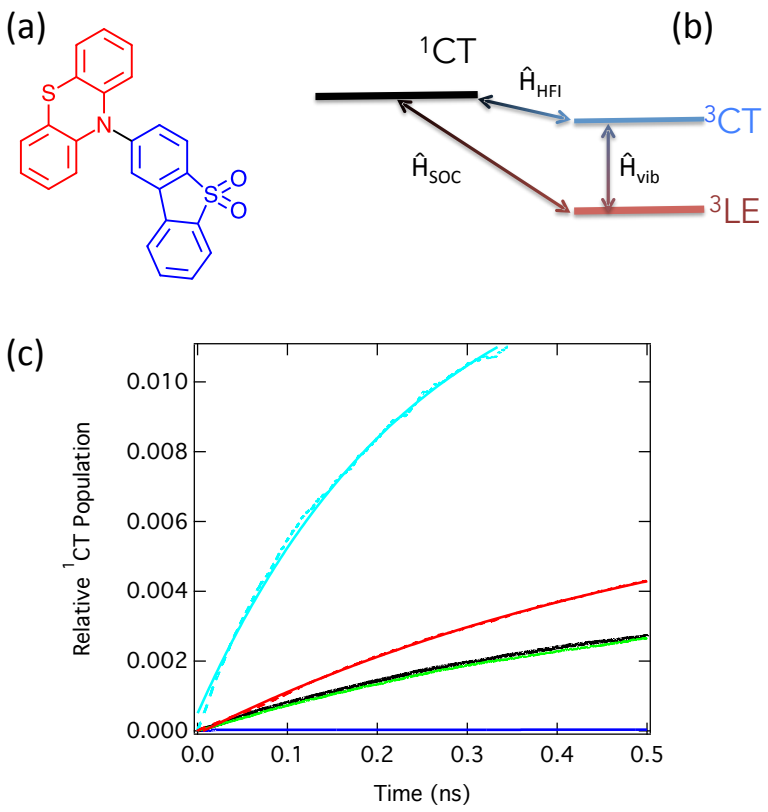

Figure 34: (a) Relative populations of the ^{3}LE state associated with ISC after excitation into the ^{1}CT state. (b) The relative populations of the ^{1}CT state associated with rISC after initially populating the ^{3}LE state. (c) Population kinetics of the ^{3}CT state during the rISC dynamics after initial population of the ^{3}LE state, i.e (b). Inset is a zoom into the early time kinetics. Black: Full model Hamiltonian described in Table S3, Green: No HFI, Blue: No Vibronic Coupling.

The temperature dependent rate of a thermally activated process is given by the Arrhenius equation provided that the equilibration is faster than the radiative or nonradiative deactivation of the electronically excited molecule. The exponential decrease in the rate with activation energy, which this imposes, strongly promotes processes with small activation barriers. Experimentally to elucidate the gap, there are two approaches adopted. The first is obtained by fitting the integrated DF emission as a function of temperature and therefore gives a thermal activation derived from the Arrhenius equation.[450] The second is defined as the difference between the onset of the fluorescence to phosphorescence signals and is therefore the optical gap. Importantly, it has been repeatedly found that the gap extracted

from these two approaches are different, sometimes by a much as 0.35 eV.[452] Indeed, larger differences were generally found for the higher performing molecules.

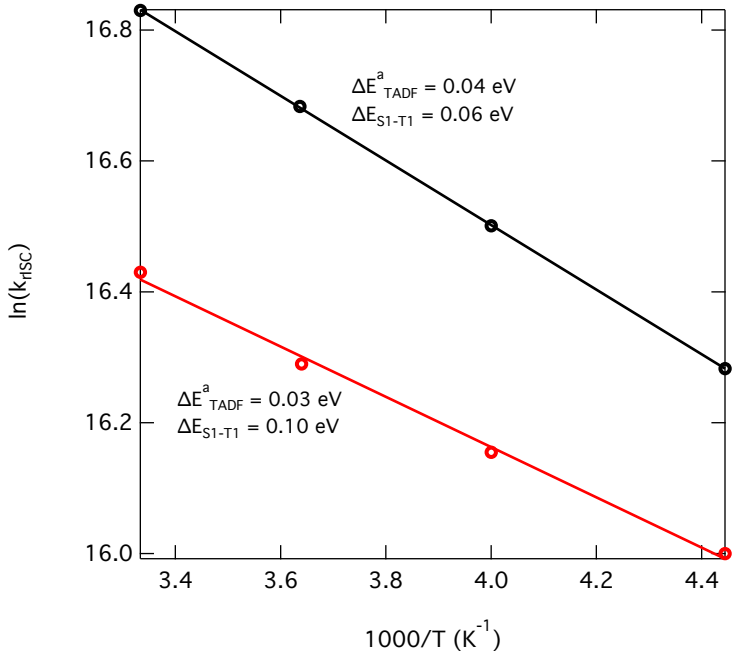

Figure 35: Energy barrier for TADF, determined from the temperature variation of k_{rISC} plotted against 1000/T (K^{-1}) for two models which have $\Delta E_{S_1-T_1} = 0.06$ and 0.1 eV. In the case of the latter, the magnitude of nonadiabatic coupling has been doubled to enable these simulations to exhibit sufficient population transfer to S_1 at lower temperatures (225 K). Figure reproced from ref.[458]

Adachi et al.[459] proposed that this difference is due to conformational changes occurring during the rather long transient lifetime of the triplet excited state. Here, coordinate dependent vibronic coupling, on-diagonal rather than nonadiabatic, alters the adiabatic energy gap between the T_1 and S_1 states. This corresponds to the strong coupling limit in the pioneering paper of Englman and Jortner.[162] However recently, Gibson *et al.*[458] proposed that the nonadiabatic coupling associated with the spin-vibronic mechanism could also play a significant role in this. Indeed, as shown in Figure 35, the nonadiabatic coupling forms an equilibrium between the two lowest triplet states, T_1 (^{3}LE) and T_2 (^{3}CT), which leads to significant population transfer, even without thermal activation. This has the effect of lowering the activation barrier for TADF because, according to second-order perturbation

theory, it becomes dominated by the S_1-T_2 energy gap, rather than the S_1-T_1 energy gap.

The mechanism proposed above is not limited to three excited states. Indeed Marian and co-workers recently studied 3-(9,9-dimethylacridin-10(9H)-yl)-9H-xanthen-9-one (ACRXTN)[460] and 10-Phenyl-10H,10'H-spiro[acridine-9,9'-anthracen]-10'-one (ACRSA).[149] In both of these cases, the important excited states involve CT, $\pi\pi^*$ and $n\pi^*$ states. Indeed in the case of the latter, the authors reported k_{rISC} $\sim 10^9$ s^{-1}, one of the largest rates observed. This is discussed in more detail in section .

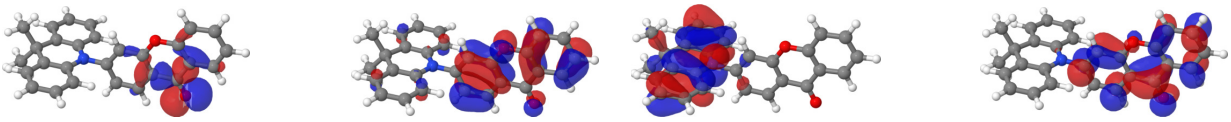

(a) n_O (b) π_{H-1} (c) π_H (d) π_L^*

Figure 36: Frontier orbitals of ACRXTN at the optimised ground-state geometry.

The ACRXTN TADF emitter is composed of an acridine donor and xanthone acceptor. The xanthone unit is well-known for its complicated photophysics,[461–465] and this is further complicated by the addition on the acridine introducing CT states. This emitter has been applied in OLEDs exhibiting low intensity roll-off with increasing currently denstiy[466] and as an assistant dopant in purely organic OLEDs.[467] The former observation suggests a high rate of rISC, minimising the lifetime of the triplet states.

The important molecular orbitals (MOs) of ACRXTN are shown in Fig. 36 and can be grouped as following:

1. MOs that are localised on the xanthone moiety: n_O (Figure 36(a)), π_{H-1} (Figure 36(b)), π_L^* (Figure 36(d)),

2. MOs that are localised on the acridine substituent: π_H (Figure 36(c))

High-level quantum chemistry calculations using DFT/MRCI-R[468,469] show that consequently, the electronic transitions involving these orbitals can be characterised as local xanthone excitations (LEX) and CT transitions. Importantly, the involvement of states with different

character means that TDDFT can struggle to correctly predict the relative ordering of these states, and therefore care should always be taken when calculating the energetics of states with these methods.

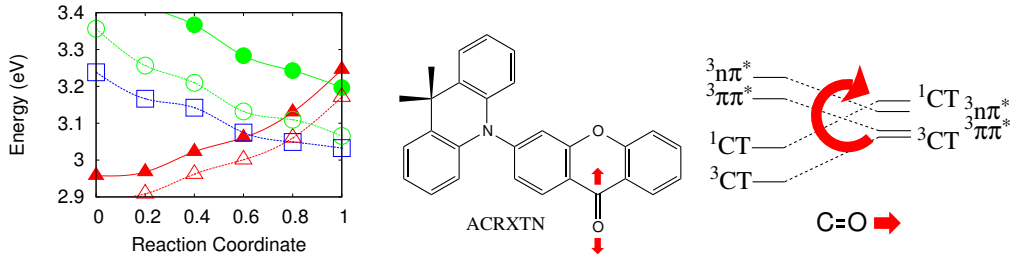

Figure 37: Left:DFT/MRCI-R energy profiles along a linearly interpolated path connecting the singlet CT minimum (R = 0.0) and the minimum of the S($n_O\pi^*$) state (R = 1.0). Solid lines, singlets; dashed lines, triplets; triangles, CT states; circles, $n_O\pi_L^*$ states; squares, $\pi\pi^*$ states with leading $\pi_{H-1}\pi_L^*$ term; Right: Schematic of the proposed ISC and rISC mechanism in ACRXTN, reproduced from ref.[460]

At the excited state geometry of the CT states, the geometry and wave function characteristics are almost identical at the singlet and triplet CT minima, corresponding to nested potentials separated by 0.06 eV and therefore the weak coupling proposed by Jortner and Englman[162] applies. However, as expected the electronic SOCME between these two states is effectively zero, and therefore it seems unlikely this can explain the fast equilibration of the singlet and triplet populations. To overcome this, vibronic coupling to close-by LE states is required. Figure 37 shows the energetic proximity of the five lowest electronically excited states (^{1}CT, ^{3}CT, $T_{\pi\pi^*}$,$T_{n\pi^*}$, $S_{n\pi^*}$) along a linearly interpolated path connecting the ^{1}CT minimum (R = 0.0) and the minimum of the $S_{n\pi^*}$ state. This, as sketched in the inset in Figure 37 and the structural changes are dominated by the elongation of the C=O bond. This clearly shows that this motion drives the potential energy surfaces of the low-lying excited states toward various intersections. Indeed, at the intersection substantial spin–orbit interactions are observed between the ^{1,3}CT and $T_{\pi\pi^*}$. Both of these strongly promote a spin-vibronic mechanism, which explains the rapid rISC, that cannot be explained with the Condon approximation at the CT-optimised geometry.

It is interesting to note that Gibson *et al.* used ρMCTDH in their studies. While this approach rigorously includes the temperature effect it is very computationally expensive because the numerical treatment of density operators is more difficult since the dimensionality of the system formally doubles.[130] In contrast in ref.[149] Lyskov *et al.* exploited the equilibrium which will be formed between singlet and triplet states in a closed quantum system, i.e. one with emission and non-radiative decay not incorporated. This equilibrium between the singlet and triplet manifolds represents the balance between the k_{ISC} and k_{rISC} pathways and it becomes possible to retrieve a rate equation:

$$[S_{all}] = \frac{k_{rISC}}{3(k_{rISC} + k_{ISC})}(1 - \exp^{-(k_{rISC}+k_{ISC})t}) \tag{43}$$

with an equilibrium triplet concentration of $k_{rISC}/3(k_{rISC} + k_{ISC})$ at $t \to \infty$. Fitting this equation to the population kinetics can be used to determine k_{ISC} and k_{rISC}.

Finally, it is emphasized that, as discussed in section , the mechanisms presented above and proposed by in ref.[460] and[149,456] are formally different, the former invoking vibrational spin–orbit, while the latter using derivative coupling. In practice these terms can hardly be told apart, and these studies highlight the importance of not only considering the energetic alignment of the states but also the vibrational motion responsible for coupling and mixing these excited states.

Environment Effect on Spin-Vibronic Dynamics

The involvement of multiple electronic states of different electronic character means that the spin-vibronic mechanism is likely to be strongly affected by the influence of the local embedding environment of the photoexcited molecule. Indeed, excited states exhibiting a larger excited-state dipole moment will be more stabilised by the electrostatic field generated by the solvent. These solvent-induced shifts will mean that the intramolecular potential surfaces are strongly displaced and their crossing points modified and therefore can suppress,

induce and/or accelerate the spin-vibronic mechanism. This effect, in the context of the spin-vibronic mechanism, was first reported by Lim *et al.*[7,470] for the solvent dependent phosphorescence lifetime of several polycyclic monoazines.

Heteroaromatic Compounds

Using the perturbation theory approaches described above, Marian and co-workers calculated the rates of ISC in a series of heteroaromatic compounds.[51–55,150,151,174,175,185,431] In all these systems, ISC is strongly influenced by the environment due to the simultaneous importance of both $n\pi^*$ and $\pi\pi^*$ states which are differently shifted by solvents of higher polarity. Particularly interesting in this respect is the photophysics of flavins and aromatic carbonyl compounds. The authors used two approaches to account for solvation, firstly one based upon purely a continuum solvation model to mimic solute-solvent interactions in non-protic media, and a second for protic solvents which also incorporated explicit solvent molecules forming hydrogen bonds.

Flavins are biologically active photosensitisers which are present, *e.g.* as cofactors in the light-oxygen-voltage (LOV) domains of blue-light receptors.[471,472] Absorption of blue light populates the S_1 state of lumiflavin which is of $\pi\pi^*$ type. In vacuum and apolar environments, a $^3(n\pi^*)$ state, T_2 crosses the S_1 potential close to its minimum, as schematically shown in Fig. 38(a), where an El-Sayed allowed ISC may occur with a computed rate constant of $k_{ISC} \approx 10^9$ s^{-1}. A polar protic solvent such as water forms hydrogen bonds with the lone orbital pairs and lead to a strong blue shift of the $^3(n\pi^*)$ state which is energetically no longer accessible for ISC from the vibrationally relaxed S_1 state. Simultaneously, solvent-solute interactions stabilise a higher-lying $^3(\pi\pi^*)$ state which becomes the T_2 state in aqueous solution (Fig. 38(b)). In Condon approximation, the El-Sayed forbidden $S_1 \rightsquigarrow T_2$ and $S_1 \rightsquigarrow T_1$ transitions are negligible and the S_1 state is predicted to deactivate radiationally by fluorescence. When vibrational SOC is switched on, $S_1 \rightsquigarrow T_2$ is substantially enhanced and proceeds at a rate of $k_{ISC} \approx 10^8$ s^{-1} which is of the same order of magnitude as the flu-

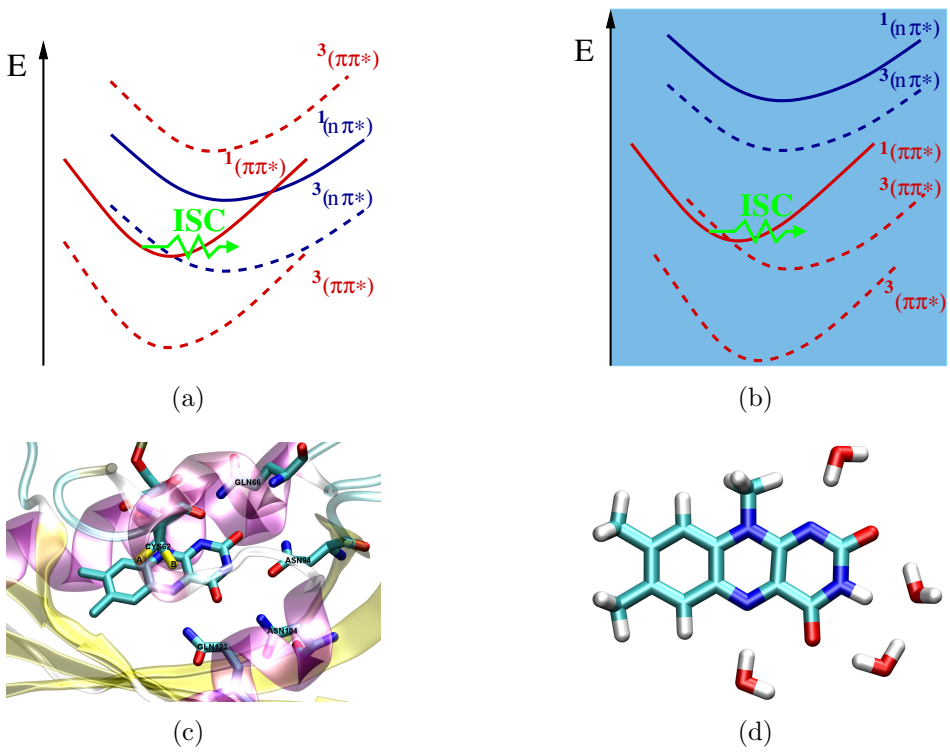

Figure 38: Schematic view of the potential energy surfaces of lumiflavin in (a) vacuum and (b) water solution. (c) Coordination of flavin mononucleotide in the LOV domain of the blue-light sensor YtvA of *Bacillus subtilis* and (d) hydrogen-bonding pattern of lumiflavin in water.

orescence rate. The solvent environment is thus seen to not only change the rate constant of the ISC but also its mechanism.[174] Like water, the protein pocket of the LOV domain forms hydrogen bonds with the flavin molecule (Fig. 38(c) and 38(d)) but the environment is less polar than bulk water with the consequence that the blue shifts of the $n\pi^*$ states are smaller in the protein, thus enabling a participation of these states in the triplet formation.[175]

One class of molecules, for which ISC can occur on the subpicosecond time scale and is thus competitive with IC, comprises the aromatic carbonyl compounds of the xanthone family (Figure 39). What makes the mechanistic picture so involved is the (at least) bi-phasic decay and the strong solvent dependence of the kinetic processes, the observation of recurrences and *inverse energy gap law* behaviour in some cases and the general lack of experimental knowledge on the location and characteristics of optically dark states that could mediate El-Sayed forbidden transitions.[55,432,473–481] A particularly remarkable feature in the

photopysics of the aromatic carbonyl compounds, besides the strong solvent dependence of their radiative and nonradiative relaxation processes, is the $T_2 \rightsquigarrow S_1$ rISC that outcompetes the $T_2 \rightsquigarrow T_1$ IC in certain solute-solvent combinations.[432,477,482] Quantum chemical studies can therefore help elucidating the mechanisms of ISC in these molecules and to understand their solvent dependence.

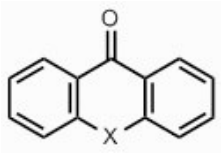

Figure 39: Chemical structures of xanthone (X = O), thioxanthone (X =S), and acridone (X =NH)

Detailed quantum chemical studies on the photophysics of xanthone, thioxanthone, and acridone in the gas phase and in various solvent environments were carried out by Marian group.[51–55] As mentioned before, a continuum model was found to be sufficient for polar aprotic environments such as acetonitrile solution. For an appropriate description of the spectral properties in polar protic solvents such as alcohols and water, a hybrid microsolvation and contiuum solvation model turned out to be necessary.

The excited-state energy landscapes of the aromatic ketones are characterized by close-lying singlet and triplet $\pi\pi^*$ and $n_O\pi^*$ configurations where n_O denotes the lone-pair orbital on the carbonyl oxygen. In vacuum and apolar solvents, $^1n_O\pi^*_L$ constitutes the lowest excited singlet state. The corresponding $^3n_O\pi^*_L$ state is nearly degenerate with the $^3\pi_H\pi^*_L$ state in thioxanthone whereas the larger exchange interaction in xanthone and acridone pushes the $^3\pi_H\pi^*_L$ state below the $^3n_O\pi^*_L$ state in all media. The photophysics of these molecules is controlled by the substantial SOC between the $\pi_H\pi^*_L$ and $n_O\pi^*_L$ configurations and by the large blue shift experienced by the $n_O\pi^*_L$ states in polar media which is even enhanced by the proticity of the solvent (Figure 40). In comparison, the $\pi_H\pi^*_L$ states experience only moderate red shifts. In addition to direct SOC, vibronic SOC plays an essential role in the photophysics of these aromatic ketones. In cases where either the $^1\pi_H\pi^*_L$ and $^1n_O\pi^*_L$ states

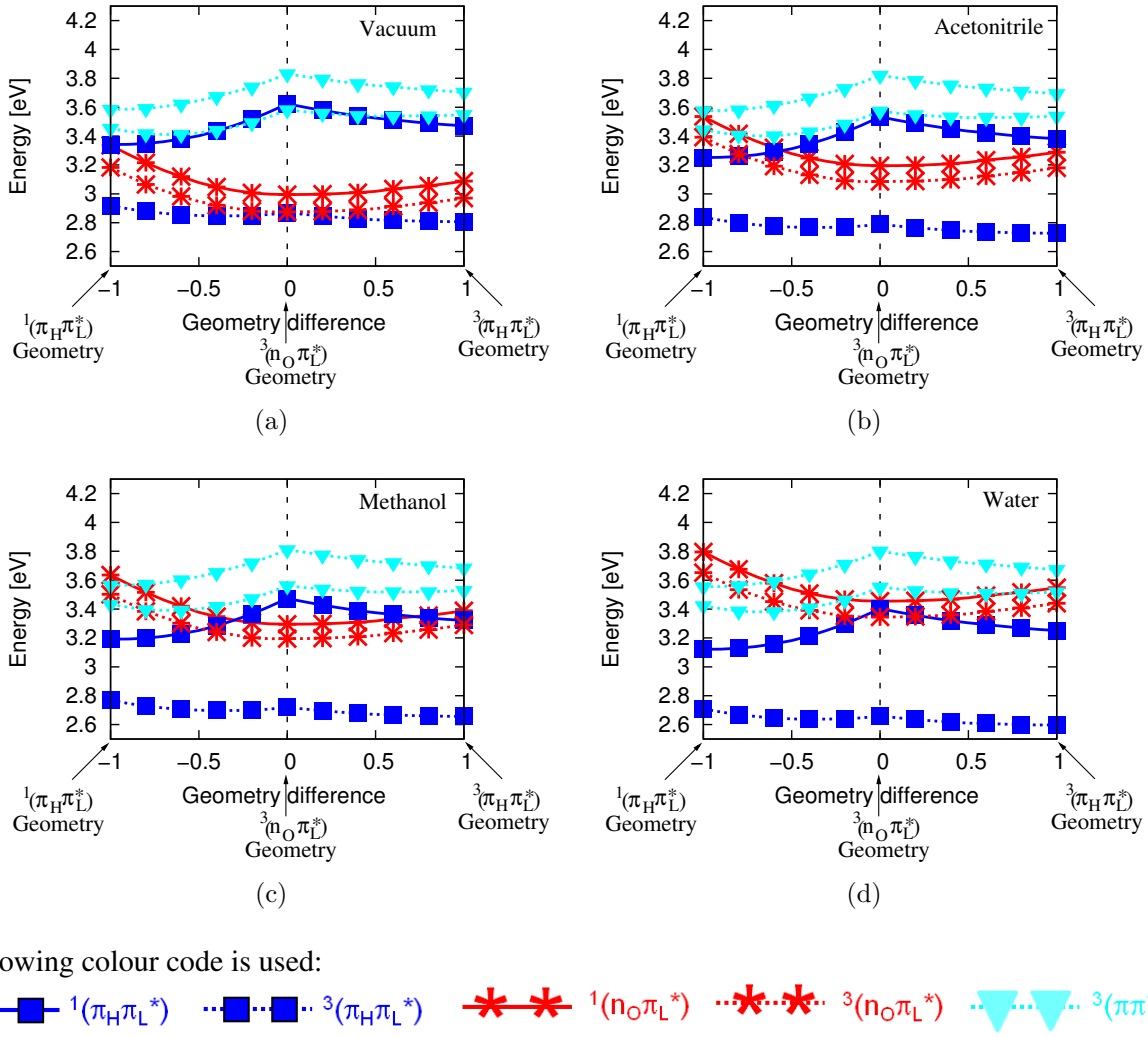

Figure 40: DFT/MRCI energy profiles of electronically excited thioxanthone in various solvents

or the corresponding triplet states are close in energy, even small out-of-plane displacements may lead to a substantial acceleration of El-Sayed forbidden transitions, with rate constants of up to 2×10^{11} s^{-1}. In these systems, DF is brought about by the reverse ISC from the T_2 (!) $^3n_O\pi_L^*$ state to the bright $^1\pi_H\pi_L^*$ state that are tuned into resonance by the surrounding medium.[482]

These studies have established the importance of theory for gaining better insight and understanding of the excited-state processes observed for these compounds in femtosecond

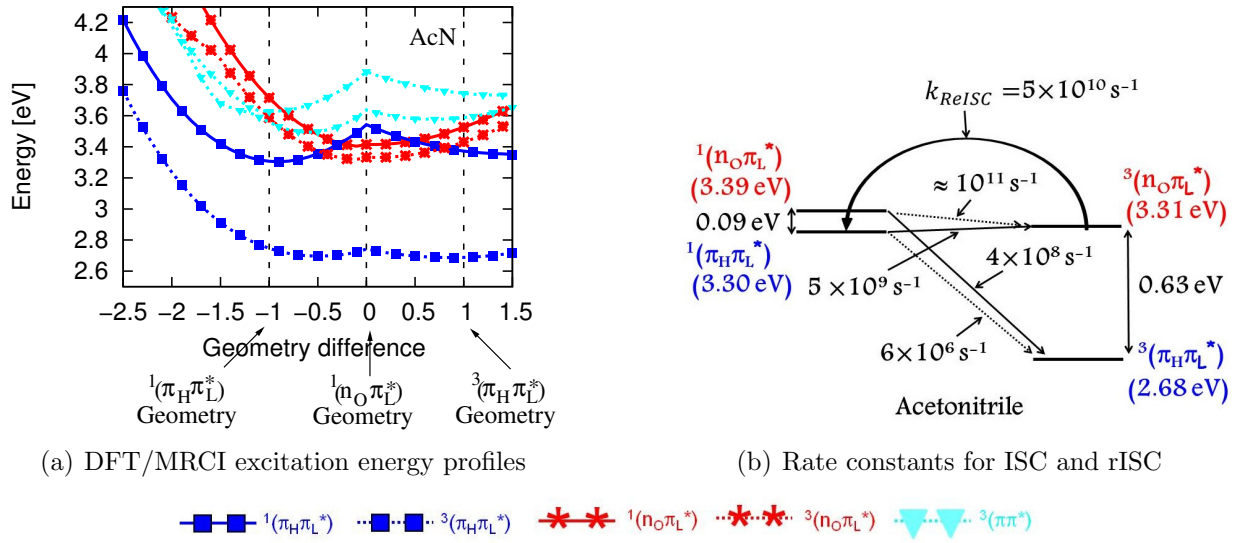

(a) DFT/MRCI excitation energy profiles

(b) Rate constants for ISC and rISC

Figure 41: DFT/MRCI energy profiles and feasible ISC channels of electronically excited acridone in acetonitrile solution. Due to strong vibronic interaction, the El-Sayed forbidden transitions proceed on the subnanosecond timescale.

time-resolved experiments. They could explain the solvent dependence of DF in xanthone[52] and successfully predict the occurrence of DF in thioxanthone in methanol solution.[51,432] The computed ISC rate constants made it possible to discriminate between alternative relaxation pathways in various solvents (methanol, tetrafluoroethanol, cyclohexane), thus aiding to unravel the complex kinetic schemes of the photorelaxation processes in this molecule.[53,55,432] The recent theoretical prediction[54] that the photoexcited acridone may also show DF in acetonitrile solution (Fig. 41) still awaits confirmation.

Transition Metal Systems

The effect of the solvent also plays a significant role for transition metal systems, which often possess states of various different characters, e.g. metal centred (MC) or charge transfer (LMCT, MLCT, etc.). Indeed, for the diplatinum complexes discussed in section 4.1, refs.[238,242] have both shown a strong solvent effect on the rate of ISC, for which the authors suggested that different solvents, most probably with higher polarity, stabilise an intermediate state providing a spin-vibronic channel from the lowest singlet into the lowest triplet

state. Whereas the ultrafast fluorescence decay τ_1 of the Re(I) complexes discussed in section 5.4 is weakly affected by solvent effects, the intermediate time-scales τ_2 may vary from 340-470 fs in acetonitrile to 1.09-1.4 ps in DMF for the Cl and Br substituted complexes, respectively.[483] This effect is hardly explained on the basis of the character and energetics of the involved excited states not really affected by the solvent effects. In contrast solvation dynamics, not included in the simulations discussed in the present review, should play a central role in this case.

Some linear two-coordinate coinage metal complexes show untypical environment effects. The absorption spectra of linear two-coordinate copper complexes of cyclic (alkyl)(amino)-carbenes (CAAC)CuX (X = halide) show negative solvatochromism, characterised by a blue shift in more polar solvents, and their solid-state emission is significantly blue shifted with respect to the solution spectra at room temperature.[355,357,358,484] Similar time- and environment-dependent shifts of the luminescence have been observed for (CAAC)-Au-Cz and (CAAC)-Cu-Cz complexes (Cz=carbazolate).[359]

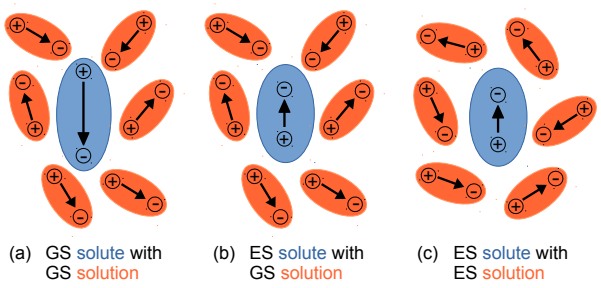

Figure 42: Schematic of the solute-solvent interactions of molecules with negative solvatochromism. (a) The highly polar electronic ground state of the solute molecule is stabilised by the polar environment. (b) The dipolar solvent-solute interactions are unfavourable for the less polar singlet or triplet excited state at short time delays after excitation or if the solvent reorientation is hindered in the solid state. (c) Solvent reorientation stabilises the excited state and leads to a red shift of the luminescence at long time delays.

Such behaviour has been rationalised recently by Föller and Marian.[361] Both types of complexes are characterised by very polar charge density distributions in the electronic ground state with the negative pole residing on the X and Cz ligands, respectively. Solute-solvent

interactions in the electronic ground and excited states are shown pictorially in Figure 42. Before electronic excitation takes place, the solid state environment and the liquid solution are well adapted to the charge distribution of the solute in the electronic ground state (Figure 42 (a)). Electronic excitation is an ultrafast process, much too fast for the solvent to reorganise instantaneously. Excitation of the linear two-coordinate complex to S_1 or T_1 moves charge from the X[355] or Cz[361] ligands to the metal center and the (CAAC) ligand. This means that the excited states do not only have much smaller static dipole moments than the electronic ground state, they also point in opposite direction. This unfavourable solute-solvent interaction explains the negative solvatochromism in absorption. In quantum chemical calculations, these electrostatic effects are well represented by continuum models such as PCM.[485] Emission of a photon is accompanied by geometry relaxation in the excited state as well as solvent reorganization. Both processes contribute to the Stokes shift, but occur on different time scales. Relaxation of the nuclear arrangement of the solute typically takes place at the subpicosecond time scale. Therefore, emission wavelengths measured in femtosecond time-resolved experiments at short delays after electronic excitation mainly reflect the solvent orientation adapted to the ground-state electron distribution (Figure 42 (b)). Because of their long luminescence decay times, solvent reorganisation is particularly important in phophorescence and TADF emitters. The time required to fully achieve solvent reorganisation (Figure 42 (c)) depends on various parameters such as the viscosity and the temperature of the medium. In the solid state (frozen solutions, films or crystalline environment), solvent reorientation is sterically hindered. For this reason, delayed luminescence in the solid state is expected to be blue shifted with respect to luminescence in liquid solution, in agreement with the experimental findings. To model the emission at longer time delays (nanosecond to microsecond time scale) in liquid solution, adaptation of the solvent environment to the charge distribution of the solute's excited state has to be taken into account. In principle, this could be achieved by QM/MM simulations, but excited-state QM/MM molecular dynamics for such long time intervals are computationally very

demanding. Alternatively, one can make use of the corrected linear response polarizable continuum model (cLR-PCM)[486] or other state-specific solvent approaches[487] in quantum chemical calculations.

Environment Effects on Metal-Free TADF Emitters

A number of studies both in solution[488] and the solid state[453,489–495] have demonstrated the effect of the local embedding environment on the photophysics of TADF molecules. This can be easily understood from the theory work[149,456,460] discussed in section . Indeed, because TADF is not simply a cyclic process between the singlet and triplet CT manifolds, but involves coupling to other states of different character and therefore different dipole moments this means that the relative shift of the states as a function of polarity will be different and crucially this will alter the gap between these states and is likely to significantly change the efficiency of TADF.

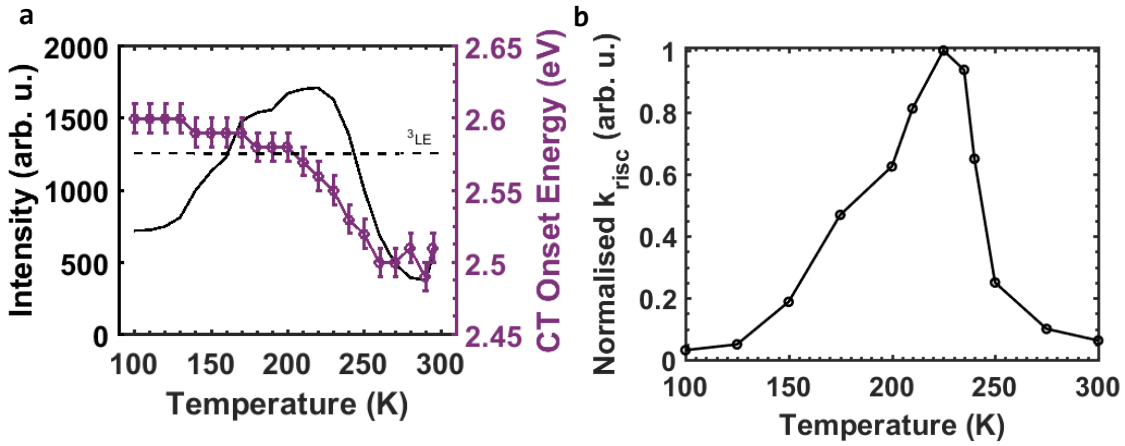

Figure 43: The temperature dependence of the intensity (black line) and CT onset energy (purple circles). The change in CT onset energy plateaus below the glass temperature, representative of the PEO film becoming rigid. The black dashed line represents the energy of the ^{3}LE at 2.58eV, with the peak in intensity apparent as the CT energy crosses resonance. b) Relative rate of rISC as a function of temperature for the D-A complex PTZ-DPTO2. The rates were extracted from the population of the 1CT state at 0.5 ns of dynamics simulations initiated from the lowest triplet state. Reproduced from ref.[492]

Indeed, in the case of PTZ-DBTO2 (section) importance of the ^{1,3}CT states, both of which will respond in the same way to changing polarity, and the ^{3}LE which will be insinuative to polarity of the environment, gives three distinct scenarios: a) the LE below the CT states, b) the LE degenerate with the CT states and c) the LE above the CT states. Clearly TADF will be most effective in the case when all three states are degenerate and mixing is most effective. Recently Etherington *et al.* used photoinduced absorption[492] to demonstrate this effect and its effect on the spin-vibronic mechanism of the D-A-D trimer analogue of PTZ-DBTO2, which gives identical photophysics to the D-A version. The TADF emitter was embedded within a polyethylene oxide (PEO) host, which importantly exhibits a temperature dependent polarity. As shown in Figure 43, by cooling the sample, it was possible to shift the onset of the ^{1}CT to higher energies, initially to bring it into degeneracy with the ^{3}LE state and then above. Figure 43a shows the integrated intensity of delayed fluorescence as a function of temperature, showing, as expected, a peak at the point of degeneracy. This is supported by simulations showing the relative rate of rISC as a function of temperature (Figure 43b) using the spin-vibronic mechanism.

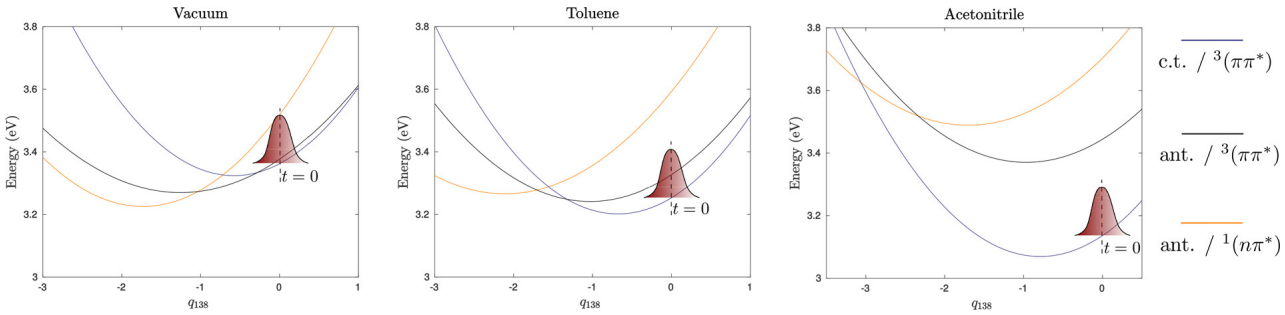

Figure 44: One-dimensional q_{138} cut through excited PESs of ACRSA in different environments. Reproduced from ref.[149]

Recently, the effect of the polarity has been simulated for ACRSA.[149] The authors used a spin-vibronic Hamiltonian and quantum nuclear dynamics to study the rate of ISC using a Hamiltonian which depended on solvation. In this case, the effect of polarity was described in an implicit manner, with a polarisable continuum model.[496]

Figure 44 shows the important $^1n\pi^*$, $^3\pi\pi^*$ and CT states along the normal mode responsible for the structural change between the $^1n\pi^*$ and $^3\pi\pi^*$ states. Importantly, while the shape of the curves remains similar, as supported by the expansion parameters of the Hamiltonian given in ref.,[149] the relative separation of the potentials changes dramatically due to the different dipole moments of the three excited states.

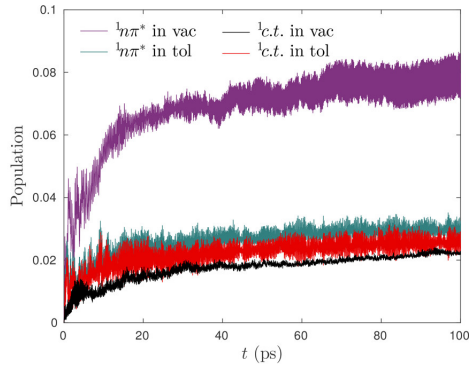

(a) Vacuum and toluene

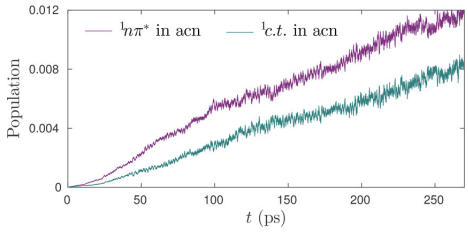

(b) Acetonitrile

Figure 45: Time-dependent population of the singlet excited states of ACRSA in vacuum, toluene, and acetonitrile following the triplet CT exciton formation. Reproduced from ref.[149]

Figure 45 shows the effect of this on the time-dependent population of the singlet excited states of ACRSA. As expected the population is fastest in low polarity solvents where the states are closest together, in agreement with finding of ref.[492] Interestingly, in the case of ACRSA, the authors reported $k_{rISC} \sim 10^9$ s^{-1}, one of the largest rates observed, and which is achieved because of the interaction between the low lying CT, $\pi\pi^*$ and $n\pi^*$ states. A polar environment such as acetonitrile destabilises $n\pi^*$ energies and stabilises CT exciton energies, by that deteriorating the efficient rISC pathway. The rate constants $k_{rISC} \sim 2 \times 10^7$ s^{-1} and $k_{ISC} \sim 5 \times 10^8$ s^{-1} for ACRSA in that solvent[149] are not much different from corresponding

values in the related spiro-acridine compound 10-phenyl-10H-spiro[acridine-9,9'-fluorene]-2'-7'-dicarbonitrile (ACRFLCN) which features a low-lying LE $^3(\pi\pi^*)$ state but lacks low-lying $n\pi^*$ states and for which a value of $k_{ISC} \sim 7 \times 10^7$ s^{-1} was reported.[497]

Summary and Outlook

In this review, we have summarised the recent work shedding new insight onto the spin-vibronic mechanism of intersystem crossing. Although the underpinning theory of this mechanism was established in the 1960's, it is only now, with the development of ultra-fast spectroscopies and high-level theoretical tools, that the importance of this phenomenon in a wide variety of molecular systems is being established.

These experimental and theoretical studies have unequivocally demonstrated that the interpretation of ISC dynamics is often not possible using simple qualitative analysis based upon empirical rules, such as the energy gap law and El-Sayed's rule. In such situations one must go beyond the assumptions based upon ISC driven only by direct SOC between states of different multiplicity, in which the coupling remains unchanged by vibrational motion, i.e. the Condon approximation. Indeed, the often strongly nonadiabatic nature of electronic excited states means that the spin, electronic and vibrational dynamics of the system cannot be described independently. Molecular excited states therefore cannot be well represented by a simple ladder of states, as depicted in a usual Jablonski diagram. Instead, the interplay amongst spin, electronic and nuclear dynamics leads to mixing and consequently to rather complicated spin-vibronic levels. This applies to molecules both with and without the presence of heavy elements.

Probing and understanding these effects in increasingly complicated systems calls for the use of new experimental techniques and more importantly for an increasing synergy between both complementary experimental techniques, and high-level theory that can underpin the experimental interpretation. New experimental procedures, such as multi-dimensional elec-

tronic spectroscopy and femtosecond X-ray spectroscopy, are offering new horizons complimentary to more established techniques such as transient optical absorption, time-resolved fluorescence spectroscopy and time-resolved vibrational spectroscopy. Indeed these are in principle capable of not only probing the correlated spin-vibronic dynamics, but also of directly probing the spin-vibronic couplings.

In the area of theory, there has been much progress including the ability to calculate the important coupling elements across a broad spectrum of quantum chemistry techniques incorporating an almost full selection of trade-off between accuracy and computational expense. It is possible to calculate the rate of spin-vibronic processes using either perturbation theory approaches or by explicit propagation of the nuclear equations of motion. For the former, spin-vibronic effects up to second order can be included alongside temperature and the effects of an environment. Compared to approaches based upon dynamics, the computational efficiency of these approaches means that it can be routinely applied to larger chemical systems.

In terms of approaches based upon nuclear dynamics, the power of grid-based quantum dynamics, which exploit model spin-vibronic Hamiltonians, has been repeatedly demonstrated. At the same time there has also been significant development in *on-the-fly* approaches, which now offer the ability to perform simulations on full dimensional potential energy surfaces and to include atomistic descriptions of the solvent environment. When comparing the two methods it is important to keep in mind that the calculation of the potentials for quantum dynamics are usually based upon interpolated models along a reduced number of collective vibrational modes. In contrast, the *on-the-fly* simulations require computations of the energies, forces, and nonadiabatic couplings at each time step of the dynamics. This implies a very different computational load for the two approaches. In this case, one has to be careful about the level of quantum chemistry used for the *on-the-fly* simulations, as generally many more quantum chemistry calculations are required, which can make the simulations prohibitive. While this is also true for grid based quantum dynamics on models, for

the latter one can also manipulate the parameters of the model to understand the physics behind the spin-vibronic mechanism. This is much harder for *on-the-fly* approaches.

In addition in terms of mechanistic understanding of spin-vibronic dynamics, although these *on-the-fly* approaches offer the ability to perform dynamics within full nuclear configuration space, for complex systems, direct analysis of the results can become quite cumbersome due to high dimensionality, especially in terms of determining the important nuclear motions and their effect. This places a greater emphasis on the quality of the post-processing of the simulations. Most importantly, it is emphasised that in many cases grid based and *on-the-fly* approaches offer completely contrasting approximations and therefore there is a huge merit in increasing the synergy of these approaches and use the *on-the-fly* approaches to build high-level first principles models.[206,498]

The criticality of spin-vibronic coupling within functional materials, such as TADF, demonstrated herein represents an important subset of a much broader research question, namely how do we efficiently exploit the excited-state properties of molecules? This is the core focus of a significant research effort aimed at a wide range of applications, such as organic and dye-sensitised solar cells, photocatalysis, OLEDs and fluorescent imaging. At present, the design of new molecules that act as the key components of these devices has largely focused upon large-scale synthetic programs aimed at developing and then exploiting structure-property relationships. However, while this can lead to incremental progress and simple design rules that can be used to manipulate a specific property, such as emission or absorption wavelength, it is usually unsuccessful in simultaneously controlling all of the required photophysical properties. This is, at least in part, due to the close interplay amongst spin, electronic and nuclear dynamics leading to mixing and rather complicated spin-vibronic levels. Consequently, to ensure continued progress in applied research fields, design procedures that go beyond the Born-Oppenheimer approximation and which explicitly take spin-vibronic couplings into account are required.

The design of new molecules can be achieved computationally, using for example virtual

high-throughput screening and has the potential to significantly speed-up material discovery. Recently, Gomez *et al.*[499] developed a virtual screening method for TADF emitters (although this can be more generally applied) with the capacity to explore the chemical space of 1.6 million molecules. However, at the heart of these approaches are a number of criteria for specific molecular properties and therefore as for experimental design, a detailed understanding of the key components of spin-vibronic must be achieved to optimise the design of these so called descriptors. Calculating couplings, both spin-orbit and nonadiabatic is obviously significantly much more computationally expensive and therefore high-throughput design adopting this approach is unlikely. We therefore recommend that such approaches could be included as an additional *medium throughput* refining step in such procedure.

Finally, we want to stress that, as shown by various examples discussed in this review, spin and vibronic coupling interplay are at work in both light organic compounds and molecular systems containing heavy-element. Internal conversion and intersystem crossing may act on a similar, ultrafast, time-scale calling for a balanced and intertwined theoretical description able to decipher the intricate mechanism of ultrafast excited-state processes, in conjunction with new experimental techniques.

Acknowledgement

TJP acknowledges the EPSRC, Projects EP/N028511/1 and EP/P012388/1 and the Leverhulme Trust, Project RPG-2016-103, for funding. CM thanks the Deutsche Forschungsgemeinschaft (MA1051/17-1 and INST 208/704-1 FUGG) and the Anton Beetz-Stiftung for financial support. CD and EG thank ANR-10-LABX-0026 Chimie des Systmes Complexes and ANR-15-CE29-0027-01 DeNeTheor as well as the Frontier Research in Chemistry Foundation, Strasbourg.

Author Biographies

Thomas Penfold was awarded his Ph.D. in 2010 from the University of Birmingham, United Kingdom, under the guidance of Prof. Graham Worth. He subsequently joined the group of Prof. Majed Chergui at the École Polytechnique Fédérale de Lausanne, Switzerland before two years within the SwissFEL project at the Paul Scherrer Institut, Switzerland. He joined Newcastle University in 2015 at Lecturer in Theoretical and Computational Chemistry. His current research interests include quantum dynamics, time-resolved spectroscopy and excited state dynamics of organic and inorganic systems.

Etienne Gindensperger received his Ph.D. in 2004 from the University Paul Sabatier, Toulouse, France, under the supervision of Profs. C. Meier and A. J. Beswick. He then joined the Theoretical Chemistry group of Prof. L. S. Cederbaum at the University of Heidelberg, Germany, as a Alexender von Humbold fellow. Since 2007, he has been CNRS-researcher at the Laboratoire de Chimie Quantique, Institut de Chimie, University of Strasbourg, France. His current interests are focused on the theoretical description of ultrafast photoinduced processes in organic and inorganic systems.

Chantal Daniel received her Ph.D. in 1985 from the University of Strasbourg. She joined the group of Keiji Morokuma at IMS, Okazaki, Japan, in 1986 as JSPS fellow and then the IBM Department in Kingston, NY, USA, as postdoctoral associate of Michel Dupuis in 1988. Since 1999, she has been CNRS-researcher at the Laboratoire de Chimie Quantique as Directeur de Recherche. Current interests are excited state properties in transition metal complexes and modeling and simulation of photochemical and photophysical properties of molecules in complex environments.

Christel M. Marian graduated in 1980 with a Ph.D in Theoretical Chemistry at the University of Bonn, Germany, under the supervision of Sigrid D. Peyerimhoff. After a post-

doctoral stay in the group of Per E. M. Siegbahn at Stockholm's University, Sweden, she became Assistant Professor at the University of Bonn where she completed her Habilitation in 1991. She headed the Computational Chemistry team at the Fraunhofer Scientific Computing and Algorithms Institute (SCAI) in Sankt Augustin, Germany, before joining the Heinrich-Heine-University Düsseldorf, Germany, as a Full Professor of Theoretical and Computational Chemistry in 2001. Since 2014 she is a regular member of the North-Rhine Westphalian Academy of Sciences and Arts. Her current research interests center on the development and application of theoretical and computational excited-state electronic structure methods, with a particular emphasis on spin-forbidden transitions.

Glossary

IC: internal conversion

ISC: intersystem crossing

rISC: reverse ISC

PES: potential energy surfaces

QD: quantum dynamics

MD: molecular dynamics

SOC: spin-orbit coupling

BO: Born-Oppenheimer

SOCME: SOC-matrix element

ECPs: effective core potentials

SOECPs: spin-orbit ECPs

DFT: density functional theory

TDDFT: time dependent DFT

UDFT: unrestricted DFT

LR-TDDFT: linear-response TDDFT

MSD: model space diabatization

FC: Franck-Condon

FCWD: FC weighted density of states

FCFs: FC factors

VDOS: vibrational density of states

DF: delayed fluorescence

TADF: thermally activated DF

TDSE: time-dependent Schrdinger equation

CI: configuration interaction

MRCI: multireference CI

MRCI-S: MRCI single

MRCI-R: MRCI redesigned

MCTDH: multi-configurational time-dependent Hartree

SPFs: single particle functions

ML-MCTDH: multi-layer MCTDH

SPDO's: single-particle density operators

LVC: linear vibronic coupling

QVC: quadratic vibronic coupling

DRE: Duschinsky rotation effects

TSH: trajectory surface hopping

QM/MM: quantum mechanics/molecular mechanics

GWP: Gaussian wavepacket

CCS: coupled-coherent states

MCE: multi-configurational Ehrenfest

vMCG: variational multi-configurational Gaussian wavepacket

GPUs: graphical processing units

ESA: excited state absorption

2D-IR: 2-dimensional infrared

FSRS: femtosecond stimulated Raman scattering

BB-IVS: broad band impulsive vibrational spectroscopy

CT: charge transfer

MLCT: metal-to-ligand CT

LLCT: ligand-to-ligand CT

LMCT: ligand-to-metal CT

XLCT: X to ligand CT

MC: metal-centered

IL: intra-ligand

LC: ligand-centered

LE: local excited

LEX: local xanthone excitations

2D-ES: 2-dimensional electronic spectroscopy

X-FELS: X-ray free electron lasers

HHG: high harmonic generation

RXES: X-ray emission spectroscopy

RIXS: Resonant Inelastic X-ray scattering

DSSCs: dye-sensitized solar cells

OLEDs: organic light-emitted diodes

JT: Jahn-Teller

PJT: pseudo-JT

LIESST: light-induced excited spin-state trapping

LEECs: light emitting electrochemical cells

RASI: rotationally assisted spin-state inversion

CMA : carbine-metalamide

TRPES: time-resolved photoelectron spectroscopy

CASSCF: complete-active-space self-consistent-field

MS-CASPT2: multi-state CAS second order perturbation theory

CC2: coupled cluster doubles

SCS-CC2: spin component scaled CC2

PDT: photodynamic therapy

FBP: free-base porphyrin

LOV: light oxygen voltage

DMF: dimethyl formamide

PCM: polarizable continuum model

cLR-PCM: corrected linear response PCM

PEO: polyethylene oxide

References

(1) Kasha, M. Phosphorescence and the Role of the Triplet State in the Electronic Excitation of Complex Molecules. *Chem. Rev.* **1947**, *41*, 401–419

.

(2) Kasha, M. Energy transfer mechanisms and the molecular exciton model for molecular aggregates. *Radiat. Res.* **1963**, *20*, 55–70

.

(3) Kasha, M. Characterization of electronic transitions in complex molecules. *Discuss Faraday Soc.* **1950**, *9*, 14–19

.

(4) El-Sayed, M. Spin Orbit Coupling and the Radiationless Processes in Nitrogen Heterocyclics. *J. Chem. Phys.* **1963**, *38*, 2834–2838

.

(5) Albrecht, A. Vibronic Spin-Orbit Perturbations and the Assignment of the Lowest Triplet State of Benzene. *J. Chem. Phys.* **1963**, *38*, 354–365

.

(6) Lim, E.; Jack, M. Vibronic Interaction between (n, π^*) and (π, π^*) States and Spin Orbit Coupling in Nitrogen Heterocyclics. *J. Chem. Phys.* **1966**, *45*, 4742–4743

.

(7) Lim, E.; Yu, J. M. Vibronic Spin–Orbit Interactions in Heteroaromatic Molecules. II. Phosphorescence of Quinoxaline and Other Diazanaphthalenes. *J. Chem. Phys.* **1968**, *49*, 3878–3884

.

(8) Henry, B. R.; Siebrand, W. Spin–Orbit Coupling in Aromatic Hydrocarbons. Calculation of the Radiative Triplet Lifetimes of Naphthalene, Anthracene, and Phenanthrene. *J. Chem. Phys.* **1969**, *51*, 2396–2405

.

(9) Henry, B. R.; Siebrand, W. Spin–Orbit Coupling in Aromatic Hydrocarbons. Analysis of Nonradiative Transitions between Singlet and Triplet States in Benzene and Naphthalene. *J. Chem. Phys.* **1971**, *54*, 1072–1085

.

(10) Rose, B. D.; Shoer, L. E.; Wasielewski, M. R.; Haley, M. M. Unusually short excited state lifetimes of indenofluorene and fluorenofluorene derivatives result from a conical intersection. *Chem. Phys. Lett.* **2014**, *616*, 137–141

.

(11) Kamkaew, A.; Lim, S. H.; Lee, H. B.; Kiew, L. V.; Chung, L. Y.; Burgess, K. BODIPY dyes in photodynamic therapy. *Chem. Soc. Rev.* **2013**, *42*, 77–88

.

(12) Singh-Rachford, T. N.; Castellano, F. N. Photon upconversion based on sensitized triplet–triplet annihilation. *Coord. Chem. Rev.* **2010**, *254*, 2560–2573

.

(13) Shatruk, M.; Phan, H.; Chrisostomo, B. A.; Suleimenova, A. A. Symmetry-breaking structural phase transitions in spin crossover complexes. *Coord. Chem. Rev.* **2015**, *289*, 62–73

.

(14) Bertoni, R.; Cammarata, M.; Lorenc, M.; Matar, S. F.; Létard, J.-F.; Lemke, H. T.; Collet, E. Ultrafast Light-induced Spin-State Trapping Photophysics Investigated in Fe (phen) 2 (NCS) 2 Spin-crossover Crystal. *Acc. Chem. Res.* **2015**, *48*, 774–781

.

(15) Ohkoshi, S.-i.; Tokoro, H. Photomagnetism in cyano-bridged bimetal assemblies. *Acc. Chem. Res.* **2012**, *45*, 1749–1758

.

(16) Knoll, J. D.; Turro, C. Control and Utilization of Ruthenium and Rhodium Metal Complex Excited States for Photoactivated Cancer Therapy. *Coord. Chem. Rev.* **2015**, *282*, 110–126

.

(17) Blanco-Rodríguez, A.M.; Busby, M. ; Gradinaru, C. ; Crane, B.R. ; Di Bilio, A.J. ; Matousek, P. ; Towrie, M. ; Leigh, B.S. ; Richards, J.H.; Vlcek, A.; et al. Excited-State Dynamics of Structurally Characterized [ReI (CO) 3 (phen)(HisX)]+(X= 83, 109) Pseudomonas a eruginosa Azurins in Aqueous Solution. *J. Am. Chem. Soc.* **2006**, *128*, 4365–4370

.

(18) Aliprandi, A.; Mauro, M.; De Cola, L. Controlling and imaging biomimetic self-assembly. *Nat. Chem.* **2016**, *8*, 10

.

(19) Wang, C.; Qin, J.; Shen, X.; Riedel, R.; Harms, K.; Meggers, E. Asymmetric Radical–Radical Cross-Coupling through Visible-Light-Activated Iridium Catalysis. *Angew. Chem. Int. Ed.* **2016**, *55*, 685–688

.

(20) Goswami, S.; Gish, M. K.; Wang, J.; Winkel, R. W.; Papanikolas, J. M.; Schanze, K. S. π-Conjugated Organometallic Isoindigo Oligomer and Polymer Chromophores: Singlet and Triplet Excited State Dynamics and Application in Polymer Solar Cells. *ACS Appl. Mater. Interfaces* **2015**, *7*, 26828–26838

.

(21) Chen, Z.; Hsu, H.-Y.; Arca, M.; Schanze, K. S. Triplet Energy Transport in Platinum-acetylide Light Harvesting Arrays. *J. Phys. Chem. B* **2014**, *119*, 7198–7209

.

(22) Zewail, A. H. Laser Femtochemistry *Science* **1988**, *242*, 1645–1653

.

(23) Zewail, A. H. Femtochemistry: Atomic-Scale Dynamics of the Chemical Bond. *J. Phys. Chem. A* **2000**, *104*, 5660–5694

.

(24) Mukamel, S. *Principles of Nonlinear Optical Spectroscopy*; Oxford University Press, USA, 1995

.

(25) Chergui, M. On the Interplay Between Charge, Spin and Structural Dynamics in Transition Metal Complexes. *Dalton Trans.* **2012**, *41*, 13022–13029

.

(26) Cannizzo, A.; Milne, C. J.; Consani, C.; Gawelda, W.; Bressler, C.; van Mourik, F.; Chergui, M. Light-induced spin crossover in Fe(II)-based complexes: The Full Photocycle Unraveled by Ultrafast Optical and X-ray Spectroscopies *Coord. Chem. Rev.* **2010**, *254*, 2677–2686

.

(27) Zhang, W. ; Alonso-Mori, R. ; Bergmann, U. ; Bressler, C. ; Chollet, M.; Galler, A. ; Gawelda, W.; Hadt, R.G. ; Hartsock, R.W. ; Kroll, T. et al. Tracking Excited State Charge and Spin Dynamics in Iron Coordination Complexes *Nature* **2014**, *509*, 345–348

.

(28) Auböck, G.; Chergui, M. Sub-50-fs Photoinduced Spin Crossover in [Fe (bpy) 3] 2+ *Nat. Chem.* **2015**, *7*, 629–633

.

(29) Lemke, H. T.; Kjær, K. S.; Hartsock, R.; Van Driel, T. B.; Chollet, M.; Glownia, J. M.; Song, S.; Zhu, D.; Pace, E.; Matar, S. F. et al. Coherent Structural Trapping Through Wavepacket Dispersion During Photoinduced Spin State Switching. *Nat. Comm.* **2017**, *8*, 15342

.

(30) Consani, C.; Prémont-Schwarz, M.; ElNahhas, A.; Bressler, C.; van Mourik, F.; Cannizzo, A.; Chergui, M. Vibrational Coherences and Relaxation in the High-Spin State of Aqueous $[Fe^{II}(bpy)_3]^{2+}$ *Angew. Chem. Int. Ed.* **2009**, *48*, 7184–7187

.

(31) McCusker, J. K.; Walda, K.; Dunn, R.; Simon, J.; Magde, D.; Hendrickson, D. Sub picosecond 1MLCT-5T2 Intersystem Crossing of Low-Spin Polypyridyl Ferrous Complexes *J. Am. Chem. Soc.* **1993**, *115*, 298–307

.

(32) Bressler, C.; Milne, C. J.; Pham, V.-T.; el Nahhas, A.; van der Veen, R. M.; Gawelda, W.; Johnson, S. L.; Beaud, P.; Grolimund, D.; Kaiser, M.; et al. Femtosecond XANES Study of the Light-Induced Spin Crossover Dynamics in an Iron(II) Complex *Science* **2009**, *323*, 489–492

.

(33) Cannizzo, A.; Blanco-Rodriguez, A. M.; El Nahhas, A.; Szebera, J.; Zalis, S.; Vlček, A., Jr; Chergui, M. Femtosecond Fluorescence and Intersystem Crossing in Rhenium (I) Carbonyl- Bipyridine Complexes. *J. Am. Chem. Soc.* **2008**, *130*, 8967–8974

.

(34) van der Veen, R. M.; Cannizzo, A.; van Mourik, F.; Vlček Jr, A.; Chergui, M. Vibrational Relaxation and Intersystem Crossing of Binuclear Metal Complexes in Solution. *J. Am. Chem. Soc* **2011**, *133*, 305–315

.

(35) Takezaki, M.; Hirota, N.; Terazima, M. Nonradiative Relaxation Processes and Electronically Excited States of Nitrobenzene Studied by Picosecond Time-Resolved Transient Grating Method. *J. Phys. Chem. A* **1997**, *101*, 3443–3448

.

(36) Takezaki, M.; Hirota, N.; Terazima, M. Relaxation of Nitrobenzene from the Excited Singlet State. *J. Chem. Phys.* **1998**, *108*, 4685–4686

.

(37) Morales-Cueto, R.; Esquivelzeta-Rabell, M.; Saucedo-Zugazagoitia, J.; Peon, J. Singlet Excited-State Dynamics of Nitropolycyclic Aromatic Hydrocarbons: Direct Measurements by Femtosecond Fluorescence Up-Conversion. *J. Phys. Chem. A* **2007**, *111*, 552–557

.

(38) Zugazagoitia, J. S.; Almora-Díaz, C. X.; Peon, J. Ultrafast Intersystem Crossing in 1-nitronaphthalene. An Experimental and Computational Study. *J. Phys. Chem. A* **2008**, *112*, 358–365

.

(39) Zugazagoitia, J. S.; Collado-Fregoso, E.; Plaza-Medina, E. F.; Peon, J. Relaxation in the Triplet Manifold of 1-Nsitronaphthalene Observed by Transient Absorption Spectroscopy. *J. Phys. Chem. A* **2009**, *113*, 805–810

.

(40) Reichardt, C.; Vogt, R. A.; Crespo-Hernández, C. E. On the Origin of Ultrafast Nonradiative Transitions in Nitro-polycyclic Aromatic Hydrocarbons: Excited State Dynamics in 1-nitronaphthalene. *J. Chem. Phys.* **2009**, *131*, 224518

.

(41) Crespo-Hernández, C. E.; Burdzinski, G.; Arce, R. Environmental Photochemistry of Nitro-PAHs: Direct Ibservation of Ultrafast Intersystem Crosing in 1-nitropyrene. *J. Phys. Chem. A* **2008**, *112*, 6313–6319

.

(42) Heinz, B.; Schmierer, T.; Laimgruber, S.; Gilch, P. Excited State Processes of Nitrobenzaldehydes Probed by Ultrafast Fluorescence and Absorption Spectroscopy. *J. Photochem. Photobio. A.* **2008**, *199*, 274–281

.

(43) Cheng, S.; Song, P.; Yang, S.; Yin, H.; Han, K. Fluorescence and Solvent-Dependent Phosphorescence Studies of *o*-nitrobenzaldehyde: A Combined Experimental and Theoretical Investigation. *Phys. Chem. Chem. Phys.* **2010**, *12*, 9067–9074

.

(44) Vogt, R. A.; Reichardt, C.; Crespo-Hernández, C. E. Excited-State Dynamics in Nitro-Naphthalene Derivatives: Intersystem Crossing to the Triplet Manifold in Hundreds of Femtoseconds. *J. Phys. Chem. A* **2013**, *117*, 6580–6588

.

(45) Vogt, R. A.; Crespo-Hernández, C. E. Conformational Control in the Population of the Triplet State and Photoreactivity of Nitronaphthalene Derivatives. *J. Phys. Chem. A* **2013**, *117*, 14100–14108

.

(46) Larsen, M. A. B.; Thøgersen, J.; Stephansen, A. B.; Peon, J.; Sølling, T. I.; Keiding, S. R. Transient IR Spectroscopic Observation of Singlet and Triplet States of 2-Nitrofluorene: Revisiting the Photophysics of Nitroaromatics *J. Phys. Chem. A* **2016**, *120*, 28–35

.

(47) Orozco-Gonzalez, Y.; Coutinho, K.; Peon, J.; Canuto, S. Theoretical Study of the Absorption and Nonradiative Deactivation of 1-nitronaphthalene in the Low Lying Singlet and Triplet Excited States Including Methanol and Ethanol Solvent Effects. *J. Chem. Phys.* **2012**, *137*, 054307

.

(48) Giussani, A. Understanding of the Photophysics and Photochemistry of 1-Nitronaphthalene under Solar Radiation: The First Theoretical Evidence of a Photodegradation Intramolecular Rearrangement Mechanism Involving the Triplet States. *J. Chem. Theory Comput.* **2014**, *10*, 3987–3995

.

(49) Quenneville, J.; Greenfield, M.; Moore, D. S.; McGrane, S. D.; Scharff, R. J. Quantum Chemistry Studies of Electronically Excited Nitrobenzene, TNA, and TNT. *J. Phys. Chem. A* **2011**, *115*, 12286–12297

.

(50) Mewes, J.-M.; Jovanović, V.; Marian, C. M.; Dreuw, A. On the Molecular Mechanism of Non-radiative Decay of Nitrobenzene and the Unforeseen Challenges this Simple

Molecule Holds for Electronic Structure Theory. *Phys. Chem. Chem. Phys.* **2014**, *16*, 12393–12406

.

(51) Rai-Constapel, V.; Salzmann, S.; Marian, C. M. Isolated and Solvated Thioxanthone: A Photophysical Study. *J. Phys. Chem. A* **2011**, *115*, 8589–8596

.

(52) Rai-Constapel, V.; Etinski, M.; Marian, C. M. Photophysics of Xanthone: A Quantum Chemical Perusal. *J. Phys. Chem. A* **2013**, *117*, 3935–3944

.

(53) Rai-Constapel, V.; Villnow, T.; Ryseck, G.; Gilch, P.; Marian, C. M. Chimeric Behavior of Excited Thioxanthone in Protic Solvents: II. Theory. *J. Phys. Chem. A* **2014**, *118*, 11708–11717

.

(54) Rai-Constapel, V.; Marian, C. M. Solvent Tunable Photophysics of Acridone: A Quantum Chemical Perspective. *RSC Adv.* **2016**, *6*, 18530–18537

.

(55) Mundt, R.; Villnow, T.; Ziegenbein, C. T.; Gilch, P.; Marian, C. M.; Rai-Constapel, V. Thioxanthone in Apolar Solvents: Ultrafast Internal Conversion Precedes Fast Intersystem Crossing. *Phys. Chem. Chem. Phys.* **2016**, *18*, 6637–6647

.

(56) Morita, A.; Kato, S. Theoretical Study on the Intersystem Crossing Mechanism of a Diradical in Norrish type II Reactions in Solution. *J. Phys. Chem.* **1993**, *97*, 3298–3313

.

(57) Daniel, C.; Heitz, M.-C.; Manz, J.; Ribbing, C. Spin Orbit Induced Radiationless Transitions in Organometallics: Quantum Simulation of the 1E 3A1 Intersystem Crossing Process in HCo(CO)4 *J. Chem. Phys.* **1995**, *102*, 905–912

.

(58) Heitz, M.-C.; Ribbing, C.; Daniel, C. Spin Orbit Induced Radiationless Transitions in Organometallics: Quantum Simulation of the Intersystem Crossing Processes in the Photodissociation of HCo (CO)4. *J. Chem. Phys.* **1997**, *106*, 1421–1428

.

(59) Parker, D.; Minns, R.; Penfold, T.; Worth, G.; Fielding, H. Ultrafast Dynamics of the S1 Excited State of Benzene. *Chem. Phys. Lett.* **2009**, *469*, 43–47

.

(60) Minns, R. S.; Parker, D. S. N.; Penfold, T. J.; Worth, G. A.; Fielding, H. H. Competing Iltrafast Intersystem Crossing and Internal Conversion in the "Channel 3" Region of Benzene *Phys. Chem. Chem. Phys.* **2010**, *12*, 15607–15615

.

(61) Tavernelli, I.; Curchod, B. F.; Rothlisberger, U. Nonadiabatic Molecular Dynamics with Solvent Effects: A LR-TDDFT QM/MM Study of Ruthenium (II) tris(bipyridine) in Water. *Chem. Phys.* **2011**, *391*, 101–109

.

(62) Mai, S.; Marquetand, P.; González, L. Non-adiabatic and Intersystem Crossing Dynamics in SO2. II. The Role of Triplet States in the Bound State Dynamics Studied by Surface-Hopping Simulations. *J. Chem. Phys.* **2014**, *140*, 204302

.

(63) Polyak, B. M.; Sakovich, R. A.; Gularyan, S. K.; Romanov, A. N.; Isakova, S. I. Modeling Processes of Non-Radiative Relaxation of Electronically Excited States of

Fluorescent Probe 4-dimethylaminochalcone and its Complexes With Water Using Non Adiabatic Molecular Dynamics. *J. Photochem. Photobiol.* **2014**, *278*, 89–96

.

(64) Richter, M.; Mai, S.; Marquetand, P.; González, L. Ultrafast Intersystem Crossing Dynamics in Uracil Unravelled by Ab Initio Molecular Dynamics. *Phys. Chem. Chem. Phys.* **2014**, *16*, 24423–24436

.

(65) Martínez-Fernández, L.; Corral, I.; Granucci, G.; Persico, M. Competing Ultrafast Intersystem Crossing and Internal Conversion: A Time Resolved Picture for the Deactivation of 6-Thioguanine. *Chem. Sci.* **2014**, *5*, 1336–1347

.

(66) Cui, G.; Thiel, W. Generalized Trajectory Surface-Hopping Method for Internal Conversion and Intersystem Crossing. *J. Chem. Phys.* **2014**, *141*, 124101

.

(67) Freitag, L.; Gonzalez, L. Theoretical Spectroscopy and Photodynamics of a Ruthenium Nitrosyl Complex. *Inorg. Chem.* **2014**, *53*, 6415–6426

.

(68) Mai, S.; Marquetand, P.; González, L. A General Method to Describe Intersystem Crossing Dynamics in Trajectory Surface Hopping. *Int. J. Quantum Chem.* **2015**, *115*, 1215–1231

.

(69) Crespo-Hernandez, C. E.; Martínez-Fernndez, L.; Rauer, C.; Reichardt, C.; Mai, S.; Pollum, M.; Marquetand, P.; Gonzaez, L.; Corral, I. Electronic and Structural Elements that Regulate the Excited-State Dynamics in Purine Nucleobase Derivatives. *J. Am. Chem. Soc.* **2015**, *137*, 4368–4381

.

(70) Iuchi, S.; Koga, N. Insight into the Light-Induced Spin Crossover of [Fe(bpy)3] 2+ in Aqueous Solution from Molecular Dynamics Simulation of d–d Excited States. *Phys. Chem. Chem. Phys.* **2016**, *18*, 4789–4799

.

(71) Franco de Carvalho, F.; Tavernelli, I. Nonadiabatic Dynamics with Intersystem Crossings: A Time-Dependent Density Functional Theory Implementation. *J. Chem. Phys.* **2015**, *143*, 224105

.

(72) Mai, S.; Marquetand, P.; Gonzalez, L. Intersystem Crossing Pathways in the Noncanonical Nucleobase 2-Thiouracil: A time-Dependent Picture. *J. Phys. Chem. Lett.* **2016**, *7*, 1978–1983

.

(73) Cao, J.; Xie, Z.-Z. Internal Conversion and Intersystem Crossing in α, β-enones: A Combination of Electronic Structure Calculations and Dynamics Simulations. *Phys. Chem. Chem. Phys.* **2016**, *18*, 6931–6945

.

(74) Pederzoli, M.; Pittner, J. A New Approach to Molecular Dynamics with Non-Adiabatic and Spin Orbit Effects with Applications to QM/MM Simulations of Thiophene and Selenophene *J. Chem. Phys.* **2017**, *146*, 114101

.

(75) Mai, S.; Richter, M.; Marquetand, P.; González, L. The DNA Nucleobase Thymine in Motion–Intersystem Crossing Simulated with Surface Hopping. *Chem. Phys.* **2017**, *482*, 9–15

.

(76) Borin, A. C.; Mai, S.; Marquetand, P.; González, L. Ab Initio Molecular Dynamics Relaxation and Intersystem Crossing Mechanisms of 5-azacytosine. *Phys. Chem. Chem. Phys.* **2017**, *19*, 5888–5894

.

(77) Ando, H.; Iuchi, S.; Sato, H. Theoretical Study on Ultrafast Intersystem Crossing of Chromium (III) Acetylacetonate. *Chem. Phys. Lett.* **2012**, *535*, 177–181

.

(78) Papai, M.; Vanko, G.; Rozgonyi, T.; Penfold, T. J. High-Efficiency Iron Photosensitizer Explained with Quantum Wavepacket Dynamics *J. Phys. Chem. Lett.* **2016**, *7*, 2009–2014

.

(79) Pápai, M.; Penfold, T. J.; Møller, K. B. Effect of tert-Butyl Functionalization on the Photoexcited Decay of a Fe (II)-N-Heterocyclic Carbene Complex *J. Phys. Chem. C* **2016**, *120*, 17234–17241

.

(80) Lévêque, C.; Taïeb, R.; Köppel, H. Communication: Theoretical Prediction of the Importance of the 3B2 state in the Dynamics of Sulfur Dioxide. *J. Chem. Phys.* **2014**, *140*, 091101

.

(81) Eng, J.; Gourlaouen, C.; Gindensperger, E.; Daniel, C. Spin-Vibronic Quantum Dynamics for Ultrafast Excited-State Processes. *Acc. Chem. Res.* **2015**, *48*, 809–817

.

(82) Fumanal, M.; Gindensperger, E.; Daniel, C. Ultrafast Excited-State Decays in [Re (CO) 3 (N, N)(L)] n+: Nonadiabatic Quantum Dynamics. *J. Chem. Theory Comput.* **2017**, *13*, 1293–1306

.

(83) Harabuchi, Y.; Eng, J.; Gindensperger, E.; Taketsugu, T.; Maeda, S.; Daniel, C. Exploring the Mechanism of Ultrafast Intersystem Crossing in Rhenium (I) Carbonyl Bipyridine Halide Complexes: Key Vibrational Modes and Spin–Vibronic Quantum Dynamics. *J. Chem. Theory Comput.* **2016**, *12*, 2335–2345

.

(84) Xie, C.; Hu, X.; Zhou, L.; Xie, D.; Guo, H. Ab initio Determination of Potential Energy Surfaces for the First Two UV Absorption Bands of SO2. *J. Chem. Phys.* **2013**, *139*, 014305

.

(85) Mondal, P.; Domcke, W. Infrared Absorption Spectra of Jahn–Teller Systems: Application to the Transition-Metal Trifluorides MnF3 and NiF3. *J. Phys. Chem. A* **2014**, *118*, 3726–3734

.

(86) Baryshnikov, G.; Minaev, B.; Ågren, H. Theory and Calculation of the Phosphorescence Phenomenon. *Chem. Rev.* **2017**, *117*, 6500–6537

.

(87) Hess, B. A.; Marian, C. M.; Wahlgren, U.; Gropen, O. A Mean-Field Spin-Orbit Method Applicable to Correlated Wavefunctions. *Chem. Phys. Lett.* **1996**, *251*, 365–371

.

(88) Marian, C. M.; Wahlgren, U. A New Mean-Field and ECP-based Spin-Orbit Method. Applications to Pt and PtH. *Chem. Phys. Lett.* **1996**, *251*, 357–364

.

(89) Pyykkö, P. Relativistic Effects in Chemistry: More Common Than You Thought. *Ann. Rev. Phys. Chem.* **2012**, *63*, 45–64

.

(90) Marian, C. M. Spin-Orbit Coupling and Intersystem Crossing in Molecules *Wiley Interdiscip. Rev. Comput. Mol. Sci.* **2011**, *2*, 187–203

.

(91) Koseki, S.; Schmidt, M. W.; Gordon, M. S. MCSCF/6-31G (d, p) Calculations of One-Electron Spin-Orbit Coupling Constants in Diatomic Molecules. *J. Phys. Chem.* **1992**, *96*, 10768–10772

.

(92) Ermler, W. C.; Ross, R. B.; Christiansen, P. A. Spin-Orbit Coupling and Other Relativistic Effects in Atoms and Molecules.*Adv. Quantum Chem.* **1988**, *19*, 139–182

.

(93) Cao, X.; Dolg, M. Pseudopotentials and Model Potentials. *Wiley Interdiscip. Rev. Comput. Mol. Sci.* **2011**, *1*, 200–210

.

(94) Dolg, M.; Cao, X. Relativistic Pseudopotentials: Their Development and Scope of Applications. *Chem. Rev.* **2012**, *112*, 403–480

.

(95) Pitzer, R. M.; Winter, N. W. Electronic-Structure Methods for Heavy-Atom Molecules. *J. Phys. Chem.* **1988**, *92*, 3061–3063

.

(96) Walker, T.; Richards, W. Calculation of Spin-Orbit Coupling Constants in Diatomic Molecules from Hartree-Fock Wave Functions.*Phys. Rev.* **1969**, *177*, 100

.

(97) Malmqvist, P. Å.; Roos, B. O.; Schimmelpfennig, B. The Restricted Active Space (RAS) State iInteraction Approach With Spin–Orbit Coupling. *Chem. Phys. Lett.* **2002**, *357*, 230–240

.

(98) Sjøvoll, M.; Gropen, O.; Olsen, J. A Determinantal Approach to Spin-Orbit Configuration Interaction *Theor. Chem. Acc.* **1997**, *97*, 301

.

(99) Buenker, R. J.; Alekseyev, A. B.; Liebermann, H.-P.; Lingott, R.; Hirsch, G. Comparison of Spin-Orbit Configuration Interaction Methods Employing Relativistic Effective Core Potentials for the Calculation of Zero-Field Splittings of Heavy Atoms with a 2Po Ground State *J. Chem. Phys.* **1998**, *108*, 3400–3408

.

(100) Yabushita, S.; Zhang, Z.; Pitzer, R. M. Spin-Orbit Configuration Interaction Using the Graphical Unitary Group Approach and Relativistic Core Potential and Spin-Orbit Operators *J. Phys. Chem. A* **1999**, *103*, 5791–5800

.

(101) Vallet, V.; Maron, L.; Teichteil, C.; Flament, J.-P. A Two-Step Uncontracted Determinantal Effective Hamiltonian-Based SO-CI Method *J. Chem. Phys.* **2000**, *113*, 1391–1402

.

(102) Kleinschmidt, M.; Tatchen, J.; Marian, C. M. Spin-Orbit Coupling of DFT/MRCI Wavefunctions: Method, Test Calculations, and Application to Thiophene *J. Comp. Chem.* **2002**, *23*, 824–833

.

(103) Jovanović, V.; Lyskov, I.; Kleinschmidt, M.; Marian, C. M. On the Performance of

DFT/MRCI-R and MR-MP2 in Spin–Orbit Coupling Calculations on Diatomics and Polyatomic Organic Molecules. *Mol. Phys.* **2017**, *115*, 109–137

.

(104) Krauter, C. M.; Schimmelpfennig, B.; Pernpointner, M.; Dreuw, A. Algebraic Diagrammatic Construction for the Polarization Propagator with Spin-Orbit Coupling. *Chem. Phys.* **2017**, *482*, 286 – 293

.

(105) Wang, Z.; Tu, Z.; Wang, F. Equation-of-Motion Coupled-Cluster Theory for Excitation Energies of Closed-Shell Systems with Spin-Orbit Coupling. *J. Chem. Theory Comput.* **2014**, *10*, 5567–5576

.

(106) Epifanovsky, E.; Klein, K.; Stopkowicz, S.; Gauss, J.; Krylov, A. I. Spin–Orbit Couplings Within the Equation-of-Motion Coupled-Cluster Framework: Theory, Implementation, and Benchmark Calculations. *J. Chem. Phys.* **2015**, *143*, 064102

.

(107) Cao, Z.; Wang, F.; Yang, M. Coupled-Cluster Method for Open-Shell Heavy-Element Systems with Spin-Orbit Coupling. *J. Chem. Phys.* **2017**, *146*, 134108

.

(108) Böckmann, M.; Klessinger, M.; Zerner, M. C. Spin- Orbit Coupling in Organic Molecules: A Semiempirical Configuration Interaction Approach toward Triplet State Reactivity. *J. Phys. Chem.* **1996**, *100*, 10570–10579

.

(109) Wang, F.; Ziegler, T. A Simplified Relativistic Time-Dependent Density-Functional Theory Formalism for the Calculations of Excitation Energies Including Spin-Orbit Coupling Effect. *J. Chem. Phys.* **2005**, *123*, 152102

.

(110) Chiodo, S.; Russo, N. Determination of Spin-Orbit Coupling Contributions in the Framework of Density Functional Theory. *J. Comput. Chem.* **2008**, *29*, 912–920

.

(111) Chiodo, S. G.; Russo, N. DFT Spin–Orbit Coupling Between Singlet and Triplet Excited States: A Case of Psoralen Compounds. *Chem. Phys. Lett.* **2010**, *490*, 90–96

.

(112) Franco de Carvalho, F.; Curchod, B.; Penfold, T. J.; Tavernelli, I. Derivation of Spin-Orbit Couplings in Collinear Linear-Response TDDFT: A Rigorous Formulation *J. Chem. Phys.* **2014**, *140*, 144103

.

(113) Tavernelli, I.; Curchod, B. F. E.; Laktionov, A.; Rothlisberger, U. Nonadiabatic Coupling Vectors for Excited States within Time-Dependent Density Functional Theory in the Tamm-Dancoff Approximation and Beyond. *J. Chem. Phys.* **2010**, *133*, 194104

.

(114) Tavernelli, I.; Curchod, B. F. E.; Rothlisberger, U. On Nonadiabatic Coupling Vectors in Time-Dependent Density Functional Theory. *J. Chem. Phys.* **2009**, *131*, 196101

.

(115) Dinkelbach, F.; Kleinschmidt, M.; Marian, C. M. Assessment of Interstate Spin–Orbit Couplings from Linear Response Amplitudes. *J. Chem. Theory Comput.* **2017**, *13*, 749–766

.

(116) Gao, X.; Bai, S.; Fazzi, D.; Niehaus, T.; Barbatti, M.; Thiel, W. Evaluation of Spin-Orbit Couplings with Linear-Response Time-Dependent Density Functional Methods. *J. Chem. Theory Comput.* **2017**, *13*, 515–524

.

(117) Born, M.; Huang, K. *Dynamical theory of crystal lattices*; Oxford university press, 1998

.

(118) Born, M.; Oppenheimer, R. Zur Quantentheorie der Molekeln *Annalen der Physik* **1927**, *389*, 457–484

.

(119) Worth, G.; Cederbaum, L. Beyond Born-Oppenheimer: Molecular Dynamics Through a Conical Intersection *Ann. Rev. Phys. Chem.* **2004**, *55*, 127–158

.

(120) Fatehi, S.; Alguire, E.; Shao, Y.; Subotnik, J. E. Analytic Derivative Couplings Between Configuration-Interaction-Singles States with Built-in Electron-Translation Factors for Translational Invariance. *J. Chem. Phys.* **2011**, *135*, 234105

.

(121) Dallos, M.; Lischka, H.; Shepard, R.; Yarkony, D. R.; Szalay, P. G. Analytic Evaluation of Nonadiabatic Coupling Terms at the MR-CI Level. II. Minima on the Crossing Seam: Formaldehyde and the Photodimerization of Ethylene. *J. Chem. Phys.* **2004**, *120*, 7330–7339

.

(122) Lischka, H.; Dallos, M.; Szalay, P. G.; Yarkony, D. R.; Shepard, R. Analytic evaluation of nonadiabatic coupling terms at the MR-CI level. I. Formalism. *J. Chem. Phys.* **2004**, *120*, 7322–7329

.

(123) Kuhlman, T. S.; Glover, W. J.; Mori, T.; Møller, K. B.; Martínez, T. J. Between

Ethylene and Polyenes-the Non-Adiabatic Dynamics of Cis-dienes. *Faraday Discuss.* **2012**, *157*, 193–212

.

(124) Mori, T.; Glover, W. J.; Schuurman, M. S.; Martinez, T. J. Role of Rydberg States in the Photochemical Dynamics of Ethylene. *J. Phys. Chem. A* **2012**, *116*, 2808–2818

.

(125) Park, J. W.; Shiozaki, T. Analytical Derivative Coupling for Multistate CASPT2 Theory. *J. Chem. Theory Comput.* **2017**, *13*, 3676–3683

.

(126) Chernyak, V.; Mukamel, S. Density-Matrix Representation of Nonadiabatic Couplings in Time-Dependent Density Functional (TDDFT) Theories. *J. Chem. Phys.* **2000**, *112*, 3572–3579

.

(127) Send, R.; Furche, F. First-Order Nonadiabatic Couplings from Time-Dependent Hybrid Density Functional Response Theory: Consistent Formalism, Implementation, and Performance *J. Chem. Phys.* **2010**, *132*, 044107

.

(128) Ou, Q.; Fatehi, S.; Alguire, E.; Shao, Y.; Subotnik, J. E. Derivative Couplings Between TDDFT Excited States Obtained by Direct Differentiation in the Tamm-Dancoff Approximation. *J. Chem. Phys.* **2014**, *141*, 024114

.

(129) Domcke, W.; Yarkony, D.R. and Horst, K.A. *Conical intersections: Electronic Structure, Dynamics and Spectroscopy*; World Scientific, 2004; Vol. 15

.

(130) Tannor, D. J. *Introduction to quantum mechanics*; University Science Books, 2007

.

(131) Mead, C. A.; Truhlar, D. G. Conditions for the Definition of a Strictly Diabatic Electronic Basis for Molecular Systems. *J. Chem. Phys.* **1982**, *77*, 6090–6098

.

(132) Subotnik, J. E.; Yeganeh, S.; Cave, R. J.; Ratner, M. A. Constructing Diabatic States from Adiabatic states: Extending Generalized Mulliken–Hush to Multiple Charge Centers with Boys Localization. *J. Chem. Phys.* **2008**, *129*, 244101

.

(133) Van Voorhis, T.; Kowalczyk, T.; Kaduk, B.; Wang, L.-P.; Cheng, C.-L.; Wu, Q. The Diabatic Picture of Electron Transfer, Reaction Barriers, and Molecular Dynamics. *Ann. Rev. Phys. Chem.* **2010**, *61*, 149–170

.

(134) Subotnik, J. E.; Alguire, E. C.; Ou, Q.; Landry, B. R.; Fatehi, S. The Requisite Electronic Structure Theory to Describe Photoexcited Nonadiabatic Dynamics: Nonadiabatic Derivative Couplings and Diabatic Electronic Couplings. *Acc. of Chem. Res.* **2015**, *48*, 1340–1350

.

(135) Werner, H.-J.; Meyer, W. MCSCF study of the Avoided Curve Crossing of the Two Lowest 1Σ+ states of LiF. *J. Chem. Phys.* **1981**, *74*, 5802–5807

.

(136) Cave, R. J.; Newton, M. D. Generalization of the Mulliken-Hush Treatment for the Calculation of Electron Transfer Matrix Elements. *Chem. Phys. Lett.* **1996**, *249*, 15–19

.

(137) Cave, R. J.; Newton, M. D. Calculation of Electronic Coupling Matrix Elements for Ground and Excited State Electron Transfer Reactions: Comparison of the General-

ized Mulliken–Hush and Block Diagonalization Methods. *J. Chem. Phys.* **1997**, *106*, 9213–9226

.

(138) Subotnik, J. E.; Vura-Weis, J.; Sodt, A. J.; Ratner, M. A. Predicting Accurate Electronic Excitation Transfer Rates via Marcus Theory with Boys or Edmiston- Ruedenberg Localized Diabatization *J. Phys. Chem. A* **2010**, *114*, 8665–8675

.

(139) Fatehi, S.; Alguire, E.; Subotnik, J. E. Derivative Couplings and Analytic Gradients for Diabatic States, with an Implementation for Boys-Localized Configuration-Interaction Singles. *J. Chem. Phys.* **2013**, *139*, 124112

.

(140) Zhu, X.; Yarkony, D. R. On the Construction of Property Based Diabatizations: Diabolical Singular Points. *J. Phys. Chem. A* **2015**, *119*, 12383–12391

.

(141) Hoyer, C. E.; Xu, X.; Ma, D.; Gagliardi, L.; Truhlar, D. G. Diabatization Based on the Dipole and Quadrupole: The DQ method. *J. Chem. Phys.* **2014**, *141*, 114104

.

(142) Hoyer, C. E.; Parker, K.; Gagliardi, L.; Truhlar, D. G. The DQ and DQΦ Electronic Structure Diabatization Methods: Validation for General Applications. *J. Chem. Phys.* **2016**, *144*, 194101

.

(143) Köppel, H.; Domcke, W.; Cederbaum, L. S. Multimode Molecular Dynamics Beyond the Born-Oppenheimer Approximation. *Adv. in Chem. Phys.* **1984**, *57*, 59–246

.

(144) Pacher, T.; Cederbaum, L.; Köppel, H. Approximately Diabatic States from Block Diagonalization of the Electronic Hamiltonian. *J. Chem. Phys.* **1988**, *89*, 7367–7381

.

(145) Domcke, W.; Woywod, C. Direct Construction of Diabatic States in the CASSCF Approach. Application to the Conical Intersection of the 1A2 and 1B1 Excited States of Ozone. *Chem. Phys. Lett.* **1993**, *216*, 362–368

.

(146) Domcke, W.; Woywod, C.; Stengle, M. Diabatic CASSCF Orbitals and Wavefunctions. *Chem. Phys. Lett.* **1994**, *226*, 257–262

.

(147) Wittenbrink, N.; Venghaus, F.; Williams, D.; Eisfeld, W. A New Approach for the Development of Diabatic Potential Energy Surfaces: Hybrid Block-Diagonalization and Diabatization by Ansatz. *J. Chem. Phys.* **2016**, *145*, 184108

.

(148) Zeng, T. A Diabatization Protocol that Includes Spin-Orbit Coupling *J. Chem. Phys.* **2017**, *146*, 144103

.

(149) Lyskov, I.; Marian, C. M. Climbing up the Ladder: Intermediate Triplet States Promote the Reverse Intersystem Crossing in the Efficient TADF Emitter ACRSA. *J. Phys. Chem. C* **2017**, *121*, 21145–21153

.

(150) Tatchen, J.; Gilka, N.; Marian, C. M. Intersystem Crossing Driven by Vibronic Spin–Orbit Coupling: A Case Study on Psoralen. *Phys. Chem. Chem. Phys.* **2007**, *9*, 5209–5221

.

(151) Etinski, M.; Rai-Constapel, V.; Marian, C. M. Time-dependent Approach to Spin-Vibronic Coupling: Implementation and Assessment. *J. Chem. Phys.* **2014**, *140*, 114104

.

(152) Penfold, T.; Spesyvtsev, R.; Kirkby, O. M.; Minns, R.; Parker, D.; Fielding, H.; Worth, G. Quantum Dynamics Study of the Competing Ultrafast Intersystem Crossing and Internal Conversion in the "channel 3" Region of Benzene *J. Chem. Phys.* **2012**, *137*, 204310

.

(153) Granucci, G.; Persico, M.; Spighi, G. Surface Hopping Trajectory Simulations with Spin-Orbit and Dynamical Couplings. *J. Chem. Phys.* **2012**, *137*, 22A501

.

(154) Capano, G.; Chergui, M.; Rothlisberger, U.; Tavernelli, I.; Penfold, T. J. A Quantum Dynamics Study of the Ultrafast Relaxation in a Prototypical Cu(I)–Phenanthroline. *J. Phys. Chem. A* **2014**, *118*, 9861–9869.

.

(155) Curchod, B. F.; Rauer, C.; Marquetand, P.; González, L.; Martínez, T. J. Communication: GAIMS Generalized Ab Initio Multiple Spawning for Both Internal Conversion and Intersystem Crossing Processes. *J. Chem. Phys.* **2016**, *144*, 101102.

.

(156) Siddique, Z.; Yamamoto, Y.; Ohno, T.; Nozaki, K. Structure-Dependent Photophysical Properties of Singlet and Triplet Metal-to-Ligand Charge Transfer States in Copper(I) Bis(diimine) Compounds *Inorg. Chem.* **2003**, *42*, 6366–6378

.

(157) Capano, G.; Rothlisberger, U.; Tavernelli, I.; Penfold, T. J. Theoretical Rationaliza-

tion of the Emission Properties of Prototypical Cu (I)–Phenanthroline Complexes. *J. Phys. Chem. A* **2015**, *119*, 7026–7037

.

(158) Hsu, C.-W.; Lin, C.-C.; Chung, M.-W.; Chi, Y.; Lee, G.-H.; Chou, P.-T.; Chang, C.-H.; Chen, P.-Y. Systematic Investigation of the Metal-Structure–Photophysics Relationship of Emissive d 10-Complexes of Group 11 Elements: The Prospect of Application in Organic Light Emitting Devices *J. Am. Chem. Soc.* **2011**, *133*, 12085–12099

.

(159) Lim, B. T.; Okajima, S.; Chandra, A.; Lim, E. Radiationless Transitions in Electron Donor-Acceptor Complexes: Selection Rules for S 1- T1 Intersystem Crossing and Efficiency of S 1-S 0 Internal Conversion. *Chem. Phys. Lett.* **1981**, *79*, 22–27

.

(160) Dance, Z. E.; Mickley, S. M.; Wilson, T. M.; Ricks, A. B.; Scott, A. M.; Ratner, M. A.; Wasielewski, M. R. Intersystem Crossing Mediated by Photoinduced Intramolecular Charge Transfer: Julolidine- Anthracene Molecules with Perpendicular π Systems*J. Phys. Chem. A* **2008**, *112*, 4194–4201

.

(161) Balzani, V.; Juris, A.; Venturi, M.; Campagna, S.; Serroni, S. Luminescent and Redox-Active Polynuclear Transition Metal Complexes. *Chem. Rev.* **1996**, *96*, 759–834

.

(162) Englman, R.; Jortner, J. The Energy Gap Law for Radiationless Transitions in Large Molecules *Mol. Phys.* **1970**, *18*, 145–164

.

(163) Etinski, M.; Marian, C. M. Overruling the Energy Gap Law: Fast Triplet Formation in 6-azauracil. *Phys. Chem. Chem. Phys.* **2010**, *12*, 15665–15671

.

(164) Perun, S.; Tatchen, J.; Marian, C. M. Singlet and Triplet Excited States and Intersystem Crossing in Free-Base Porphyrin: TDDFT and DFT/MRCI Study. *ChemPhysChem* **2008**, *9*, 282–292

.

(165) Berkelbach, T. C.; Hybertsen, M. S.; Reichman, D. R. Microscopic Theory of Singlet Exciton Fission. II. Application to Pentacene Dimers and the Role of Superexchange. *J. Chem. Phys.* **2013**, *138*, 114103

.

(166) Symalla, F.; Friederich, P.; Massé, A.; Meded, V.; Coehoorn, R.; Bobbert, P.; Wenzel, W. Charge Transport by Superexchange in Molecular Host-Guest Systems. *Phys. Rev. Lett.* **2016**, *117*, 276803

.

(167) Duschinsky, F. The Importance of the Electron Spectrum in Multi Atomic Molecules Concerning the Frank-Condon Principle. *Acta Physicochim.* **1937**, *7*, 551–566

.

(168) Hougen, J. T.; Watson, J. K. G. Anomalous Rotational Line Intensities in Electronic Transitions of Polyatomic Molecules: Axis-Switching *Canad. J. Phys.* **1965**, *43*, 298–320

.

(169) Özkan, I. Franck-Condon Principle for Polyatomic Molecules: Axis-Switching Effects and Transformation of Normal Coordinates *J. Mol. Spectrosc.* **1990**, *139*, 147–162

.

(170) Tatchen, J. E. Spin-verbotene photophysikalische Prozesse in organischen Molekülen:

Entwicklung quantenchemischer Methoden und Anwendung auf Psoralene. Ph.D. thesis, Heinrich Heine University Düsseldorf, Germany, 2006

.

(171) Reimers, J. R. A Practical Method For the Use of Curvilinear Coordinates in Calculations of Normal-Mode-Projected Displacements and Duschinsky Rotation Matrices for Large Molecules. *J. Chem. Phys.* **2001**, *115*, 9103–9109

.

(172) Toniolo, A.; Persico, M. Efficient Calculation of Franck-Condon Factors and Vibronic Couplings in Polyatomics. *J. Comput. Chem.* **2001**, *22*, 968–975

.

(173) Toniolo, A.; Persico, M. A Theoretical Study of Spectroscopy and Predissociation Dynamics in Nitrosoalkanes. *J. Chem. Phys.* **2001**, *115*, 1817–1827

.

(174) Salzmann, S.; Tatchen, J.; Marian, C. M. The Photophysics of Flavins: What Makes the Difference Between Gas Phase and Aqueous Solution? *J. Photochem. Photobiol. A* **2008**, *198*, 221–231

.

(175) Salzmann, S.; Silva-Junior, M. R.; Thiel, W.; Marian, C. M. Influence of the LOV Domain on Low-Lying Excited States of Flavin: A Combined Quantum-Mechanics / Nolecular-Mechanics Investigation. *J. Phys. Chem. B* **2009**, *113*, 15610–15618

.

(176) Rodriguez-Serrano, A.; Rai-Constapel, V.; Daza, M. C.; Doerr, M.; Marian, C. M. A Theoretical Study of Thionine: Spin-Orbit Coupling and Intersystem Crossing. *Photochem. Photobiol. Sci.* **2012**, *11*, 1860–1867

.

(177) Rodriguez-Serrano, A.; Rai-Constapel, V.; Daza, M. C.; Doerr, M.; Marian, C. M. Internal Heavy Atom Effects in Phenothiazinium Dyes: Enhancement of Intersystem Crossing via Vibronic Spin-Orbit Coupling. *Phys. Chem. Chem. Phys.* **2015**, *17*, 11350–11358

.

(178) Haarhoff, P. The Density of Vibrational Energy Levels of Polyatomic Molecules. *Mol. Phys.* **1964**, *7*, 101–117

.

(179) Dierksen, M.; Grimme, S. An Efficient Approach for the Calculation of Franck-Condon Integrals of Large Molecules *J. Chem. Phys.* **2005**, *122*, 244101

.

(180) Jankowiak, H. C.; Stuber, J. L.; Berger, R. Vibronic Transitions in Large Molecular Systems: Rigorous Prescreening Conditions for Franck-Condon Factors. *J. Chem. Phys.* **2007**, *127*, 234101

.

(181) Santoro, F.; Lami, A.; Improta, R.; Bloino, J.; Barone, V. Effective Method for the Computation of Optical Spectra of Large Molecules at Finite Temperature Including the Duschinsky and Herzberg–Teller Effect: The Q_x Band of Porphyrin as a Case Study. *J. Chem. Phys.* **2008**, *128*, 224311

.

(182) von Mehler, F. G. Ueber die Entwicklung einer Function von beliebig vielen Variablen nach Laplaceschen Functionen höherer Ordnung. *J. Reine Angew. Math.* **1866**, *66*, 161–176

.

(183) Markham, J. J. Interaction of Normal modes with Electron Traps. *Rev. Mod. Phys.* **1959**, *31*, 956–989

.

(184) Etinski, M.; Tatchen, J.; Marian, C. M. Time-Dependent Approaches for the Calculation of Intersystem Crossing Rates. *J. Chem. Phys.* **2011**, *134*, 154105–154114

.

(185) Etinski, M.; Tatchen, J.; Marian, C. M. Thermal and Solvent Effects on the Triplet Formation in Cinnoline. *Phys. Chem. Chem. Phys.* **2014**, *16*, 4740–4751

.

(186) Peng, Q.; Niu, Y.; Deng, C.; Shuai, Z. Vibration Correlation Function Formalism of Radiative and Non-Radiative Rates for Complex Molecules. *Chem. Phys.* **2010**, *370*, 215 – 222

.

(187) Peng, Q.; Niu, Y.; Shi, Q.; Gao, X.; Shuai, Z. Correlation Function Formalism for Triplet Excited State Decay: Combined Spin–orbit and Nonadiabatic Couplings. *J. Chem. Theory Comput.* **2013**, *9*, 1132–1143

.

(188) Banerjee, S.; Baiardi, A.; Bloino, J.; Barone, V. Temperature Dependence of Radiative and Nonradiative Rates from Time-Dependent Correlation Function Methods. *J. Chem. Theory Comput.* **2016**, *12*, 774–786

.

(189) Beck, M. H.; Jäckle, A.; Worth, G. A.; Meyer, H.-D. The Multiconfiguration Time-Dependent Hartree Method: A Highly Efficient Algorithm for Propagating Wavepackets. *Phys. Rep.* **2000**, *324*, 1–105

.

(190) Wang, H.; Thoss, M. Multilayer Formulation of the Multiconfiguration Time-Dependent Hartree Theory *J. Chem. Phys.* **2003**, *119*, 1289–1299

.

(191) Vendrell, O.; Meyer, H.-D. Multilayer Multiconfiguration Time-Dependent Hartree Method: Implementation and Applications to a Henon–Heiles Hamiltonian and to Pyrazine *J. Chem. Phys.* **2011**, *134*, 044135

.

(192) Meyer, H.-D., Gatti, F., Worth, G. A., Eds. *High dimensional quantum dynamics: Basic Theory, Extensions, and Applications of the MCTDH method*; VCH: Weinheim, Germany, 2008

.

(193) Raab, A.; Burghardt, I.; Meyer, H.-D. The Multiconfiguration Time-Dependent Hartree Method Generalized to the Propagation of Density Operators. *J. Chem. Phys.* **1999**, *111*, 8759–8772

.

(194) Raab, A.; Meyer, H.-D. Multiconfigurational Expansions of Density Operators: Equations of Motion and Their Properties. *Theo. Chem. Acc.* **2000**, *104*, 358–369

.

(195) Lorenz, U.; Saalfrank, P. Comparing Thermal Wavefunction Methods for Multi-Configuration Time-Dependent Hartree Simulations. *J. Chem. Phys.* **2014**, *140*, 044106

.

(196) Penfold, T.; Worth, G. A model Hamiltonian to Simulate the Complex Photochemistry of Benzene II *J. Chem. Phys.* **2009**, *131*, 190–199

.

(197) Cattarius, C.; Worth, G.; Meyer, H.-D.; Cederbaum, L. All Mode Dynamics at the Conical Intersection of an Octa-atomic Molecule: Multi-Configuration Time-Dependent Hartree (MCTDH) Investigation on the Butatriene Cation. *J. Chem. Phys.* **2001**, *115*, 2088–2100

.

(198) Poluyanov, L.; Domcke, W. The Relativistic Renner–Teller Effect Revisited. *Chem. Phys.* **2004**, *301*, 111–127

.

(199) Domcke, W.; Mishra, S.; Poluyanov, L. V. The Relativistic E× E Jahn–Teller Effect Revisited. *Chem. Phys.* **2006**, *322*, 405–410

.

(200) Poluyanov, L. V.; Domcke, W. Relativistic E× T Jahn–Teller Effect in Tetrahedral Systems. *J. Chem. Phys.* **2008**, *129*, 224102

.

(201) Poluyanov, L. V.; Domcke, W. Relativistic T× T and T× E Jahn–Teller Coupling in Tetrahedral Systems. *Chem. Phys.* **2010**, *374*, 86–93

.

(202) Poluyanov, L. V.; Domcke, W. Relativistic Jahn–Teller and Pseudo-Jahn–Teller Couplings in D2d Systems. *Chem. Phys.* **2012**, *407*, 1–8

.

(203) Poluyanov, L. V.; Domcke, W. Jahn-Teller, Pseudo-Jahn-Teller, and Spin-Orbit Coupling Hamiltonian of an Electron in an Octahedral Environment. *J. Chem. Phys.* **2012**, *137*, 114101

.

(204) Weike, T.; Eisfeld, W. Development of Multi-Mode Diabatic Spin-Orbit Models at Arbitrary Order. *J. Chem. Phys.* **2016**, *144*, 104108

.

(205) Li, S. L.; Truhlar, D. G.; Schmidt, M. W.; Gordon, M. S. Model Space Diabatization for Quantum Photochemistry. *J. Chem. Phys.* **2015**, *142*, 064106

.

(206) Capano, G.; Penfold, T.; Chergui, M.; Tavernelli, I. Photophysics of a Copper Phenanthroline Elucidated by Trajectory and Wavepacket-based Quantum Dynamics: A Synergetic Approach. *Phys. Chem. Chem. Phys.* **2017**, *19*, 19590-19600

.

(207) Poirier, B. Using Wavelets to Extend Quantum Dynamics Calculations to Ten or More Degrees of Freedom. *J. Chem. Theory Comput.* **2003**, *2*, 65–72

.

(208) Richings, G. W.; Polyak, I.; Spinlove, K. E.; Worth, G.; Burghardt, I.; Lasorne, B. Quantum Dynamics Simulations using Gaussian Wavepackets: The vMCG method *Int. Rev. Phys. Chem.* **2015**, *34*, 269–308

.

(209) Tully, J. C.; Preston, R. K. Trajectory Surface Hopping Approach to Nonadiabatic Molecular Collisions: The Reaction of H+ with D2. *J. Chem. Phys.* **1971**, *55*, 562–572

.

(210) Tully, J. C. Molecular Dynamics with Electronic Transitions. *J. Chem. Phys.* **1990**, *93*, 1061–1071

.

(211) Tavernelli, I.; Curchod, B.; Rothlisberger, U. Nonadiabatic Molecular Dynamics with

Solvent Effects: A LR-TDDFT QM/MM Study of Ruthenium (II) Tris (Bipyridine) in Water. *Chem. Phys.* **2011**, *391*, 101–109

.

(212) Subotnik, J. E.; Jain, A.; Landry, B.; Petit, A.; Ouyang, W.; Bellonzi, N. Understanding the Surface Hopping View of Electronic Transitions and Decoherence. *Ann. Rev. Phys. Chem.* **2016**, *67*, 387–417

.

(213) Amatatsu, Y.; Morokuma, K.; Yabushita, S. Ab Initio Potential Energy Surfaces and Trajectory Studies of A-band Photodissociation Dynamics: CH3I-CH3+ I and CH3+ I *J. Chem. Phys.* **1991**, *94*, 4858–4876

.

(214) Richter, M.; Marquetand, P.; González-Vázquez, J.; Sola, I.; González, L. SHARC: Ab Initio Molecular Dynamics with Surface Hopping in the Adiabatic Representation Including Arbitrary Couplings. *J. Chem. Theory Comput.* **2011**, *7*, 1253–1258

.

(215) Richter, M.; Marquetand, P.; Gonzalez-Vazquez, J.; Sola, I.; Gonzalez, L. Femtosecond Intersystem Crossing in the DNA Nucleobase Cytosine. *J. Phys. Chem. Lett.* **2012**, *3*, 3090–3095

.

(216) Mai, S.; Marquetand, P.; Richter, M.; González-Vázquez, J.; González, L. Singlet and Triplet Excited-State Dynamics Study of the Keto and Enol Tautomers of Cytosine. *ChemPhysChem* **2013**, *14*, 2920–2931

.

(217) Sanchez-Rodriguez, J. A.; Mohamadzade, A.; Mai, S.; Ashwood, B.; Pollum, M.; Marquetand, P.; Gonzalez, L.; Crespo-Hernandez, C. E.; Ullrich, S. 2-Thiouracil In-

tersystem Crossing Photodynamics Studied By Wavelength-Dependent Photoelectron And Transient Absorption Spectroscopies. *Phys. Chem. Chem. Phys.* **2017**, *19*, 19756-19766

.

(218) Marazzi, M.; Mai, S.; Roca-Sanjuan, D.; Delcey, M. G.; Lindh, R.; Gonzalez, L.; Monari, A. A. Benzophenone Ultrafast Triplet Population: Revisiting the Kinetic Model by Surface-Hopping Dynamics *J. Phys. Chem. Lett.* **2016**, *7*, 622–626

.

(219) Atkins, A. J.; González, L. Trajectory Surface-Hopping Dynamics Including Intersystem Crossing in [Ru (bpy) 3] 2+ *J. Phys. Chem. Lett.* **2017**, *8*, 3840–3845

.

(220) Cannizzo, A.; van Mourik, F.; Gawelda, W.; Zgrablic, G.; Bressler, C.; Chergui, M. Broadband Femtosecond Fluorescence Spectroscopy of $[Ru(bpy)_3]^{2+}$ *Angew. Chem. Int. Ed.* **2006**, *45*, 3174–3176

.

(221) Martinez, T. J.; Ben-Nun, M.; Levine, R. Multi-Electronic-State Molecular Dynamics: A Wavefunction Approach with Applications. *J. Phys. Chem.* **1996**, *100*, 7884–7895

.

(222) Ben-Nun, M.; Martınez, T. J. Nonadiabatic Molecular Dynamics: Validation of the Multiple Spawning Method for a Multidimensional Problem. *J. Chem. Phys.* **1998**, *108*, 7244–7257

.

(223) Shalashilin, D. V.; Child, M. S. The Phase Space CCS Approach to Quantum and Semiclassical Molecular Dynamics for High-Dimensional Systems. *Chem. Phys.* **2004**, *304*, 103–120

.

(224) Shalashilin, D. V. Quantum Mechanics with the Basis Set Guided by Ehrenfest Trajectories: Theory and Application to Spin-Boson Model. *J. Chem. Phys.* **2009**, *130*, 244101

.

(225) Worth, G. A.; Burghardt, I. Full Quantum Mechanical Molecular Dynamics using Gaussian Wavepackets. *Chem. Phys. Lett.* **2003**, *368*, 502–508

.

(226) Makhov, D. V.; Glover, W. J.; Martinez, T. J.; Shalashilin, D. V. Ab initio Multiple Cloning Algorithm for Quantum Nonadiabatic Molecular Dynamics. *J. Chem. Phys.* **2014**, *141*, 054110

.

(227) Heller, E. J. Time-Dependent Approach to Semiclassical Dynamics. *J. Chem. Phys.* **1975**, *62*, 1544–1555

.

(228) Heller, E. J. Frozen Gaussians: A Very Simple Semiclassical Approximation. *J. Chem. Phys.* **1981**, *75*, 2923–2931

.

(229) Titov, A. V.; Ufimtsev, I. S.; Luehr, N.; Martinez, T. J. Generating Efficient Quantum Chemistry Codes for Novel Architectures. *J. Chem. Theory Comput.* **2012**, *9*, 213–221

.

(230) Curchod, B. F.; Sisto, A.; Martínez, T. J. Ab Initio Multiple Spawning Photochemical Dynamics of DMABN Using GPUs *J. Phys. Chem. A* **2017**,

.

(231) Snyder Jr, J. W.; Curchod, B. F.; Martínez, T. J. GPU-Accelerated State-Averaged Complete Active Space Self-Consistent Field Interfaced with Ab Initio Multiple Spawning Unravels the Photodynamics of Provitamin D3. *J. Phys. Chem. Lett.* **2016**, *7*, 2444–2449

.

(232) Penfold, T. Accelerating Direct Quantum Dynamics Using Graphical Processing Units. *Phys. Chem. Chem. Phys.* **2017**, *19*,19601-19608

.

(233) Heicklen, J.; Kelly, N.; Partymiller, K. The Photophysics and Photochemistry of SO2 *Rev. Chem. Intermed.* **1980**, *3*, 315

.

(234) Hofbeck, T.; Lam, Y. C.; Kalbáč, M.; Záliš, S.; Vlček Jr, A.; Yersin, H. Tunable Dual Emission of the d8–d8 Dimer [Pt2 (μ-P2O5 (BF2) 2) 4] 4– *Inorg. Chem* **2016**, *55*, 2441–2449

.

(235) Rice, S. F.; Gray, H. B. Electronic Absorption and Emission Spectra of Binuclear Platinum(II) Complexes. Characterization of the Lowest Singlet and Triplet Excited States of Tetrakis(diphosphonato)diplatinate(4-) Anion (Pt2(H2P2O5)44-). *J. Am. Chem. Soc.* **1983**, *105*, 4571–4575

.

(236) van der Veen, R. M.; Kas, J. J.; Milne, C. J.; Pham, V.-T.; el Nahhas, A.; Lima, F. A.; Vithanage, D. A.; Rehr, J. J.; Abela, R.; Chergui, M. L-edge XANES Analysis of Photoexcited Metal Complexes in Solution *Phys. Chem. Chem. Phys.* **2010**, *12*, 5551–5561

.

(237) van der Veen, R.; Milne, C.; el Nahhas, A.; Lima, F.; Pham, V.; Best, J.; Weinstein, J.; Borca, C.; Abela, R.; Bressler, C. et al. Structural Determination of a Photochemically Active Diplatinum Molecule by Time-Resolved EXAFS Spectroscopy *Angew. Chem. Int. Ed.)* **2009**, *48*, 2711–2714

.

(238) van der Veen, R. M.; Cannizzo, A.; van Mourik, F.; Vlcek, A. J.; Chergui, M. Vibrational Relaxation and Intersystem Crossing of Binuclear Metal Complexes in Solution *J. Am. Chem. Soc.* **2011**, *133*, 305–315

.

(239) Novozhilova, I.; Volkov, A.; Coppens, P. Theoretical Analysis of the Triplet Excited State of the [Pt-2(H2P2O5)(4)](4-) Ion and Comparison with Time-Resolved X-ray and Spectroscopic Results *J. Am. Chem. Soc.* **2003**, *125*, 1079–1087

.

(240) Christensen, M.; Haldrup, K.; Bechgaard, K.; Feidenhans'l, R.; Kong, Q.; Cammarata, M.; lo Russo, M.; Wulff, M.; Harrit, N.; Nielsen, M. M. Time-Resolved X-Ray Scattering of an Electronically Excited State in Solution. Structure of the $^3A_{2u}$ State of Tetrakis-mu-Pyrophosphitodiplatinate(Ii) *J. Am. Chem. Soc.* **2009**, *131*, 502–508

.

(241) Lam, Y. C.; Gray, H. B.; Winkler, J. R. Intersystem Crossing in Diplatinum Complexes. *J. Phys. Chem. A* **2016**, *120*, 7671–7676

.

(242) Monni, R.; Auböck, G.; Kinschel, D.; Aziz-Lange, K. M.; Gray, H. B.; Vlček, A.; Chergui, M. Conservation of Vibrational Coherence in Ultrafast Electronic Relaxation: The Case of Diplatinum Complexes in Solution. *Chem. Phys. Lett* **2017**, *693*, 112-120

.

(243) Záliš, S.; Lam, Y.-C.; Gray, H. B.; Vlček, A. Spin–Orbit TDDFT Electronic Structure of Diplatinum (II, II) Complexes. *Inorg. Chem* **2015**, *54*, 3491–3500

.

(244) Milder, S. J.; Brunschwig, B. S. Factors Affecting Nonradiative Decay: Temperature Dependence of the Picosecond Fluorescence Lifetime of Tetrakis (dihydrogen diphosphate) Diplatinum (4-). *J. Phys. Chem.* **1992**, *96*, 2189–2196

.

(245) Stiegman, A.; Rice, S.; Gray, H.; Miskowski, V. Electronic Spectroscopy of d8-d8 Diplatinum Complexess - Excited States of PT2(P2O5H2)44- *Inorg. Chem.* **1987**, *26*, 1112–1116

.

(246) Nibbering, E. T.; Fidder, H.; Pines, E. Ultrafast Chemistry: Using Time-Resolved Vibrational Spectroscopy for Interrogation of Structural Dynamics. *Annu. Rev. Phys. Chem.* **2005**, *56*, 337–367

.

(247) Horvath, R.; Huff, G. S.; Gordon, K. C.; George, M. W. Probing the Excited State Nature of Coordination Complexes with Blended Organic and Inorganic Chromophores using Vibrational Spectroscopy. *Coord. Chem. Rev.* **2016**, *325*, 41–58

.

(248) Bredenbeck, J.; Helbing, J.; Kolano, C.; Hamm, P. Ultrafast 2D–IR Spectroscopy of Transient Species. *ChemPhysChem* **2007**, *8*, 1747–1756

.

(249) Hunt, N. Transient 2D-IR spectroscopy of inorganic excited states. *Dalton Trans.* **2014**, *43*, 17578–17589

.

(250) Kukura, P.; McCamant, D. W.; Mathies, R. A. Femtosecond Stimulated Raman Spectroscopy *Ann. Rev. Phys. Chem.* **2007**, *58*, 461–488

.

(251) Lee, S.-Y.; Zhang, D.; McCamant, D. W.; Kukura, P.; Mathies, R. A. Theory of Femtosecond Stimulated Raman Spectroscopy *J. Chem. Phys.* **2004**, *121*, 3632

.

(252) Dietze, D. R.; Mathies, R. A. Femtosecond Stimulated Raman Spectroscopy *ChemPhysChem* **2016**, *17*, 1224–1251

.

(253) Pollard, W. T.; Mathies, R. A. Analysis of Femtosecond Dynamic Absorption Spectra of Nonstationary States *Ann. Rev. Phys. Chem.* **1992**, *43*, 497–523

.

(254) Liebel, M.; Schnedermann, C.; Wende, T.; Kukura, P. Principles and Applications of Broadband Impulsive Vibrational Spectroscopy. *J. Phys. Chem. A* **2015**, *119*, 9506–9517

.

(255) Smeigh, A. L.; Creelman, M.; Mathies, R. A.; McCusker, J. K. Femtosecond Time-Resolved Optical and Raman Spectroscopy of Photoinduced Spin Crossover: Temporal Resolution of Low-to-High Spin Optical Switching. *J. Am. Chem. Soc.* **2008**, *130*, 14105–14107

.

(256) Yoon, S.; Kukura, P.; Stuart, C. M.; Mathies, R. A. Direct Observation of the Ultrafast Intersystem Crossing in tris (2, 2-bipyridine) Ruthenium (II) Using Femtosecond Stimulated Raman Spectroscopy. *Mol. Phys.* **2006**, *104*, 1275–1282

.

(257) Damrauer, N. H. Femtosecond Dynamics of Excited-State Evolution in [Ru(bpy)3]2+ *Science* **1997**, *275*, 54–57

.

(258) Musser, A. J.; Liebel, M.; Schnedermann, C.; Wende, T.; Kehoe, T. B.; Rao, A.; Kukura, P. Evidence for Conical Intersection Dynamics Mediating Ultrafast Singlet Exciton Fission. *Nat. Phys.* **2015**, *11*, 352–357

.

(259) Schnedermann, C.; Muders, V.; Ehrenberg, D.; Schlesinger, R.; Kukura, P.; Heberle, J. Vibronic Dynamics of the Ultrafast All-Trans to 13-Cis Photoisomerization of Retinal in Channelrhodopsin-1. *J. Am. Chem. Soc* **2016**, *138*, 4757–4762

.

(260) Delor, M.; Scattergood, P. A.; Sazanovich, I. V.; Parker, A. W.; Greetham, G. M.; Meijer, A. J.; Towrie, M.; Weinstein, J. A. Toward Control of Electron Transfer in Donor-Acceptor Molecules by Bond-Specific Infrared Excitation. *Science* **2014**, *346*, 1492–1495

.

(261) Delor, M.; Keane, T.; Scattergood, P. A.; Sazanovich, I. V.; Greetham, G. M.; Towrie, M.; Meijer, A. J.; Weinstein, J. A. On the Mechanism of Vibrational Control of Light-Induced Charge Transfer in Donor–Bridge–Acceptor Assemblies. *Nat. Chem.* **2015**, *7*, 689–695

.

(262) Delor, M.; Archer, S. A.; Keane, T.; Meijer, A. J.; Sazanovich, I. V.; Greetham, G. M.; Towrie, M.; Weinstein, J. A. Directing The Path of Lght-Induced Electron Transfer at a Molecular Fork Using Vibrational Excitation. *Nat. Chem.* **2017**, doi:10.1038/nchem.2793.

.

(263) Jonas, D. M. Two-Dimensional Femtosecond Spectroscopy. *Ann. Rev. Phys. Chem.* **2003**, *54*, 425–463

.

(264) Hamm, P.; Zanni, M. *Concepts and methods of 2D infrared spectroscopy*; Cambridge University Press, 2011

.

(265) Mukamel, S. Multidimensional Femtosecond Correlation Spectroscopies of Electronic and Vibrational Excitations. *Ann. Rev. Phys. Chem.* **2000**, *51*, 691–729

.

(266) Halpin, A.; Johnson, P. J.; Tempelaar, R.; Murphy, R. S.; Knoester, J.; Jansen, T. L.; Miller, R. D. Two-Dimensional Spectroscopy of a Molecular Dimer Unveils the Effects of Vibronic CCoupling on Exciton Coherences. *Nat. Chem.* **2014**, *6*, 196–201

.

(267) Carbery, W. P.; Verma, A.; Turner, D. B. Spin–Orbit Coupling Drives Femtosecond Nonadiabatic Dynamics in a Transition Metal Compound. *J. Phys. Chem. Lett.* **2017**, *8*, 1315–1322

.

(268) Bizimana, L. A.; Brazard, J.; Carbery, W. P.; Gellen, T.; Turner, D. B. Resolving Molecular Vibronic Structure Using High-Sensitivity Two-Dimensional Electronic Spectroscopy. *J. Chem. Phys.* **2015**, *143*, 164203

.

(269) Bakulin, A. A.; Morgan, S. E.; Kehoe, T. B.; Wilson, M. W.; Chin, A. W.; Zigmantas, D.; Egorova, D.; Rao, A. Real-time Observation of Multiexcitonic States in Ul-

trafast Singlet Fission Using Coherent 2D Electronic Spectroscopy. *Nat. Chem.* **2016**, *8*, 16–23

.

(270) Reis, D. A.; Lindenberg, A. M. *Light Scattering In Solids IX* **2007**, *108*, 371–422

.

(271) Elsaesser, T.; Woerner, M. Photoinduced Structural Dynamics of Polar Solids Studied by Femtosecond X-ray Diffraction *Acta Crystallogr. A* **2010**, *66*, 168–178

.

(272) Johnson, S. L.; Beaud, P.; Vorobeva, E.; Milne, C. J.; Murray, E. D.; Fahy, S.; Ingold, G. Non-Equilibrium Phonon Dynamics Studied by Grazing-Incidence Femtosecond X-ray Crystallography *Acta Crystallogr. A* **2010**, *66*, 157–167

.

(273) Sciaini, G.; Miller, R. J. D. Femtosecond Electron Diffraction: Heralding The Era of Atomically Resolved Dynamics *Rep. Prog. Phys.* **2011**, *74*, 096101

.

(274) Chergui, M.; Zewail, A. H. Electron and X-Ray Methods of Ultrafast Structural Dynamics: Advances and Applications *ChemPhysChem* **2009**, *10*, 28–43

.

(275) Penfold, T.; Milne, C.; Chergui, M. Recent Advances in Ultrafast X-ray Absorption Spectroscopy of Solutions *Adv. Chem. Phys.* **2013**, *153*, 1–41

.

(276) Bressler, C.; Chergui, M. Molecular Structural Dynamics Probed by Ultrafast X-Ray Absorption Spectroscopy *Ann. Rev. Phys. Chem.* **2010**, *61*, 263–282

.

(277) Chen, L. Probing Transient Molecular Structures with Time-Resolved Pump/Probe XAFS using Synchrotron X-ray Sources *J. Electron Spectrosc. Relat. Phenom.* **2001**, *119*, 161–174

.

(278) Milne, C.; Penfold, T.; Chergui, M. Recent Experimental and Theoretical Developments in Time-Resolved X-ray Spectroscopies. *Coord. Chem. Rev.* **2014**, *277*, 44-68.

.

(279) Zewail, A. 4D Ultrafast Electron Diffraction, Crystallography, and Microscopy *Ann. Rev. Phys. Chem.* **2006**, *57*, 65–103

.

(280) van der Veen, R. M.; Penfold, T. J.; Zewail, A. H. Ultrafast Core-Loss Spectroscopy in Four-Dimensional Electron Microscopy. *Struct. Dyn.* **2015**, *2*, 024302

.

(281) Zholents, A.; Zolotorev, M. S. Femtosecond X-ray Pulses of Synchrotron Radiation *Phys. Rev. Lett.* **1996**, *76*, 912–915

.

(282) Schoenlein, R. W.; Chattopadhyay, S.; Chong, H. H. W.; Glover, T. E.; Heimann, P. A.; Shank, C.; Zholents, A.; Zolotorev, M. S. Generation of Femtosecond Pulses of Synchrotron Radiation *Science* **2000**, *287*, 2237–2240

.

(283) Pham, V.-T.; Penfold, T. J.; van der Veen, R. M.; Lima, F.; el Nahhas, A.; Johnson, S. L.; Beaud, P.; Abela, R.; Bressler, C.; Tavernelli, I.; et al. Probing the Transition from Hydrophilic to Hydrophobic Solvation with Atomic Scale Resolution *J. Am. Chem. Soc.* **2011**, *133*, 12740–12748

.

(284) Huse, N.; Cho, H.; Hong, K.; Jamula, L.; de Groot, F.; Kim, T.; McCusker, J.; Schoenlein, R. Femtosecond Soft X-ray Spectroscopy of Solvated Transition-Metal Complexes: Deciphering the Interplay of Electronic and Structural Dynamics *J. Phys. Chem. Lett.* **2011**, *2*, 880–884

.

(285) Abo-Bakr, M.; Feikes, J.; Holldack, K.; Kuske, P.; Peatman, W.; Schade, U.; Wustefeld, G.; Hubers, H. Brilliant, Coherent Far-Infrared (THz) Synchrotron Radiation *Phys. Rev. Lett.* **2003**, *90*, 094801

.

(286) Feikes, J.; Holldack, K.; Kuske, P.; Wustefeld, G. Compressed Electron Bunches for THz Generation - Operating BESSY II in a Dedicated Low Alpha Mode. Proceedings of EPAC 2004, Lucerne, Switzerland. 2004

.

(287) Pertot, Y.; Schmidt, C.; Matthews, M.; Chauvet, A.; Huppert, M.; Svoboda, V.; von Conta, A.; Tehlar, A.; Baykusheva, D.; Wolf, J.-P.; et al. Time-Resolved X-Ray Absorption Spectroscopy With a Water Window High-Harmonic Source *Science* **2017**, *355*, 264–267

.

(288) Attar, A. R.; Bhattacherjee, A.; Pemmaraju, C.; Schnorr, K.; Closser, K. D.; Prendergast, D.; Leone, S. R. Femtosecond X-ray Spectroscopy of an Electrocyclic Ring-Opening Reaction. *Science* **2017**, *356*, 54–59

.

(289) Wernet, P. et al. Orbital-Specific Mapping of the Ligand Exchange Dynamics of Fe(CO)5 in Solution *Nature* **2015**, *520*, 78–81

.

(290) de Groot, F. High-Resolution X-ray Emission and X-ray Absorption Spectroscopy *Chem. Rev.* **2001**, *101*, 1779–1808

.

(291) Glatzel, P.; Bergmann, U. High Resolution 1s Core Hole X-ray Spectroscopy in 3d Transition Metal Complexes - Electronic and Structural Information *Coord. Chem. Rev.* **2005**, *249*, 65–95

.

(292) Vankó, G. ; Bordage, A; Glatzel, P; Gallo, E; Rovezzi, M.; Gawelda, W.; Galler, A; Bressler, C; Doumy, G.; March, A.M¿ et al. Spin-State Studies with XES and RIXS: From Static to Ultrafast *J. Electron Spectrosc. Relat. Phenom.* **2013**, *188*, 166–171

.

(293) Capano, G.; Milne, C.; Chergui, M.; Rothlisberger, U.; Tavernelli, I.; Penfold, T. Probing Wavepacket Dynamics using Ultrafast X-ray Spectroscopy. *J. Phys. B: At., Mol. Opt. Phys.* **2015**, *48*, 214001

.

(294) Penfold, T.; Pápai, M.; Rozgonyi, T.; Møller, K. B.; Vankó, G. Probing Spin–Vibronic Dynamics using Femtosecond X-ray Spectroscopy. *Faraday Discuss.* **2016**, *194*, 731–746

.

(295) Kumar, B.; Llorente, M.; Froehlich, J.; Dang, T.; Sathrum, A.; Kubiak, C. P. Photochemical and Photoelectrochemical Reduction of CO2 *Ann. Rev. Phys. Chem.* **2012**, *63*, 541–569

.

(296) Gratzel, M. Dye-Sensitized Solar Cells *J. Photochem. Photobiol. C* **2003**, *4*, 145–153

.

(297) Ponseca Jr, C. S.; Chabera, P.; Uhlig, J.; Persson, P.; Sundstrom, V. Ultrafast Electron Dynamics in Solar Energy Conversion *Chem. Rev.* **2017**, *117* 10940-11024.

.

(298) Holder, E.; Langeveld, B.; Schubert, U. New Trends in the Use of Transition Metal–Ligand Complexes for Applications in Electroluminescent Devices. *Adv. Mater.* **2005**, *17*, 1109–1121

.

(299) Lo, K. K.-W.; Louie, M.-W.; Zhang, K. Y. Design of Luminescent Iridium (III) and Rhenium (I) Polypyridine Complexes As In Vitro and In Vivo Ion, Molecular and Biological Probes. *Coord. Chem. Rev.* **2010**, *254*, 2603–2622

.

(300) Lo, K. K.-W.; Choi, A. W.-T.; Law, W. H.-T. Applications of Luminescent Inorganic and Organometallic Transition Metal Complexes as Biomolecular and Cellular Probes. *Dalton Trans.* **2012**, *41*, 6021–6047

.

(301) Yin Zhang, K.; Ka-Shun Tso, K.; Louie, M.-W.; Liu, H.-W.; Kam-Wing Lo, K. A Phosphorescent Rhenium (I) Tricarbonyl Polypyridine Complex Appended with a Fructose Pendant that Exhibits Photocytotoxicity and Enhanced Uptake by Breast Cancer Cells. *Organomet.* **2013**, *32*, 5098–5102

.

(302) Herman, L.; Ghosh, S.; Defrancq, E.; Mesmaekera, A. K.-D. Ru (II) Complexes and Light: Molecular Tools for Biomolecules. *J. Phys. Org. Chem.* **2008**, *21*, 670–681

.

(303) Zeglis, B. M.; Pierre, V. C.; Barton, J. K. Metallo-Intercalators and Metallo-Insertors. *Chem. Comm.* **2007**, *44*, 4565–4579

.

(304) Bonnet, S.; Collin, J.-P. Ruthenium-based Light-Driven Molecular Machine Prototypes: Synthesis and Properties. *Chem. Soc. Rev.* **2008**, *37*, 1207–1217

.

(305) Yam, V. W.-W.; Ko, C.-C.; Zhu, N. Photochromic and Luminescence Switching Properties of a Versatile Diarylethene-Containing 1, 10-Phenanthroline Ligand and its Rhenium (I) Complex. *J. Am. Chem. Soc.* **2004**, *126*, 12734–12735

.

(306) Bingol, B.; Durrell, A. C.; Keller, G. E.; Palmer, J. H.; Grubbs, R. H.; Gray, H. B. Electron Transfer Triggered by Optical Excitation of Phenothiazine-tris (meta-phenyleneethynylene)-(tricarbonyl)(bpy)(py) rhenium (I). *J. Phys. Chem. B* **2012**, *117*, 4177–4182

.

(307) Blanco-Rodríguez, A.M.; Di Bilio, A.J.; Shih, C. ; Museth, A.K.; Clark, I.P.; Towrie, M. and Cannizzo, A.; Sudhamsu, J.; Crane, B.R. Sỳkora, J.; et al. Phototriggering Electron Flow through ReI-modified Pseudomonas aeruginosa Azurins. *Chem. Eur. J.* **2011**, *17*, 5350–5361

.

(308) Önfelt, B.; Lincoln, P.; Nordén, B.; Baskin, J. S.; Zewail, A. H. Femtosecond Linear Dichroism of DNA-Intercalating Chromophores: Solvation and Charge Separation Dynamics of [Ru(phen)2dppz]2+ Systems. *Proc. Natl. Acad. Sci. U.S.A.* **2000**, *97*, 5708–5713

.

(309) Coates, C. G.; Olofsson, J.; Coletti, M.; McGarvey, J. J.; Önfelt, B.; Lincoln, P.; Norden, B.; Tuite, E.; Matousek, P.; Parker, A. W. Picosecond time-resolved resonance

Raman probing of the light-switch states of [Ru (Phen) 2dppz] 2+ *J. Phys. Chem. B* **2001**, *105*, 12653–12664

.

(310) Sun, Y.; Liu, Y.; Turro, C. Ultrafast Dynamics of the Low-Lying 3MLCT States of [Ru(bpy)2(dppp2)]2+. *J. Am. Chem. Soc.* **2010**, *132*, 5594–5595

.

(311) McCusker, J. K.; Vlcek Jr, A. Ultrafast Excited-State Processes in Inorganic Systems. 2015

.

(312) Mondal, P.; Opalka, D.; Poluyanov, L. V.; Domcke, W. Jahn–Teller and Spin–Orbit Coupling Effects in Transition-Metal Trifluorides. *Chem. Phys.* **2011**, *387*, 56–65

.

(313) Decurtins, S.; Gütlich, P.; Köhler, C.; Spiering, H.; Hauser, A. A. Light-Induced Excited Spin State Trapping in a Transition-Metal Complex: The Hexa-1-propyltetrazole-iron (II) Tetrafluoroborate Spin-Crossover System. *Chem. Phys. Lett.* **1984**, *105*, 1–4

.

(314) Gütlich, P.; Hauser, A.; Spiering, H. Thermal and Optical Switching of Iron (II) Complexes. *Angew. Chem. Int. Ed.* **1994**, *33*, 2024–2054

.

(315) Hauser, A. Intersystem Crossing in the [Fe (ptz) 6](BF4) 2 Spin Crossover System (ptz= 1-propyltetrazole). *J. Chem. Phys.* **1991**, *94*, 2741–2748

.

(316) Hauser, A. *Spin Crossover In Transition Metal Compounds Ii* **2004**, *234*, 155–198

.

(317) Lorenc, M. ; Hébert, J.; Moisan, N.; Trzop, E.; Servol, M.; Buron-Le Cointe, M.; and Cailleau, H.; and Boillot, M-L.; Pontecorvo, E.; and Wulff, M.; et al. Successive Dynamical Steps of Photoinduced Switching of a Molecular Fe (III) Spin-Crossover Material by Time-Resolved X-ray Diffraction. *Phys. Rev. Lett.* **2009**, *103*, 028301

.

(318) Cammarata, M.; Bertoni, R.; Lorenc, M.; Cailleau, H.; Di Matteo, S.; Mauriac, C.; Matar, Samir F.; Lemke, H.; Chollet, M.; Ravy, S; et al. Sequential Activation of Molecular Breathing and Bending during Spin-Crossover Photoswitching Revealed by Femtosecond Optical and X-Ray Absorption Spectroscopy. *Phys. Rev. Lett.* **2014**, *113*, 227402

.

(319) Vankó, G.; Bordage, A.; Pápai, M.; Haldrup, K.; Glatzel, P.; and March, A.M.; Doumy, G.; and Britz, A.; Galler, A.; Assefa, T. et al. Detailed Characterization of a Nanosecond-Lived Excited State: X-ray and Theoretical Investigation of the Quintet State in Photoexcited $[Fe(terpy)_2]^{2+}$ *J. Phys. Chem. C* **2015**, *119*, 5888–5902

.

(320) Vanko, G.; Glatzel, P.; Pham, V.-T.; Abela, R.; Grolimund, D.; Borca, C. N.; Johnson, S. L.; Milne, C. J.; Bressler, C. Picosecond Time-Resolved X-Ray Emission Spectroscopy: Ultrafast Spin-State Determination in an Iron Complex *Angew. Chem. Int. Ed.* **2010**, *49*, 5910–5912

.

(321) Pápai, M.; Vanko, G.; de Graaf, C.; Rozgonyi, T. Theoretical Investigation of the Electronic Structure of Fe(II) Complexes at Spin-State Transitions *J. Chem. Theory Comput.* **2013**, *9*, 509–519

.

(322) Gawelda, W.; Cannizzo, A.; Pham, V.-T.; van Mourik, F.; Bressler, C.; Chergui, M. Ultrafast Nonadiabatic Dynamics of [FeII (bpy) 3] 2+ in Solution. *J. Am. Chem. Soc.* **2007**, *129*, 8199–8206

.

(323) Huse, N.; Kim, T. K.; Jamula, L.; McCusker, J. K.; de Groot, F. M. F.; Schoenlein, R. W. Photo-Induced Spin-State Conversion in Solvated Transition Metal Complexes Probed via Time-Resolved Soft X-ray Spectroscopy *J. Am. Chem. Soc.* **2010**, *132*, 6809–6816

.

(324) Cho, H.; Strader, M. L.; Hong, K.; Jamula, L.; Gullikson, E. M.; Kim, T. K.; de Groot, F. M. F.; McCusker, J. K.; Schoenlein, R. W.; Huse, N. Ligand-field symmetry effects in Fe(II) Polypyridyl Compounds Probed by Transient X-ray Absorption Spectroscopy *Faraday Discuss.* **2012**, *157*, 463

.

(325) Sousa, C.; de Graaf, C.; Rudavskyi, A.; Broer, R.; Tatchen, J.; Etinski, M.; Marian, C. M. Ultrafast Deactivation Mechanism of the Excited Singlet in the Light-Induced Spin Crossover of [Fe (2, 2-bipyridine) 3] 2+ *Chem. Eur. J.* **2013**, *19*, 17541–17551

.

(326) Ardo, S.; Meyer, G. J. Photodriven Heterogeneous Charge Transfer with Transition-Metal Compounds Anchored to TiO 2 Semiconductor Surfaces. *Chem. Soc. Rev.* **2009**, *38*, 115–164

.

(327) Liu, Y.; Harlang, T.; Canton, S.; Chabera, P.; Suarez-Alcantara, K.; Fleckhaus, A.; Vithanage, D. A.; Göransson, E.; Corani, A.; Lomoth, R.; Sundström, V.;

Wärnmark, K. Towards Longer-Lived Metal-to-Ligand Charge Transfer States of Iron(ii) Complexes: an N-Heterocyclic Carbene Approach *Chem. Comm.* **2013**, *49*, 6412

.

(328) Harlang, T. C. B; Liu, Y.; Gordivska, O.; and Fredin, L.A.; Ponseca Jr, C.S.; Huang, P.; Chabera, P.; Kjaer, K.S.; Mateos, H.; Uhlig, J. et al. Iron Sensitizer Converts Light to Electrons with 92% Yield *Nat. Chem.* **2015**, *7*, 883–889

.

(329) Yersin, H. *Highly efficient OLEDs with Phosphorescent Materials*; John Wiley & Sons, 2008

.

(330) Kafafi, Z. H. *Organic Electroluminescence*; CRC Press, 2005

.

(331) Shinar, J.; Savvateev, V. *Introduction to Organic Light-Emitting Devices*; Springer, 2004

.

(332) Su, H.-C.; Chen, H.-F.; Fang, F.-C.; Liu, C.-C.; Wu, C.-C.; Wong, K.-T.; Liu, Y.-H.; Peng, S.-M. Solid-State White Light-Emitting Electrochemical Cells Using Iridium-Based Cationic Transition Metal Complexes. *J. Am. Chem. Soc.* **2008**, *130*, 3413–3419, cited By 117

.

(333) Slinker, J.; Bernards, D.; Houston, P.; Abruña, H.; Bernhard, S.; Malliaras, G. Solid-State Electroluminescent Devices Based on Transition Metal Complexes. *Chem. Comm.* **2003**, *9*, 2392–2399.

.

(334) Zhao, Q.; Li, F.; Huang, C. Phosphorescent Chemosensors Based on Heavy-Metal Complexes. *Chem. Soc. Rev.* **2010**, *39*, 3007–3030.

.

(335) Keefe, M.; Benkstein, K.; Hupp, J. Luminescent Sensor Molecules Based on Coordinated Metals: A Review of Recent Developments. *Coord. Chem. Rev.* **2000**, *205*, 201–228.

.

(336) Barbieri, A.; Accorsi, G.; Armaroli, N. *Chem. Comm.* **2008**, 2185–2193.

(337) Armaroli, N. Luminescent Complexes Beyond the Platinum Group: The d10 Avenue *Chem. Soc. Rev.* **2001**, *30*, 113–124

.

(338) Lazorski, M. S.; Castellano, F. N. Advances in the Light Conversion Properties of Cu (I)-based Photosensitizers *Polyhedron* **2014**,

.

(339) Juris, A.; Balzani, V.; Barigelletti, F.; Campagna, S.; Belser, P.; von Zelewsky, A. Ru(II) Polypyridine Complexes: Photophysics, Photochemistry, Eletrochemistry, and Chemiluminescence. *Coord. Chem. Rev.* **1988**, *84*, 85 – 277

.

(340) McMillin, D. R.; Kirchhoff, J. R.; Goodwin, K. V. Exciplex Quenching of Photo-Excited Copper Complexes *Coord. Chem. Rev.* **1985**, *64*, 83–92

.

(341) Cunningham, C.; Cunningham, K.; Michalec, J.; McMillin, D. Cooperative Substituent Effects on the Excited States of Copper Phenanthrolines *Inorg. Chem.* **1999**, *38*, 4388–4392

.

(342) Eggleston, M. K.; McMillin, D. R.; Koenig, K. S.; Pallenberg, A. J. Steric Effects in the Ground and Excited States of Cu (NN) 2+ Systems *Inorg. Chem.* **1997**, *36*, 172–176

.

(343) Chen, L.; Shaw, G.; Novozhilova, I.; Liu, T.; Jennings, G.; Attenkofer, K.; Meyer, G.; Coppens, P. MLCT State Structure and Dynamics of a Copper(I) Diimine Complex Characterized by Pump-Probe X-ray and Laser Spectroscopies and DFT Calculations *J. Am. Chem. Soc.* **2003**, *125*, 7022–7034

.

(344) Capano, G.; Penfold, T. J.; Rothlisberger, U.; Tavernelli, I. A Vibronic Coupling Hamiltonian to Describe the Ultrafast Excited State Dynamics of a Cu(I)-phenanthroline Complex *Chimia* **2014**, *68*, 227–230

.

(345) Iwamura, M.; Takeuchi, S.; Tahara, T. Ultrafast Excited-State Dynamics of Copper (I) Complexes. *Acc. Chem. Res.* **2015**, *48*, 782–791

.

(346) Iwamura, M.; Takeuchi, S.; Tahara, T. Real-time Observation of the Photoinduced Structural Change of Bis(2,9-dimethyl-1,10-phenanthroline)copper(I) by Femtosecond Fluorescence Spectroscopy: A Realistic Potential Curve of the Jahn-Teller Distortion *J. Am. Chem. Soc.* **2007**, *129*, 5248–5256

.

(347) Shaw, G. B.; Grant, C. D.; Shirota, H.; Castner, E. W.; Meyer, G. J.; Chen, L. X. Ultrafast Structural Rearrangements in the MLCT Excited State for Copper(I) Bis-Phenanthrolines in Solution *J. Am. Chem. Soc.* **2007**, *129*, 2147–2160

.

(348) Iwamura, M.; Watanabe, H.; Ishii, K.; Takeuchi, S.; Tahara, T. Coherent Nuclear Dynamics in Ultrafast Photoinduced Structural Change of Bis (diimine) copper (I) Complex *J. Am. Chem. Soc.* **2011**, *133*, 7728

.

(349) Iwamura, M.; Takeuchi, S.; Tahara, T, Substituent Effect on the Photoinduced Structural Change of Cu(I) Complexes Observed by Femtosecond Emission Spectroscopy *Phys. Chem. Chem. Phys.* **2014**, *16*, 4143–4154

.

(350) Zgierski, M. Cu(I)-2,9-dimethyl-1,10-phenanthroline: Density Functional Study of the Structure, Vibrational Force-Field, and Excited Electronic States *J. Chem. Phys* **2003**, *118*, 4045

.

(351) Agena, A.; Iuchi, S.; Higashi, M. Theoretical Study on Photoexcitation Dynamics of a Bis-diimine Cu (I) Complex in Solutions. *Chem. Phys. Lett.* **2017**, *679*, 60–65

.

(352) Garakyaraghi, S.; Danilov, E. O.; McCusker, C. E.; Castellano, F. N. Transient Absorption Dynamics of Sterically Congested Cu (I) MLCT Excited States. *J. Phys. Chem. A* **2015**, *119*, 3181–3193

.

(353) Huang, J.; and Buyukcakir, O.; and Mara, M.W.; Coskun, A.; Dimitrijevic, N.M.; Barin, G.; Kokhan, O.; Stickrath, A.B.; Ruppert, R.; and Tiede, D.M.; et al. Highly Efficient Ultrafast Electron Injection From the Singlet MLCT Excited State of Copper (I) Diimine Complexes to TiO2 Nanoparticles. *Angew. Chem. Int. Ed.* **2012**, *51*, 12711–12715

.

(354) Krylova, V. A.; Djurovich, P. I.; Aronson, J. W.; Haiges, R.; Whited, M. T.; Thompson, M. E. Structural and Photophysical Studies of Phosphorescent Three-Coordinate Copper (I) Complexes Supported by an N-Heterocyclic Carbene Ligand. *Organometallics* **2012**, *31*, 7983–7993

.

(355) Gernert, M.; Müller, U.; Haehnel, M.; Pflaum, J.; Steffen, A. Cyclic Alkyl(amino)carbene as Two-Atom π-Chromophore Leading to the First Phosphorescent Linear Cu^I Complexes *Chem. Eur. J.* **2017**, *23*, 2206–2216

.

(356) Shi, S.; Collins, L. R.; Mahon, M. F.; Djurovich, P. I.; Thompson, M. E.; Whittlesey, M. K. Synthesis and Characterization of Phosphorescent Two Coordinate Copper(i) Complexes Bearing Diamidocarbene Ligands. *Dalton Trans.* **2017**, *46*, 745–752

.

(357) Romanov, A. S.; Di, D.; Yang, L.; Fernandez-Cestau, J.; Becker, C. R.; James, C. E.; Zhu, B.; Linnolahti, M.; Credgington, D.; Bochmann, M. Highly Photoluminescent Copper Carbene Complexes Based on Prompt Rather than Delayed Fluorescence. *Chem. Commun.* **2016**, *52*, 6379–6382

.

(358) Romanov, A. S.; Becker, C. R.; James, C. E.; Di, D.; Credgington, D.; Linnolahti, M.; Bochmann, M. Copper and Gold Cyclic (Alkyl)(amino)carbene Complexes with Sub-Microsecond Photoemissions: Structure and Substituent Effects on Redox and Luminescent Properties. *Chem. Eur. J.* **2017**, *23*, 4625–4637

.

(359) Di, D.; Romanov, A. S.; Yang, L.; Richter, J. M.; Rivett, J. P. H.; Jones, S.; Thomas, T. H.; Abdi Jalebi, M.; Friend, R. H.; Linnolahti, M.; Bochmann, M.; Credg-

ington, D. High-Performance Light-Emitting Diodes Based on Carbene-Metal-Amides. *Science* **2017**, *356*, 159–163

.

(360) Liske, A.; Wallbaum, L.; Föller, J.; Gernert, M.; Ganter, C.; Marian, C. M.; Steffen, A. Highly Efficient Blue to Blue-Green ^{3}MLCT Phosphorescence from a Novel Class of Linear Cu^I complexes. *Chem. Eur. J. submitted*

.

(361) Föller, J.; Marian, C. M. Rotationally Assisted Spin-State Inversion in Carbene-Metal-Amides Is an Artifact *submitted*

.

(362) Wrighton, M.; Morse, D. L. Nature of the Lowest Excited State in Tricarbonylchloro-1, 10-phenanthrolinerhenium (I) and Related Complexes. *J. Am. Chem. Soc.* **1974**, *96*, 998–1003

.

(363) Kumar Arvind, L. A. J., Sun Shih Sheng Photophysics and Photochemistry of Rhenium Diimine Complexes. *Top. Organomet. Chem.* **2010**, *29*, 1–35

.

(364) Vlček, A.; Busby, M. Ultrafast ligand-to-ligand electron and energy transfer in the complexes fac-[Re I (L)(CO)$_3$ (bpy)] $^{n+}$ *Coord. Chem. Chem.* **2006**, *250*, 1755–1762

.

(365) Leonidova, A.; Gasser, G. Underestimated Potential of Organometallic Rhenium Complexes as Anticancer Agents. *ACS Chem. Bio.* **2014**, *9*, 2180–2193

.

(366) Wenger, O. S. Proton-coupled electron transfer with photoexcited ruthenium (II), rhenium (I), and iridium (III) complexes. *Coord. Chem. Chem.* **2015**, *282*, 150–158

.

(367) Warren, J. J.; Ener, M. E.; Vlček, A.; Winkler, J. R.; Gray, H. B. Electron Hopping Through Proteins. *Coord. Chem. Chem.* **2012**, *256*, 2478–2487

.

(368) Lo, K. K.-W. Luminescent Rhenium (I) and Iridium (III) Polypyridine Complexes as Biological Probes, Imaging Reagents, and Photocytotoxic Agents. *Acc. Chem. Res.* **2015**, *48*, 2985–2995

.

(369) Zhao, G.-W.; Zhao, J.-H.; Hu, Y.-X.; Zhang, D.-Y.; Li, X. Recent Advances of Neutral Rhenium (I) Tricarbonyl Complexes for Application in Organic Light-Emitting Diodes. *Synth. Met.* **2016**, *212*, 131–141

.

(370) Lees, A. J. Luminescence Properties of Organometallic Complexes. *Chem Rev.* **1987**, *87*, 711–743

.

(371) El Nahhas, A.; Van Der Veen, R.; Penfold, T.; Pham, V.; Lima, F.; Abela, R.; Blanco-Rodriguez, A.; Zalis, S.; Vlcek, A.; Tavernelli, I.; Rothlisberger, U.; Milne, C.; Chergui, M. X-ray Absorption Spectroscopy of Ground and Excited Rhenium–Carbonyl–Diimine Complexes: Evidence for a Two-Center Electron Transfer. *J. Phys. Chem. A* **2013**, *117*, 361–369

.

(372) Heydova, R.; Gindensperger, E.; Romano, R.; Saokora, J.; Vlček Jr, A.; Záliš, S.; Daniel, C. Spin–orbit treatment of UV–vis absorption spectra and photophysics of rhenium (I) carbonyl–bipyridine complexes: MS-CASPT2 and TD-DFT Analysis. *J. Phys. Chem. A* **2012**, *116*, 11319–11329

.

(373) El Nahhas, A.; Consani, C.; Blanco-Rodríguez, A. M.; Lancaster, K. M.; Braem, O.; Cannizzo, A.; Towrie, M.; Clark, I. P.; Zalis, S.; Chergui, M.; Vlček Jr, A. Ultrafast Excited-State Dynamics of Rhenium (I) Photosensitizers [Re (Cl)$(CO)_3$ (N, N)] and [Re (imidazole)$(CO)_3$ (N, N)]$^+$: Diimine Effects. *Inorg. Chem.* **2011**, *50*, 2932–2943

.

(374) Vlček Jr, A. *Photophysics of organometallics*; Springer, 2009; 115–158

.

(375) Blanco-Rodríguez, A. M.; Towrie, M.; Collin, J.-P.; Záliš, S.; Vlček Jr, A. Excited-State Relaxation Dynamics of Re (I) Tricarbonyl Complexes with Macrocyclic Phenanthroline Ligands Studied by Time-Resolved IR Spectroscopy. *Dalton Trans.* **2009**, 3941–3949

.

(376) Vlček Jr, A.; Kvapilova, H.; Towrie, M.; Záliš, S. Electron-Transfer Acceleration Investigated by Time Resolved Infrared Spectroscopy. *Acc. Chem. Res.* **2015**, *48*, 868–876

.

(377) Busby, M.; Matousek, P.; Towrie, M.; Vlček, A. Ultrafast excited-state dynamics of photoisomerizing complexes fac-[Re (Cl)$(CO)_3$ $(papy)_2$] and fac-[Re (papy)$(CO)_3$ (bpy)]$^+$(papy= trans-4-phenylazopyridine). *Inorg. Chim. Acta.* **2007**, *360*, 885–896

.

(378) Ko, C.-C.; Kwok, W.-M.; Yam, V. W.-W.; Phillips, D. L. Triplet MLCT Photosensitization of the Ring-Closing Reaction of Diarylethenes by Design and Synthesis of a Photochromic Rhenium (I) Complex of a Diarylethene-Containing 1,10-Phenanthroline Ligand. *Chem. Eur. J.* **2006**, *12*, 5840–5848

.

(379) Busby, M.; Hartl, F.; Matousek, P.; Towrie, M.; Vlček, A. Ultrafast Excited State Dynamics Controlling Photochemical Isomerization of N-Methyl-4-[trans-2-(4-pyridyl) ethenyl] pyridinium Coordinated to a {ReI $(CO)_3$(2, 2'-bipyridine)} Chromophore. *Chem. Eur. J.* **2008**, *14*, 6912–6923

.

(380) Kiefer, L. M.; King, J. T.; Kubarych, K. J. Dynamics of Rhenium Photocatalysts Revealed Through Ultrafast Multidimensional Spectroscopy. *Acc. Chem. Res.* **2015**, *48*, 1123–1130

.

(381) Yang, L.; Ren, A.-M.; Feng, J.-K.; Liu, X.-J.; Ma, Y.-G.; Zhang, M.; Liu, X.-D.; Shen, J.-C.; Zhang, H.-X. Theoretical Studies of Ground and Excited Electronic States in a Series of Halide Rhenium (I) bipyridine Complexes. *J. Phys. Chem. A* **2004**, *108*, 6797–6808

.

(382) Vlček, A.; Záliš, S. Comments on Theoretical Studies of Ground and Excited Electronic States in a Series of Halide Rhenium (I) Bipyridine Complexes. *J. Phys. Chem. A* **2005**, *109*, 2991–2992

.

(383) Nahhas, A. E.; Cannizzo, A.; Mourik, F. v.; Blanco-Rodrguez, A. M.; Záliš, S.; Vlček, A., Jr; Chergui, M. Ultrafast Excited-State Dynamics of [Re (L)$(CO)_3$ (bpy)]$^{n+}$ Complexes: Involvement of the Solvent. *J. Phys. Chem. A* **2010**, *114*, 6361–6369

.

(384) Baková, R.; Chergui, M.; Daniel, C.; Vlček, A.; Záliš, S. Relativistic effects in spectroscopy and photophysics of heavy-metal complexes illustrated by spin–orbit calculations of [Re (imidazole)$(CO)_3$ (phen)]$^+$ *Coord. Chem. Rev.* **2011**, *255*, 975–989

.

(385) Gourlaouen, C.; Eng, J.; Otsuka, M.; Gindensperger, E.; Daniel, C. Quantum Chemical Interpretation of Ultrafast Luminescence Decay and Intersystem Crossings in Rhenium (I) Carbonyl Bipyridine Complexes. *J. Chem. Theory. Comput.* **2015**, *11*, 99–110

.

(386) Fumanal, M.; Daniel, C. Description of Excited States in [Re (Imidazole)$(CO)_3$ (Phen)]$^+$ Including Solvent and Spin-Orbit Coupling Effects: Density Functional Theory Versus Multiconfigurational Wavefunction Approach. *J. Comp. Chem.* **2016**, *37*, 2454–2466

.

(387) Fumanal, M.; Daniel, C. Electronic and Photophysical Properties of [Re (L)$(CO)_3$ (phen)]+ and [Ru $(L)_2$ (bpy) 2] $^{2+}$ (L= imidazole), Building Units for Long-Range Electron Transfer in Modified Blue Copper Proteins. *J. Phys. Chem. A* **2016**, *120*, 6934–6943

.

(388) Fumanal, M.; Gindensperger, E.; Daniel, C. Ligand Substitution and Conformational Effects on the Ultrafast Luminescent Decay of (L=imidazole, pyridine): Nonadiabatic Quantum Dynamics. *to be published*

.

(389) Parmenter, C. S. Radiative and Nonradiative Processes in Benzene. *Adv. Chem. Phys.* **1972**, *22*, 365–421

.

(390) Clara, M.; Hellerer, T.; Neusser, H. J. Fast Decay of High Vibronic S_1 States in Gas-Phase Benzene. *Appl. Phys. B* **2000**, *71*, 431

.

(391) Penfold, T.; Worth, G. The Effect of Molecular Distortions on Spin-Orbit Coupling in Simple Hydrocarbons *Chem. Phys.* **2010**, *375*, 58–66

.

(392) Becker, R. S.; Seixas de Melo, J.; Macanita, A. L.; Elisei, F. Comprehensive Evaluation of the Absorption, Photophysical, Energy Transfer, Structural, and Theoretical Properties of α-oligothiophenes with One to Seven Rings. *J. Phys. Chem.* **1996**, *100*, 18683–18695

.

(393) Weinkauf, R.; Lehr, L.; Schlag, E.; Salzmann, S.; Marian, C. Ultrafast Dynamics in Thiophene Investigated by Femtosecond Pump Probe Photoelectron Spectroscopy and Theory. *Phys. Chem. Chem. Phys.* **2008**, *10*, 393–404

.

(394) Salzmann, S.; Kleinschmidt, M.; Tatchen, J.; Weinkauf, R.; Marian, C. M. Excited States of Thiophene: Ring Opening as Deactivation Mechanism. *Phys. Chem. Chem. Phys.* **2008**, *10*, 380–392

.

(395) Cui, G.; Fang, W. Ab Initio Trajectory Surface-Hopping Study on Ultrafast Deactivation Process of Thiophene. *J. Phys. Chem. A* **2011**, *115*, 11544–11550

.

(396) Prlj, A.; Curchod, B. F.; Corminboeuf, C. Excited state dynamics of thiophene and bithiophene: new insights into theoretically challenging systems. *Phys. Chem. Chem. Phys.* **2015**, *17*, 14719–14730

.

(397) Schnappinger, T.; Kölle, P.; Marazzi, M.; Monari, A.; González, L.; de Vivie-Riedle, R.

Ab initio Molecular Dynamics of Thiophene: The Interplay of Internal Conversion and Intersystem Crossing. *Phys. Chem. Chem. Phys.* **2017**,

.

(398) Middleton, C. T.; de La Harpe, K.; Su, C.; Law, Y. K.; Crespo-Hernández, C. E.; Kohler, B. DNA Excited-State Dynamics: From Single Bases to the Double Helix *Ann. Rev. Phys. Chem.* **2009**, *60*, 217–239

.

(399) Crespo-Hernández, C. E.; Cohen, B.; Hare, P. M.; Kohler, B. Ultrafast Excited-State Dynamics in Nucleic Acids *Chem. Rev.* **2004**, *104*, 1977–2020

.

(400) McFarland, B.K. ; Farrell, J.P. ; Miyabe, S. ; Tarantelli, F. ; Aguilar, A.; Berrah, N.; Bostedt, C.; Bozek, J.D. ; Bucksbaum, P.H. ; Castagna, J.C.; et al. Ultrafast X-ray Auger Probing of Photoexcited Molecular Dynamics. *Nat. Comm.* **2014**, *5*, 4235

.

(401) Wolf, T.J.A.; Myhre, R.H. ; Cryan, J.P.; Coriani, S. ; Squibb, R.J. ; Battistoni, A. ; Berrah, N.; Bostedt, C.; Bucksbaum, P.; Coslovich, G, et al. Probing ultrafast $\pi\pi^*/n\pi^*$ internal conversion in organic chromophores via K-edge resonant absorption. *Nat. Comm.* **2017**, *8*

.

(402) Samoylova, E.; Lippert, H.; Ullrich, S.; Hertel, I. V.; Radloff, W.; Schultz, T. Dynamics of Photoinduced Processes in Adenine and Thymine Base Pairs *J. Am. Chem. Soc.* **2005**, *127*, 1782–1786

.

(403) Ullrich, S.; Schultz, T.; Zgierski, M. Z.; Stolow, A. Direct Observation of Electronic

Relaxation Dynamics in Adenine via Time-Resolved Photoelectron Spectroscopy *J. Am. Chem. Soc.* **2004**, *126*, 2262–2263

.

(404) Canuel, C.; Mons, M.; Piuzzi, F.; Tardivel, B.; Dimicoli, I.; Elhanine, M. Excited states dynamics of DNA and RNA bases: Characterization of a stepwise deactivation pathway in the gas phase *J. Chem. Phys.* **2005**, *122*, 074316

.

(405) González-Vázquez, J.; González, L.; Samoylova, E.; Schultz, T. Thymine Relaxation after UV Irradiation: The Role of Tautomerization and $\pi\sigma^*$ States *Phys. Chem. Chem. Phys.* **2009**, *11*, 3927

.

(406) Lobsiger, S.; Etinski, M.; Blaser, S.; Frey, H.-M.; Marian, C.; Leutwyler, S. Intersystem Crossing Rates of S1 State Keto-Amino Cytosine at Low Excess Energy. *J. Chem. Phys.* **2015**, *143*, 234301

.

(407) Pecourt, J.-M. L.; Peón, J.; Kohler, B. Ultrafast Internal Conversion of Electronically Excited RNA and DNA Nucleosides in Water *J. Am. Chem. Soc.* **2000**, *122*, 9348–9349

.

(408) Gustavsson, T.; Sarkar, N.; Lazzarotto, E.; Markovitsi, D.; Improta, R. Singlet excited state dynamics of uracil and thymine derivatives: A femtosecond fluorescence upconversion study in acetonitrile *Chem. Phys. Lett.* **2006**, *429*, 551–557

.

(409) Sharonov, A.; Gustavsson, T.; Carré, V.; Renault, E.; Markovitsi, D. Cytosine ex-

cited state dynamics studied by femtosecond fluorescence upconversion and transient absorption spectroscopy *Chem. Phys. Lett.* **2003**, *380*, 173–180

.

(410) Kohler, B. Nonradiative Decay Mechanisms in DNA Model Systems *J. Phys. Chem. Lett.* **2010**, *1*, 2047–2053

.

(411) Cohen, B.; Hare, P. M.; Kohler, B. Ultrafast Excited-State Dynamics of Adenine and Monomethylated Adenines in Solution: Implications for the Nonradiative Decay Mechanism *J. Am. Chem. Soc.* **2003**, *125*, 13594–13601

.

(412) Ismail, N.; Blancafort, L.; Olivucci, M.; Kohler, B.; Robb, M. A. Ultrafast Decay of Electronically Excited Singlet Cytosine via a State Switch. *J. Am. Chem. Soc.* **2002**, *124*, 6818–6819.

.

(413) Lan, Z.; Fabiano, E.; Thiel, W. Photoinduced Nonadiabatic Dynamics of Pyrimidine Nucleobases: On-the-Fly Surface-Hopping Study with Semiempirical Methods *J. Phys. Chem. B* **2009**, *113*, 3548–3555

.

(414) Blancafort, L.; Cohen, B.; Hare, P. M.; Kohler, B.; Robb, M. A. Singlet Excited-State Dynamics of 5-Fluorocytosine and Cytosine: An Experimental and Computational Study *J. Phys. Chem. A* **2005**, *109*, 4431–4436

.

(415) Merchan, M.; Serrano-Andres, L.; Robb, M. A.; Blancafort,L Triplet-State Formation along the Ultrafast Decay of Excited Singlet Cytosine. *J. Am. Chem. Soc.* **2005**, *127*, 1820–1825

.

(416) Boggio-Pasqua, M.; Groenhof, G.; Schäfer, L. V.; Grubmüller, H.; Robb, M. A. Ultrafast Deactivation Channel for Thymine Dimerization *J. Am. Chem. Soc.* **2007**, *129*, 10996–10997

.

(417) Serrano-Pérez, J. J.; González-Ramírez, I.; Coto, P. B.; Merchán, M.; Serrano-Andrés, L. Theoretical Insight into the Intrinsic Ultrafast Formation of Cyclobutane Pyrimidine Dimers in UV-Irradiated DNA: Thymine versus Cytosine *J. Phys. Chem. B* **2008**, *112*, 14096–14098

.

(418) Asturiol, D.; Lasorne, B.; Robb, M. A.; Blancafort, L. Photophysics of the π,π^* and n,π^* States of Thymine: MS-CASPT2 Minimum-Energy Paths and CASSCF on-the-Fly Dynamics *J. Phys. Chem. A* **2009**, *113*, 10211–10218

.

(419) Hudock, H. R.; Levine, B. G.; Thompson, A. L.; Satzger, H.; Townsend, D.; Gador, N.; Ullrich, S.; Stolow, A.; Martínez, T. J. Ab Initio Molecular Dynamics and Time-Resolved Photoelectron Spectroscopy of Electronically Excited Uracil and Thymine *J. Phys. Chem. A* **2007**, *111*, 8500–8508

.

(420) Perun, S.; Sobolewski, A. L.; Domcke, W. Conical Intersections in Thymine *J. Phys. Chem. A* **2006**, *110*, 13238–13244

.

(421) Marian, C. M. A new pathway for the rapid decay of electronically excited adenine *J. Chem. Phys.* **2005**, *122*, 104314

.

(422) Mai, S.; Pollum, M.; Martínez-Fernández, L.; Dunn, N.; Marquetand, P.; Corral, I.; Crespo-Hernández, C. E.; González, L. The Origin of Efficient Triplet State Population in Sulfur-Substituted Nucleobases. *Nat. Comm.* **2016**, *7* 13077

.

(423) Lobsiger, S.; Leutwyler, S. The Adiabatic Ionization Energy and Triplet T1 Energy of Jet-Cooled Keto-Amino Cytosine. *J. Phys. Chem. Lett.* **2012**, *3*, 3576–3580

.

(424) Lobsiger, S.; Trachsel, M. A.; Frey, H.-M.; Leutwyler, S. Excited-State Structure and Dynamics of KetoAmino Cytosine: The $1\pi\pi*$ $StateIsNonplanarandItsRadiationlessDecayIsNotUltrafast.J.$ *Phys. Chem. B***2013**, *117*, 6106−−6115

.

(425) Etinski, M.; Fleig, T.; Marian, C. M. Intersystem Crossing and Characterization of Dark States in the Pyrimidine Nucleobases Uracil, Thymine, and 1-Methylthymine. *J. Phys. Chem. A* **2009**, *113*, 11809–11816

.

(426) Kunitski, M.; Nosenko, Y.; Brutschy, B. On the Nature of the Long-Lived Dark State of Isolated 1-Methylthymine. *ChemPhysChem* **2011**, *12*, 2024–2030

.

(427) Kobayashi, T.; Harada, Y.; Suzuki, T.; Ichimura, T. Excited State Characteristics of 6-Azauracil in Acetonitrile: Drastically Different Relaxation Mechanism from Uracil. *J. Phys. Chem. A* **2008**, *112*, 13308–13315

.

(428) Gobbo, J. P.; Borin, A. C.; Serrano-Andrés, L. On the Relaxation Mechanisms of 6-Azauracil. *J. Phys. Chem. B* **2011**, *115*, 6243–6251

.

(429) Bishop, S. M.; Malone, M.; Phillips, D.; Parker, A. W.; Symons, M. C. R. Singlet Oxygen Sensitisation by Excited State DNA *J. Chem. Soc., Chem. Commun.* **1994**, 871–872

.

(430) PM Hare, PM; Middleton, CT; Mertel, KI; Herbert, JM and Kohler, B Time-resolved infrared spectroscopy of the lowest triplet state of thymine and thymidine *Chem. Phys.* **2008**, *347*, 383 – 392

.

(431) Etinski, M.; Marian, C. M. Ab initio Investigation of the Methylation and Hydration Effects on the Electronic Spectra of Uracil and Thymine. *Phys. Chem. Chem. Phys.* **2010**, *12*, 4915–4923

.

(432) Villnow, T.; Ryseck, G.; Rai-Constapel, V.; Marian, C. M.; Gilch, P. Chimeric Behavior of Excited Thioxanthone in Protic Solvents: I. Experiments. *J. Phys. Chem. A* **2014**, *118*, 11696–11707

.

(433) Bonnett, R. Photosensitizers of the Porphyrin and Phthalocyanine Series for Photodynamic Therapy. *Chem. Soc. Rev.* **1995**, *24*, 19–33

.

(434) Ochsner, M. Photophysical and photobiological processes in the photodynamic therapy of tumours. *J. Photochem. Photobiol. B.* **1997**, *39*, 1 – 18

.

(435) Schweitzer, C.; Schmidt, R. Physical Mechanisms of Generation and Deactivation of Singlet Oxygen. *Chem. Rev.* **2003**, *103*, 1685–1757

.

(436) Shim, S. C. In *CRC Handbook of Organic Photochemistry and Photobiology*; Horspool, W. M., Song, P.-S., Eds.; CRC Press: Boca Raton, 1995; Chapter 8, pp 1347–1356

.

(437) Wainwright, M. The Development of Phenothiazinium Photosensitisers. *Photodiag. Photodyn. Ther.* **2005**, *2*, 263–272

.

(438) Kennedy, J. C.; Pottier, R. H.; Pross, D. Photodynamic Therapy with Endogeneous Protoporphyrin IX: Basic Principles and Present Clinical Experience *J. Photochem. Photobiol. B* **1990**, *6*, 143–148

.

(439) Tatchen, J.; Kleinschmidt, M.; Marian, C. M. Electronic Excitation Spectra and Singlet-Triplet Coupling in Psoralen and Its Sulfur and Selenium Analogs *J. Photochem. Photobiol. A.* **2004**, *167*, 201–212

.

(440) Tatchen, J.; Marian, C. M. Electronic Excitation Spectra and Vibronic Absorption and Emission Spectra of Psoralen: A Quantum Chemical Investigation *Phys. Chem. Chem. Phys.* **2006**, *8*, 2133–2144

.

(441) Gradyushko, A.; M.P.Tsvirko, Probabilities of Intercombination Transitions in Porphyrin and Metalloporphyrin Molecules. *Opt. Spektrosk.* **1971**, *31*, 291–295

.

(442) Gouterman, M. Spectra of Porphyrins. *J. Mol. Spec.* **1961**, *6*, 138 – 163

.

(443) Minaev, B.; Wang, Y.-H.; Wang, C.-K.; Luo, Y.; Ågren, H. Density functional theory study

of vibronic structure of the first absorption Qx band in free-base porphin. *Spectrochimica Acta Part A* **2006**, *65*, 308 – 323

.

(444) Niu, Y.; Peng, Q.; Deng, C.; Gao, X.; Shuai, Z. Theory of Excited State Decays and Optical Spectra: Application to Polyatomic Molecules. *J. Phys. Chem. A* **2010**, *114*, 7817–7831

.

(445) Nagashima, U.; Takada, T.; Ohno, K. Ab initio SCF-CI Calculation on Free Base Porphin and Chlorin; Theoretical Analysis on Intensities of the Absorption Spectra. *J. Chem. Phys.* **1986**, *85*, 4524–4529

.

(446) Baskin, J. S.; Yu, H.-Z.; Zewail, A. H. Ultrafast Dynamics of Porphyrins in the Condensed Phase: I. Free Base Tetraphenylporphyrin. *J. Chem. Phys. A* **2002**, *106*, 9837–9844

.

(447) Rodriguez-Serrano, A.; Daza, M. C.; Doerr, M.; Marian, C. M. A Quantum Chemical Investigation of the Electronic Structure of Thionine. *Photochem. Photobiol. Sci.* **2012**, *11*, 397–408

.

(448) Parker, C.; Hatchard, C. Triplet-Singlet Emission in Fluid Solutions. Phosphorescence of eosin. *Trans. Farad. Soc.* **1961**, *57*, 1894–1904

.

(449) Uoyama, H.; Goushi, K.; Shizu, K.; Nomura, H.; Adachi, C. Highly efficient organic light-emitting diodes from delayed fluorescence *Nature* **2012**, *492*, 234–238

.

(450) Dias, F. B.; Penfold, T. J.; Monkman, A. P. Photophysics of Thermally Activated Delayed Fluorescence Molecules. *Methods Appl. Fluoresc.* **2017**, *5*, 012001

.

(451) Reineke, S.; Walzer, K.; Leo, K. Triplet-Exciton Quenching in Organic Phosphorescent Light-Emitting Diodes with Ir-Based Emitters. *Phys. Rev. B* **2007**, *75*, 125328

.

(452) Dias, F. B.; Bourdakos, K. N.; Jankus, V.; Moss, K. C.; Kamtekar, K. T.; Bhalla, V.; Santos, J.; Bryce, M. R.; Monkman, A. P. Triplet harvesting with 100% efficiency by way of thermally activated delayed fluorescence in charge transfer OLED emitters. *Adv. Mater.* **2013**, *25*, 3707–3714

.

(453) Santos, P. L.; Ward, J. S.; Data, P.; Batsanov, A. S.; Bryce, M. R.; Dias, F. B.; Monkman, A. P. Engineering the singlet–triplet energy splitting in a TADF molecule. *J. Mater. Chem. C* **2016**, *4*, 3815-24.

.

(454) Etherington, M.K.; Franchello, F. ; Gibson, J. ; Northey, T. ; Santos, J. ; Ward, J.S; Higginbotham, H.F. ; Data, P. ; Kurowska, A. ; Dos Santos, P.L. et al. Regio-and conformational isomerization critical to design of efficient thermally-activated delayed fluorescence emitters *Nat. Comm.* **2017**, *8*, 14987

.

(455) Ward, J. S.; Nobuyasu, R. S.; Batsanov, A. S.; Data, P.; Monkman, A. P.; Dias, F. B.; Bryce, M. R. The interplay of thermally activated delayed fluorescence (TADF) and room temperature organic phosphorescence in sterically-constrained donor–acceptor charge-transfer molecules. *Chem. Commun.* **2016**, *52* 2612-5

.

(456) Gibson, J.; Monkman, A.; Penfold, T. The Importance of Vibronic Coupling for Efficient Reverse Intersystem Crossing in TADF molecules. *ChemPhysChem* **2016**, *17* 2956

.

(457) Nobuyasu, R. S.; Ren, Z.; Griffiths, G. C.; Batsanov, A. S.; Data, P.; Yan, S.; Monkman, A. P.; Bryce, M. R.; Dias, F. B. Rational Design of TADF Polymers Using a Donor–Acceptor Monomer with Enhanced TADF Efficiency Induced by the Energy Alignment of Charge Transfer and Local Triplet Excited States. *Adv. Opt. Mater. 4* 597-607 **2016**,

.

(458) Gibson, J.; Penfold, T. Nonadiabatic coupling reduces the activation energy in thermally activated delayed fluorescence. *Physical Chemistry Chemical Physics* **2017**, *19*, 8428–8434

.

(459) Hirata, S.; Sakai, Y.; Masui, K.; Tanaka, H.; Lee, S. Y.; Nomura, H.; Nakamura, N.; Yasumatsu, M.; Nakanotani, H.; Zhang, Q.; Shizu, K.; Miyazaki, H.; Adachi, C. Highly efficient blue electroluminescence based on thermally activated delayed fluorescence *Nat. Mater.* **2015**, *14* 330-336

.

(460) Marian, C. M. On the Mechanism of the Triplet-to-Singlet Upconversion in the Assistant Dopant ACRXTN *J. Phys. Chem. C* **2016**, *120*, 3715-21

.

(461) Pownall, H. J.; Huber, J. R. Absorption and emission spectra of aromatic ketones and their medium dependence. Excited states of xanthone. *J. Am. Chem. Soc.* **1971**, *93*, 6429–6436

.

(462) Connors, R. E.; Christian, W. R. Origin of the unusual triplet-state properties of xanthones. *J. Phys. Chem.* **1982**, *86*, 1524–1528

.

(463) Cavaleri, J. J.; Prater, K.; Bowman, R. M. An investigation of the solvent dependence on the ultrafast intersystem crossing kinetics of xanthone. *Chem. Phys. Lett.* **1996**, *259*, 495–502

.

(464) Heinz, B.; Schmidt, B.; Root, C.; Satzger, H.; Milota, F.; Fierz, B.; Kiefhaber, T.; Zinth, W.; Gilch, P. On the unusual fluorescence properties of xanthone in water. *Phys. Chem. Chem. Phys.* **2006**, *8*, 3432–3439

.

(465) Satzger, H.; Schmidt, B.; Root, C.; Zinth, W.; Fierz, B.; Krieger, F.; Kiefhaber, T.; Gilch, P. Ultrafast quenching of the xanthone triplet by energy transfer: new insight into the intersystem crossing kinetics. *J. Phys. Chem. A* **2004**, *108*, 10072–10079

.

(466) Inoue, M.; Serevičius, T.; Nakanotani, H.; Yoshida, K.; Matsushima, T.; Juršėnas, S.; Adachi, C. Effect of reverse intersystem crossing rate to suppress efficiency roll-off in organic light-emitting diodes with thermally activated delayed fluorescence emitters. *Chem. Phys. Lett.* **2016**, *644*, 62–67

.

(467) Nakanotani, H.; Higuchi, T.; Furukawa, T.; Masui, K.; Morimoto, K.; Numata, M.; Tanaka, H.; Sagara, Y.; Yasuda, T.; Adachi, C. High-efficiency organic light-emitting diodes with fluorescent emitters. *Nat. Comm.* **2014**, *5*

.

(468) Grimme, S.; Waletzke, M. A combination of Kohn–Sham density functional theory and multi-reference configuration interaction methods. *J. Chem. Phys.* **1999**, *111*, 5645–5655

.

(469) Lyskov, I.; Kleinschmidt, M.; Marian, C. M. Redesign of the DFT/MRCI Hamiltonian. *J. Chem. Phys.* **2016**, *144*, 034104

.

(470) Lim, E.; Yu, J. M. Spin-Orbit Interactions in Heteroaromatic Molecules. I. Polycyclic Monoazines. *J. Chem. Phys.* **1967**, *47*, 3270–3275

.

(471) Losi, A. Flavin-based Blue-Light Photosensors: A Photobiophysics Update. *Photochem. Photobiol.* **2007**, *83*, 1283–1300

.

(472) Losi, A.; Gärtner, W. Solving Blue Light Riddles: New Lessons from Flavin-binding LOV Photoreceptors. *Photochem. Photobiol.* **2017**, *93*, 141–158

.

(473) Connors, R. E.; Christian, W. M. Origin of the Unusual Triplet-State Properties of Xanthone *J. Phys. Chem.* **1992**, *86*, 1524–1528

.

(474) Cavaleri, J. J.; Prater, K.; Bowman, R. M.An investigation of the solvent dependence on the ultrafast intersystem crossing kinetics of xanthone *Chem. Phys. Lett.* **1996**, *259*, 495–502

.

(475) Allonas, X.; Ley, C.; Bibaut, C.; Jacques, P.; Fouassier, J. P. Investigation of the triplet quantum yield of thioxanthone by time-resolved thermal lens spectroscopy: solvent and population lens effects. *Chem. Phys. Lett.* **2000**, *322*, 483–490

.

(476) Satzger, H.; Schmidt, B.; Root, C.; Zinth, W.; Fierz, B.; Krieger, F.; Kiefhaber, T.; Gilch, P. Ultrafast Quenching of the Xanthone Triplet by Energy Transfer: New Insights into the Intersystem Crossing Kinetics. *J. Phys. Chem. A* **2004**, *108*, 10072–10079

.

(477) Heinz, B.; Schmidt, B.; Root, C.; Satzger, H.; Milota, F.; Fierz, B.; Kiefhaber, T.; Zinth, W.; Gilch, P. On the unusual fluorescence properties of xanthone in water. *Phys. Chem. Chem. Phys.* **2006**, *8*, 3432–3439

.

(478) Burget, D.; Jacques, P. Dramatic Solvent Effects on Thioxanthone Fluorescence Lifetime. *J. Luminesc.* **1992**, *54*, 177–181

.

(479) Ley, C.; Morlet-Savary, F.; Jacques, P.; Fouassier, J. P. Solvent Dependence of the Intersystem Crossing Kinetics of Thioxanthone. *Chem. Phys.* **2000**, *255*, 335–346

.

(480) Krystkowiak, E.; Maciejewski, A.; Kubicki, J. Spectral and Photophysical Properties of Thioxanthone in Protic and Aprotic Solvents: The Role of Hydrogen Bonds in S_1-Thioxanthone Deactivation. *ChemPhysChem* **2006**, *7*, 597–606

.

(481) Mitsui, M.; Ohshima, Y.; Kajimoto, O. Structure and Dynamics of 9(10H)-Acridone and Its hydrated Clusters. III. Microscopic Solvation Effects on Nonradiative Dynamics *J. Phys. Chem. A* **2000**, *104*, 8660–8670

.

(482) Torres Ziegenbein, C.; Fröbel, S.; Glöß, M.; Nobuyasu, R. S.; Data, P.; Monkman, A.; Gilch, P. Triplet Harvesting with a Simple Aromatic Carbonyl. *ChemPhysChem* **2017**, *18*, 2314–2317

.

(483) el Nahhas, A.; Cannizzo, A.; van Mourik, F.; Blanco-Rodriguez, A. M.; Zalis, S.; Vlcek, A. J.; Chergui, M. Ultrafast Excited-State Dynamics ef [Re(L)(CO)(3)(bpy)](n) Complexes: Involvement of the Solvent *J. Phys. Chem. A* **2010**, *114*, 6361–6369

.

(484) Hamze, R.; Jazzar, R.; Soleilhavoup, M.; Djurovich, P. I.; Bertrand, G.; Thompson, M. E. Phosphorescent 2-, 3- and 4-coordinate cyclic (alkyl)(amino)carbene (CAAC) Cu(i) complexes. *Chem. Commun.* **2017**, *53*, 9008–9011

.

(485) Miertuš, S.; Scrocco, E.; Tomasi, J. Electrostatic interaction of a solute with a continuum. A direct utilizaion of Ab initio molecular potentials for the prevision of solvent effects. *Chem. Phys.* **1981**, *55*, 117 – 129

.

(486) Caricato, M.; Mennucci, B.; Tomasi, J.; Ingrosso, F.; Cammi, R.; Corni, S.; Scalmani, G. Formation and relaxation of excited states in solution: A new time dependent polarizable continuum model based on time dependent density functional theory. *J. Chem. Phys.* **2006**, *124*, 124520

.

(487) Mewes, J.-M.; Herbert, J. M.; Dreuw, A. On the accuracy of the general, state-specific polarizable-continuum model for the description of correlated ground- and excited states in solution. *Phys. Chem. Chem. Phys.* **2017**, *19*, 1644–1654

.

(488) Ishimatsu, R.; Matsunami, S.; Shizu, K.; Adachi, C.; Nakano, K.; Imato, T. Solvent Effect on Thermally Activated Delayed Fluorescence by 1,2,3,5-Tetrakis(carbazol-9-yl)-4,6-dicyanobenzene *J. Phys. Chem. A* **2013**, *117*, 5607–5612

.

(489) Lee, J.; Shizu, K.; Tanaka, H.; Nomura, H.; Yasuda, T.; Adachi, C. Oxadiazole- and triazole-based highly-efficient thermally activated delayed fluorescence emitters for organic light-emitting diodes *J. Mater. Chem. C* **2013**, *1*, 4599

.

(490) Noriega, R.; Barnard, E. S.; Ursprung, B.; Cotts, B. L.; Penwell, S. B.; Schuck, P. J.; Ginsberg, N. S. Uncovering single-molecule photophysical heterogeneity of bright, thermally activated delayed fluorescence emitters dispersed in glassy hosts. *J. Am. Chem. Soc.* **2016**, *138*, 13551–13560

.

(491) dos Santos, P. L.; Ward, J. S.; Bryce, M. R.; Monkman, A. P. Using Guest–Host Interactions To Optimize the Efficiency of TADF OLEDs. *J. Phys. Chem. Lett.* **2016**, *7*, 3341–3346

.

(492) Etherington, M. K.; Gibson, J.; Higginbotham, H. F.; Penfold, T. J.; Monkman, A. P. Revealing the spin–vibronic coupling mechanism of thermally activated delayed fluorescence. *Nat. Comm.* **2016**, *7*, 13680

.

(493) Méhes, G.; Goushi, K.; Potscavage, W. J.; Adachi, C. Influence of host matrix on thermally-activated delayed fluorescence: Effects on emission lifetime, photoluminescence quantum yield, and device performance. *Org. Elec.* **2014**, *15*, 2027–2037

.

(494) Dias, F.; Santos, J.; Graves, D.; Data, P.; Nobuyasu, R.; Fox, M.; Batsanov, A.; Palmeira, T.; Berberan-Santos, M.; Bryce, M.; Monkman, A. The Role of Local Triplet Excited States and D-A Relative Orientation in Thermally Activated Delayed Fluorescence: Photophysics and Devices. *Adv. Sci.* **2016**, *3*, 1600080

.

(495) Northey, T.; Stacey, J.; Penfold, T. J. The Role of Solid State Solvation on the Charge Transfer State of a Thermally Activated Delayed Fluorescence Emitter *J. Mater. Chem. C submitted* **2017**, DOI: 10.1039/c7tc04099g

.

(496) Cossi, M.; Barone, V.; Cammi, R.; Tomasi, J. Ab initio study of solvated molecules: a new implementation of the polarizable continuum model. *Chem. Phys. Lett.* **1996**, *255*, 327–335

.

(497) Méhes, G.; Nomura, H.; Zhang, Q.; Nakagawa, T.; Adachi, C. Enhanced Electroluminescence Efficiency in a Spiro-Acridine Derivative through Thermally Activated Delayed Fluorescence. *Angew. Chem. Int. Ed.* **2012**, *51*, 11311–11315

.

(498) Li, X.; Xie, Y.; Hu, D.; Lan, Z. Analysis of the Geometrical Evolution in On-the-Fly Surface-Hopping Nonadiabatic Dynamics with Machine Learning Dimensionality Reduction Approaches: Classical Multidimensional Scaling and Isometric Mapping. *J. Chem. Theory Comput.* **2017**,

.

(499) Gómez-Bombarelli, R.; Aguilera-Iparraguirre, J.; Hirzel, T.D. ; Duvenaud, D.; Maclaurin, D.; Blood-Forsythe, M.A.; Chae, H.S; Einzinger, M.; and Ha, D-G.; Wu, T., et al. Design of efficient molecular organic light-emitting diodes by a high-throughput virtual screening and experimental approach. *Nat. Mater.* **2016**, *15* 1120-1127 .

Graphical TOC Entry